

University of New Hampshire

University of New Hampshire Scholars' Repository

Master's Theses and Capstones

Student Scholarship

Winter 2012

Phase partitioning of soluble trace gases with size-resolved aerosols in near-surface continental air over northern Colorado, USA during winter

Andrew H. Young

University of New Hampshire, Durham

Follow this and additional works at: <https://scholars.unh.edu/thesis>

Recommended Citation

Young, Andrew H., "Phase partitioning of soluble trace gases with size-resolved aerosols in near-surface continental air over northern Colorado, USA during winter" (2012). *Master's Theses and Capstones*. 770. <https://scholars.unh.edu/thesis/770>

This Thesis is brought to you for free and open access by the Student Scholarship at University of New Hampshire Scholars' Repository. It has been accepted for inclusion in Master's Theses and Capstones by an authorized administrator of University of New Hampshire Scholars' Repository. For more information, please contact Scholarly.Communication@unh.edu.

PHASE PARTITIONING OF SOLUBLE TRACE GASES WITH SIZE-RESOLVED
AEROSOLS IN NEAR-SURFACE CONTINENTAL AIR OVER NORTHERN
COLORADO, USA DURING WINTER

BY

ANDREW H. YOUNG

B.A., Colby College, 2009

THESIS

Submitted to the University of New Hampshire

in Partial Fulfillment of

the Requirements for the Degree of

Master of Science

in

Chemistry

December, 2012

UMI Number: 1522328

All rights reserved

INFORMATION TO ALL USERS

The quality of this reproduction is dependent upon the quality of the copy submitted.

In the unlikely event that the author did not send a complete manuscript and there are missing pages, these will be noted. Also, if material had to be removed, a note will indicate the deletion.

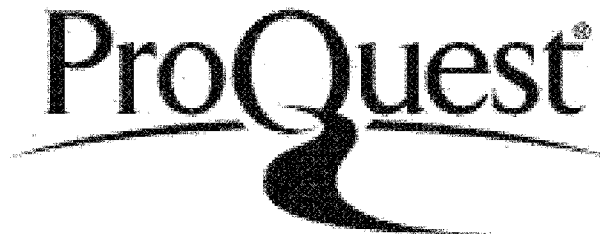


UMI 1522328

Published by ProQuest LLC 2013. Copyright in the Dissertation held by the Author.

Microform Edition © ProQuest LLC.

All rights reserved. This work is protected against unauthorized copying under Title 17, United States Code.



ProQuest LLC
789 East Eisenhower Parkway
P.O. Box 1346
Ann Arbor, MI 48106-1346

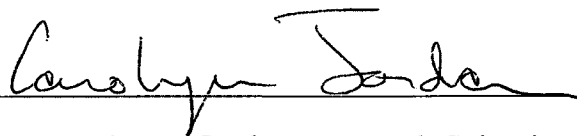
This thesis has been examined and approved.



Dr. Howard R. Mayne, Professor,
Department of Chemistry



Dr. Alexander A. P. Pszenny, Research Associate Professor,
Institute for the Study of the Earth, Oceans, and Space



Dr. Carolyn E. Jordan, Research Scientist,
Institute for the Study of the Earth, Oceans and Space

12/5/2012

Date

ACKNOWLEDGMENTS

I would like to express my immense gratitude to my advisors Dr. Alex Pszenny and Dr. Howard Mayne for their guidance, support, insight and patience during this research. I would also like to thank William Keene at the University of Virginia for sharing his knowledge of aerosols and multiphase chemistry, Dr. Carolyn Jordan of my thesis committee, and the various members of the UNH community who have offered encouragement and thoughtful discussion throughout my graduate career.

I would also like to thank my family and friends for their ongoing support and encouragement of my academic pursuits.

Financial support for this work was provided via grants through the National Science Foundation to the University of New Hampshire and the University of Virginia as part of the NACHTT campaign. Additional support was provided by the Department of Chemistry at the University of New Hampshire.

TABLE OF CONTENTS

ACKNOWLEDGEMENTS.....	iii
LIST OF TABLES.....	vi
LIST OF FIGURES.....	vii
ABSTRACT.....	viii

CHAPTER	PAGE
1. ATMOSPHERIC AEROSOLS.....	1
1.1. Aerosol Background.....	1
1.2. Aerosol Sizes, Sources, and Removal Mechanisms.....	2
1.3. Heterogeneous Reactions.....	4
2. HETEROGENEOUS HALOGEN CHEMISTRY.....	6
2.1. Introduction.....	6
2.2. Halogen Chemistry and Ozone formation.....	7
3. METHODS.....	12
3.1. Sampling Site.....	12
3.2. Measurements.....	13
3.2.1. Aerosols.....	13
3.2.2. Soluble Reactive Trace Gases.....	15
3.2.3. Meteorological Conditions and Large-Scale Atmospheric Transport.....	17
3.3. Calculations.....	19

3.3.1. Aerosol pH Inferred From Measured Phase Partitioning.....	19
3.3.2. Uncertainties in Estimated pH.....	21
4. RESULTS AND DISCUSSION.....	23
4.1. Chemical and Meteorological Characteristics.....	23
4.1.1. Meteorological Characteristics.....	23
4.1.2. Aerosol Size Distributions.....	23
4.1.3. Sources and Phase Partitioning of HCl, HNO ₃ , and NH ₃	27
4.2. Aerosol pH.....	29
4.3. Sensitivity Calculations.....	31
4.4. Implications.....	34
5. SUMMARY AND CONCLUSIONS.....	38
LIST OF REFERENCES.....	39
APPENDICES.....	46

LIST OF TABLES

Table 1. Henry's Law (K_H) and Ionization Constants for Acids (K_a), NH_3 (K_b), and Water (K_w).....	20
---	----

LIST OF FIGURES

<p>Figure 1. Location of the NOAA BAO tower in Erie, CO (diamond) and 5 day HYSPLIT back trajectories ending at the midpoint of each impactor sample. Markers on trajectories depict 24-h intervals. Additional trajectories are shown in Appendix II.....</p>	13
<p>Figure 2. Time series of (a) temperature (red) and RH (blue); (b) Wind direction (blue) and wind speed (red); (c) aerosol LWC; (d) HCl (black trace), particulate Cl⁻ based on bulk aerosol (purple bars), and ClNO₂ within ±5 m of the platform (green trace); (e) HNO₃ (black trace) and NO₃⁻ summed over impactor size bins (blue bars); and (f) NH₃ (black trace) and particulate NH₄⁺ summed over impactor size bins (orange bars). Cl⁻, NO₃⁻, and NH₄⁺ are plotted in units of equivalent nmol mol⁻¹ to facilitate direct quantitative comparison with the corresponding gas-phase mixing ratios. The shaded background intervals depict nighttime (sunset to sunrise).....</p>	18
<p>Figure 3. Box and whisker plots depicting the 10th, 25th, 50th, 75th and 90th percentiles of size-resolved particulate (a) Na⁺ (left box and whisker for each size fraction, black) and Cl⁻ (right box, purple) and (b) NO₃⁻ (left box, blue), SO₄²⁻ (middle box, red), and NH₄⁺ (right box, orange) vs ambient geometric mean diameter (GMD).....</p>	26
<p>Figure 4. Aerosol pH based on HNO₃ phase partitioning in GMD 14 μm (black circles) and 0.58 μm (blue triangles).....</p>	30
<p>Figure 5. Box and whisker plots depicting the 10th, 25th, 50th, 75th and 90th percentiles of size-resolved aerosol pH based on HNO₃ (middle box and whisker for each size fraction, blue), NH₃ (right box and whisker, orange), and HCl (HCl K_H based on <i>Marsh and McElroy</i> [1985] (left box and whisker, purple) vs ambient geometric mean diameter (GMD).....</p>	31

ABSTRACT

PHASE PARTITIONING OF SOLUBLE TRACE GASES WITH SIZE-RESOLVED AEROSOLS IN NEAR-SURFACE CONTINENTAL AIR OVER NORTHERN COLORADO, USA DURING WINTER

by

Andrew H. Young

University of New Hampshire, December 2012

Multiphase processing of reactive halogens impact important, interrelated chemical processes in Earth's troposphere. During the Nitrogen, Aerosol Composition, and Halogens on a Tall Tower (NACHTT) campaign at the National Oceanic and Atmospheric Administration Boulder Atmospheric Observatory tower, Erie, CO, USA in winter 2011, soluble trace gases, the ionic composition of size-resolved aerosols, and the associated meteorological conditions were measured. Aerosol pH was inferred from the multiphase coupling of HNO_3 , NH_3 , and HCl . pHs calculated from the measured phase partitioning and thermodynamic properties of HNO_3 and NH_3 were similar both in terms of absolute values as well as overall trends across the sampled size fractions while pHs inferred from the HCl couple were consistently higher. Aerosols were acidic across all size fractions and throughout the duration of the campaign. Total Cl was greater than ClNO_2 in sampled air parcels suggesting that Cl availability was not the limiting factor in ClNO_2 production.

CHAPTER 1

ATMOSPHERIC AEROSOLS

1.1 Aerosol Background

Pollution in the atmosphere is made up of both gaseous and particulate constituents, and for the past several decades a great deal of time has been spent to understand the fundamental sources, chemistry, and transport of these pollutants. However relatively little of the work has focused on condensed phase chemical processes involving atmospheric aerosols. Atmospheric aerosols are solid or liquid particles suspended in air and can contribute to a large range of phenomena including dust, fog, haze, smoke and soot [*Seinfeld and Pandis, 1998*].

Aerosols can play a role in the interaction of solar radiation with Earth's climate system through the scattering and absorption of light. The degree to which the aerosols will interact with the solar radiation depends on a variety of properties including loading, chemical composition, size distribution, and shape. Depending on their interaction with the incoming solar radiation, the aerosols can have a heating or cooling effect on Earth's climate. Scattering of light back towards space can lead to a cooling effect while the absorption of light can lead to a heating of the atmosphere as well as a reduction in the visible light reaching the planet's surface [*Crutzen and Andreae, 1990*]. Furthermore, long-wavelength infrared radiation emitted at the surface can be absorbed by various aerosol species leading to positive radiative forcing. Aerosols can also have several indirect effects on the interaction of light with the atmosphere. One of these indirect effects is when aerosols act as cloud condensation nuclei (CCN), which can increase the

number concentration of droplets in clouds, thereby decreasing their size distribution, leading to more scattering of shortwave radiation [Twomey, 1977]. A second indirect effect arises from the decrease in cloud droplet size noted above (because the same amount of water is divided between more droplets), resulting in a suppression of precipitation and increasing the lifetime of clouds [Forster *et al.*, 2007].

Aerosols can also have a so-called “semi-direct” effect on radiative forcing caused by radiation-absorbing atmospheric particles. One such mechanism is when aerosols aloft in the atmosphere absorb radiation and heat the surrounding air, which will decrease the condensation of water and thus cloud formation [Ackerman *et al.*, 2000]. Another example is when the absorbing aerosols are near the surface, which can slow atmospheric convection, resulting in more stable air masses. This results in less moisture aloft and thus reducing the formation of clouds. [Koren *et al.*, 2004].

1.2 Aerosol Sizes, Sources, and Removal Mechanisms

Aerosols typically range in size from a few nanometers (nm) to tens of micrometers (μm) in diameter. In the context of human health, those particles less than $2.5 \mu\text{m}$ in diameter are referred to as “fine” and those greater than $2.5 \mu\text{m}$ in diameter as “coarse” aerosols [Seinfeld and Pandis, 1998]. This is due to the fact that generally only particles below $2.5 \mu\text{m}$ can have an impact on the respiratory system. However, in the context of climate impacts and biogeochemical cycles the “cutoff” for the distinction in size is generally $1 \mu\text{m}$. This cutoff at $1 \mu\text{m}$ is due to the fact that aerosols larger than this (1) scatter light more efficiently than smaller particles and (2) the removal from the atmosphere of the larger particles via impaction and gravitational settling are more

effective. Aerosols are also recognized in terms of whether they are of anthropogenic or natural origin. Aerosols can also be described based on whether they are emitted directly (primary) or formed in the atmosphere via gas-to-particle reaction processes (secondary). The above characteristics are important, as they will influence the chemical characteristics as well as formation and removal mechanisms for the aerosol [*Seinfeld and Pandis, 1998*].

The classification of an aerosol as fine or coarse is an important distinction, as each group generally varies by transformations in the atmosphere, removal mechanisms, chemical composition, optical properties and deposition patterns in the respiratory tract. Within the fine-particle group, there are three sub-classifications: nucleation mode particles (up to 10 nm in diameter), Aitken mode particles (10 to 100 nm in diameter) and accumulation mode particles (100 nm to 1 μm in diameter). Nucleation mode particles are formed from condensation of hot vapors during combustion processes and from the nucleation of oxidation products of atmospheric trace gases to form fresh particles. These particles are then generally removed via coagulation with larger particles. Accumulation mode particles account for the largest portion of the aerosol surface area and a large portion of the aerosol mass. The sources of aerosols in this size range generally originate from coagulation of particles in the nucleation mode and from condensation of vapors onto existing particles, driving those particles into the accumulation mode size range. These particles in the accumulation mode are referred to as such because the removal mechanisms for particles in this size range are relatively inefficient, which leads to particles accumulating in this size range. Finally, coarse mode particles are formed via mechanical processes and usually consist of anthropogenic and natural dust and sea salt

particles. However, particles in this size range have reasonably high sedimentation velocities, causing them to fall out of the atmosphere in a short timeframe.

In addition to the size, aerosols can also be characterized based on the formation mechanisms of the particles. Primary aerosols are emitted directly into the atmosphere while secondary aerosols are formed via a gas-to-particle conversion process. The gas-to-particle transformation is usually a result of oxidation by O_3 or OH and NO_3 radicals.

Natural primary sources of aerosols provide a large flux of aerosols, and include sea salt, mineral dust, volcanic ash, and biological debris. Anthropogenic sources of primary aerosols are relatively small inputs to the aerosol flux and include industrial dust, black carbon from combustion, and organic aerosols from domestic and agricultural fires. Natural secondary sources include the formation of sulfate aerosols from dimethyl sulfide produced from marine sources and sulfates from volcanic emissions of sulfur dioxide (SO_2). Biogenic volatile organic compounds such as isoprene, monoterpenes and the pinenes can also be oxidized and result in the formation of secondary organic aerosols. Anthropogenic secondary sources of aerosols include fossil fuel burning, which results in sulfate and nitrate production from emitted SO_2 and nitrogen oxides ($NO_x = NO + NO_2$), respectively. These sources become especially important in urban regions.

1.3 Heterogeneous Reactions

In addition to the above-mentioned phenomena, the study of aerosols is an important area of research due to their impact on the chemical processes of the atmosphere. Heterogeneous reactions are reactions that take place between particle- and

gas-phase constituents, and these reactions can have a large impact on urban ozone formation, total reactivity of the atmosphere, and the formation of secondary aerosols. In particular, aerosols serve as a reaction surface on which chemical reactions involving atmospheric constituents can take place. These reactions are impacted by a number of factors, including the aerosols' liquid water content (LWC), aerosol composition, aerosol pH and particle density. Of particular interest in this work are heterogeneous reactions involving halogens, chlorine in particular, which is the subject of the next chapter.

CHAPTER 2

Heterogeneous Halogen Chemistry

2.1 Introduction

Chemical reactions involving inorganic halogens significantly influence the composition of the Earth's atmosphere. The importance of these reactions was first recognized in connection with stratospheric ozone loss [e.g., *Molina and Rowland*, 1974], especially within the polar vortices during spring [e.g., *Wennberg et al.*, 1994]. In the troposphere, the multiphase processing of reactive halogens significantly modifies conventional HO_x/NO_x photochemistry over Arctic and Antarctic sea ice [*Foster et al.*, 2001; *Simpson et al.*, 2007], salt flats [*Matveev et al.*, 2001], coastal-marine macroalgal beds [*Alicke et al.*, 1999], coastal cities [*Osthoff et al.*, 2008; *Riedel et al.*, 2012], other polluted coastal regions [*Finley and Saltzman*, 2006; *Pszenny et al.*, 2007; *Pechtl and von Glasow*, 2007], and the open ocean [*Read et al.*, 2008; *Keene et al.*, 2009]. Model calculations based on observations suggest that the multiphase photochemical cycling of reactive halogens from marine sources is globally significant in terms of the processing and lifetimes of climatically and ecologically important species including O₃, oxidized S and N compounds, CH₄, and reactive Hg [e.g., *von Glasow et al.*, 2002a,b; *Platt et al.*, 2004; *Read et al.*, 2008; *Lawler et al.*, 2009].

Halogen chemistry also influences the acidity of aerosols, particularly in marine regions, via the phase partitioning of HCl. Rates of important aqueous chemical transformations including sulfur oxidation and halogen "activation", as well as the phase

partitioning and associated atmospheric lifetimes of major atmospheric acids and bases are all strongly pH dependent [Keene *et al.*, 1998]. Aerosol acidity has been investigated in urban [e.g., Ludwig and Klemm, 1990] and rural [e.g., Tanner and Harrison, 1992] continental locations, in near-surface marine air [e.g., Keene *et al.*, 2002], and in the context of public health [e.g., Gwynn *et al.*, 2000]. However, persistent uncertainties in this fundamental property of multiphase systems limit the ability to assess important chemical pathways influencing Earth systems including climate [e.g., Laskin *et al.*, 2003; Keene and Pszenny, 2004; Sander *et al.*, 2004; and references therein].

Halogen-radical chemistry had been thought to be relatively unimportant in continental air remote from marine sources of halogenated precursors. However, recent measurements of ClNO₂, N₂O₅, and associated species and meteorological conditions near Boulder, CO in winter coupled with model calculations suggest that nocturnal reactions involving anthropogenic precursors in polluted continental air represent a previously unrecognized and potentially important source for atomic Cl as well as a recycling mechanism for NO₂ with important implications for oxidation processes and the physicochemical evolution of the troposphere [Thornton *et al.*, 2010; von Glasow, 2010]. Subsequent measurements at other mid-continental locations support the hypothesis that these reactions are globally significant [Mielke *et al.*, 2011; Phillips *et al.*, 2012].

2.2 Halogen Chemistry and Ozone Formation

Because photochemical reactions involving NO_x (NO + NO₂) are the dominant pathways by which ozone is formed in the troposphere, a reliable predictive capability for

oxidation processes requires explicit evaluation of NO_x cycling. At night, the reactions



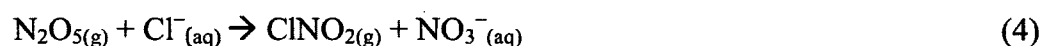
and



produce N₂O₅, which serves as a reservoir species for NO_x. The subsequent photolysis of N₂O₅ following sunrise regenerates the NO_x from which it was formed. However N₂O₅ also reacts at the surface of aerosols to produce HNO₃, NO₃⁻, and ClNO₂ via [Finlayson-Pitts et al., 1989; Behnke et al., 1997]



and



Most atmospheric models consider only reaction 3 and predict that this pathway accounts for 30% to 50% of the total NO_x sink in polluted regions [Alexander et al., 2009]. Measurements in polluted continental air during winter in Colorado, USA [Thornton et al., 2010] and Alberta, Canada [Mielke et al., 2011] revealed peak ClNO₂ mixing ratios of 450 and 250 pmol mol⁻¹, respectively. More recent measurements in rural southwestern Germany during summer detected ClNO₂ up to 800 pmol mol⁻¹ [Phillips et al., 2012]. Although somewhat lower on average, these ranges in mixing ratios overlap those for ClNO₂ measured in the polluted coastal air over Houston, Texas (from below <50 to >1 nmol mol⁻¹) [Osthoff et al., 2008] and have potentially important implications for

oxidation processes in polluted continental air. However, the pathway(s) by which ClNO₂ is produced in continental air and the overall impacts of subsequent transformations on other atmospheric constituents are poorly constrained because previous investigations in the continental troposphere did not characterize aerosol composition for size fractions greater than ~1 μm diameter or HCl vapor.

Additionally, previous investigations of ClNO₂ production and processing in polluted coastal [Osthoff *et al.*, 2008] and continental air [Thornton *et al.*, 2010] did not evaluate halogen-radical recycling via gas-phase and multiphase pathways or the associated implications for physicochemical evolution [e.g., Sander *et al.*, 1999; Pszenny *et al.*, 2004; Keene *et al.*, 2009]. Consequently, they may have underestimated the overall influences of halogen activation via reaction 4. For example, in addition to oxidizing hydrocarbons, some atomic Cl reacts with O₃ and recycles in the gas phase during the daytime via:



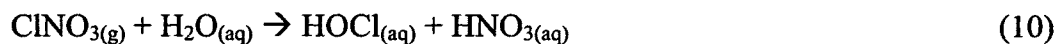
Similar reactions destroy O₃ in the stratosphere. ClO is also consumed by



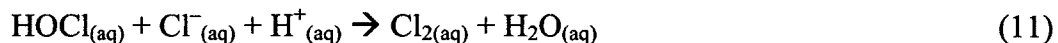
and



which, at high NO_x, suppresses atomic Cl recycling via reactions 5 through 7. Reaction 8 recycles atomic Cl without destroying NO_x but model calculations indicate that the formation of ClNO₃ via reaction 9 and its subsequent hydrolysis at aerosol surfaces (primarily those of sub-μm diameter size fractions) via:



is a major sink for NO_x and an important source for HOCl in both polluted and clean marine air [*Sander et al.*, 1999; *Pszenny et al.*, 2004; *Keene et al.*, 2009]. By extension, this pathway may also be important in polluted coastal and continental air. If so, reaction 10 would diminish both the net recycling of NO_x and the associated O₃ production relative to that based on photolysis of ClNO₂ alone. Some HOCl produced via reactions 6 and 10 is scavenged by acidic aerosols leading to additional halogen activation via:



Product Cl₂ subsequently volatilizes and, during daytime, photolyzes, yielding additional atomic Cl. Reaction 11 will proceed during both the day and night and therefore can enhance halogen activation at night and sustain halogen-radical chemistry for longer periods during daytime relative to predictions based on only ClNO₂ photolysis and the assumption that all Cl reacts with hydrocarbons (i.e., as simulated by *Osthoff et al.*, [2008] and *Thornton et al.*, [2010]).

The formation of ClNO₂ can impact oxidation processes in the troposphere in two important respects: (1) As noted above, it acts as a nocturnal reservoir for NO_x thereby slowing NO_x destruction via reaction 3 and (2) it rapidly photolyzes following sunrise to

form atomic Cl. Cl reacts with alkanes about 10-100 times faster than OH radicals and the product alkoxy radicals contribute to oxidation potential (the ability of the atmosphere to “cleanse” itself of pollutant species such as VOCs). These two aspects of ClNO₂ chemistry lead to a net increase in O₃ formation in the polluted troposphere. In addition, Cl radical production via ClNO₂ photolysis peaks in the early morning, well before the peak in OH production, which initiates volatile organic carbon (VOC)-NO_x photochemistry earlier in the day relative to conventional HO_x/NO_x photochemistry (e.g., *Behnke et al.*, [1997]; *Osthoff et al.*, [2008]).

Key outstanding uncertainties involving the size-resolved composition (including acidity) and hydration state of aerosols and of HCl mixing ratios limit current understanding of the factors that regulate ClNO₂ formation and constrain the reliability of spatial and temporal extrapolation of results. This thesis will focus on data and results from the Nitrogen, Aerosol Composition, and Halogens on a Tall Tower (NACHTT) campaign in Erie, Colorado investigating halogen reactivity and recycling and the impacts on aerosol composition and pH in the continental troposphere. These data are interpreted to assess aerosol pH and associated multiphase chemical processes that influence ClNO₂ production and processing in the polluted continental troposphere.

CHAPTER 3

Methods

3.1 Sampling Site

Between 18 February and 12 March 2011, a comprehensive suite of chemical species was measured at the National Oceanic and Atmospheric Administration (NOAA) Boulder Atmospheric Observatory (BAO) tower near Erie, CO (40.05 N, 105.01 W, and 1584 m elevation, Fig. 1) as part of the NACHTT campaign (<http://www.esrl.noaa.gov/csd/tropchem/2011NACHTT>). Unless otherwise specified, data reported herein correspond to air sampled from a platform on the BAO tower at 22 m above ground level (AGL). Additional measurements (including ClNO₂, aerosol composition, and meteorological conditions) were also characterized in parallel from a mobile instrument carriage on the tower that travelled from ground level to 250 m AGL [*Brown et al.*, manuscript in preparation]. To minimize the potential for contamination, aerosol sampling was suspended during periods of precipitation and both gas and aerosol sampling were suspended during periods of carriage maintenance.

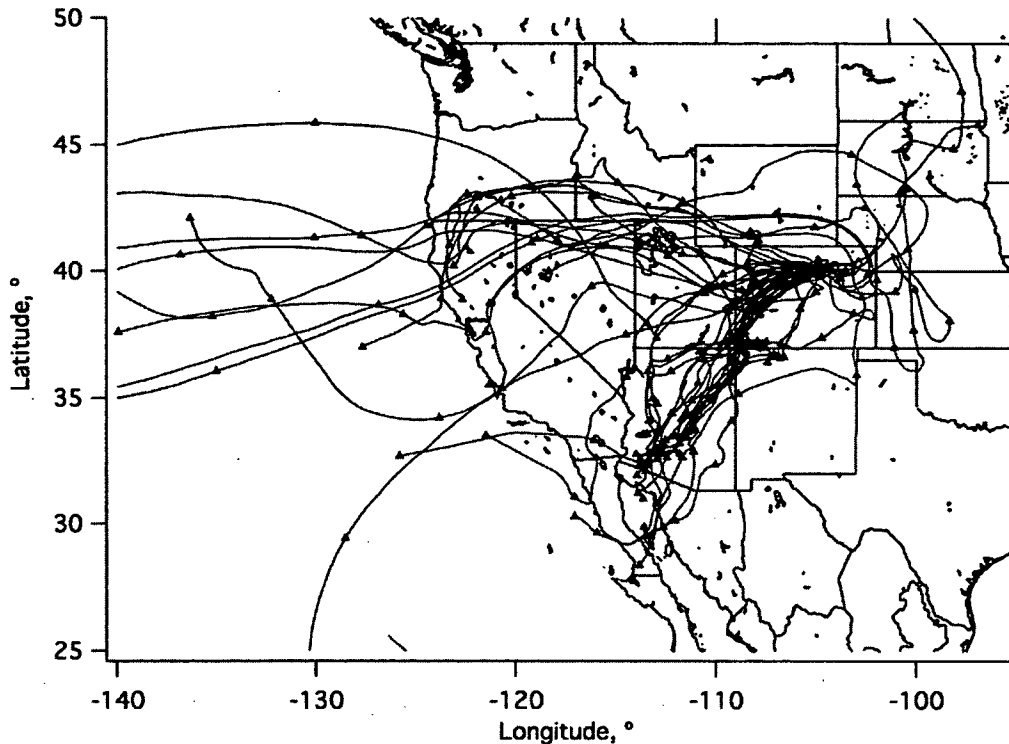


Figure 1. Location of the NOAA BAO tower in Erie, CO (diamond) and 5 day HYSPLIT back trajectories ending at the midpoint of each impactor sampling period. Markers on trajectories depict 24-h intervals. Additional trajectories are shown in Appendix II.

3.2. Measurements

3.2.1. Aerosols

Ambient aerosols were sampled over forty-five daytime (sunrise to sunset) and nighttime (sunset to sunrise) intervals with two different systems. Size-segregated aerosols were sampled with a MSP Corp. model 130 hi-flow (100 L min^{-1}) cascade impactor configured with a custom designed and fabricated inlet nozzle and Liu-Pui type inlet assembly [Liu *et al.*, 1983]. All air volumes reported herein are normalized to standard temperature and pressure (0°C , 1 atm). The calculated passing efficiency for 20- μm -diameter particles through the inlet was 95%. Relative to MSP's Micro-Orifice

Uniform Deposit Impactor (MOUDI) [Marple *et al.*, 1991] that is in more widespread use by the research community, these hi-flow impactors yield greater signal per unit deployment time while segregating aerosol size fractions using similar nozzle technology. The 50% aerodynamic diameter cut sizes for the modified impactor were 0.25, 0.44, 0.80, 1.4, 2.5, 5.0, 10, and 20 μm . The impactor was configured with 75-mm-diameter polycarbonate substrates (Whatman 111107) and 90-mm-diameter quartz fiber backup filters (Pallflex 2500 QAT-UP). Bulk aerosol was sampled in parallel on 20 x 25 cm Whatman 41 cellulose filters at an average flow rate of $1.3 \text{ m}^3 \text{ min}^{-1}$. The Whatman 41 filters were pre-washed with deionized water (DIW). Impactors and bulk filter cassettes were cleaned, dried, and loaded in a Class 100 clean bench with activated charcoal scrubbers mounted on the inlet to remove reactive trace gases. Blanks were generated by deploying loaded impactors and bulk filter cassettes on the platform, briefly exposing to ambient air (~ 15 sec), recovering, and processing using identical procedures as those for samples. After recovery, exposed impaction substrates, back filters, and bulk filters were folded in half, sealed in polyethylene bags, and stored frozen prior to analysis.

Samples and blanks were transported to and analyzed at the University of Virginia (UVA). Each impaction substrate and back filter was extracted under sonication in 8.0 ml DIW and a quarter section of each bulk filter was extracted in 16 ml DIW. Major ions (including SO_4^{2-} , Cl^- , Br^- , NO_3^- , NO_2^- , HCOO^- , CH_3COO^- , $(\text{COO})_2^{2-}$, NH_4^+ , Na^+ , K^+ , Mg^{2+} , and Ca^{2+}) were analyzed by high-performance ion chromatography (IC) using procedures similar to those described by Keene *et al.* [2009]. Data for samples were corrected based on median concentrations of analytes recovered from handling blanks

(N=10). Quarter sections of each high-volume bulk filter were shipped frozen to the University of New Hampshire (UNH) to prepare for neutron activation analysis (NAA) of elemental constituents (described below).

High-volume bulk filters were analyzed by NAA using a procedure similar to that described by *Uematsu et al.*, [1983]. A 47-mm diameter circle was punched from each high-volume sample and field blank using a stainless steel cutting die. Standards were prepared by spotting aliquots of a NIST-traceable mixed element standard solution (Ultra Scientific, North Kingstown, RI) on blank filters. Standards, samples, and field blanks were each spiked with 20 ng of indium (as an aliquot of a NIST-traceable standard solution; Ultra Scientific) as internal flux monitor, sealed in a clean polyethylene envelope and subsequently irradiated at the Rhode Island Nuclear Science Center for 300 seconds at a nominal flux of 4×10^{12} thermal neutrons $\text{cm}^{-2} \text{s}^{-1}$. Following irradiation, samples were allowed to decay for approximately 5 minutes during which time they were transferred to unirradiated envelopes, and counted for 900 s live time on a Ge(Li) gamma-ray spectrometer. Data were obtained for seven elements: Na, Mg, Al, Cl, Mn, V and Br. All laboratory manipulations of cassettes and filters prior to irradiation were carried out in class 100 clean benches.

3.2.2. Soluble Reactive Trace Gases

Unmodified air was drawn at $1.2 \text{ m}^3 \text{ min}^{-1}$ from the level of the aerosol samplers on the tower through a 10.2-cm-diameter polyvinyl chloride plenum that was passivated prior to installation [*Russell et al.*, 2003]. Prior to the experiment, passing efficiencies through the plenum for analyte gases in ambient air were measured at UVA and found to

be statistically indistinguishable from 100%. Air was subsampled from the bottom of the plenum at approximately 16 L min^{-1} through a size-fractionating inlet that inertially removed super- μm -diameter aerosols from sample air [e.g., *Keene et al.*, 1993; *Munger et al.*, 1995]. Sub- μm aerosols were removed downstream with an in-line Teflon filter (Zefluor 2 μm pore diameter). Water-soluble, volatile inorganic chloride and nitrate (dominated by and hereafter referred to as HCl and HNO_3 , respectively), NH_3 , HONO, HCOOH, and CH_3COOH in the particle-free air stream were sampled over 2-hour intervals at nominal flow rates of 20 L min^{-1} with tandem mist chambers, each of which contained 20 mL DIW, following procedures similar to those described by *Keene et al.* [2009]. Blanks were generated periodically (approximately twice daily) by loading the mist chamber, briefly (10 seconds) drawing sample air through the system, and recovering the solutions. Samples and blanks were processed and analyzed using identical procedures. Data for samples were corrected based on these handling blanks. Cl^- , NO_3^- , NH_4^+ , NO_2^- , HCOO^- , and CH_3COO^- in exposed mist solutions were analyzed on site by IC usually within an hour after recovery.

Performance of the tandem mist chamber technique for measurement of HCl, HNO_3 , NH_3 , HCOOH, and CH_3COOH has been critically evaluated and indicates that this approach yields representative results for these analytes [see *Keene et al.*, 2004, and references therein]. Although a previous intercomparison of HONO measured by this technique and by long-path differential optical absorption spectroscopy (DOAS) suggested reasonable agreement [*Keene et al.*, 2006], mixing ratios reported herein are considered semi-quantitative (because of relatively limited testing) and upper limits (based on published evidence that HONO may be produced via artifact reactions [e.g.,

Zhou et al., 2002]). Detection limits for HCl ($0.023 \text{ nmol mol}^{-1}$), HNO₃ ($0.045 \text{ nmol mol}^{-1}$), NH₃ ($1.4 \text{ nmol mol}^{-1}$), HONO ($0.032 \text{ nmol mol}^{-1}$), HCOOH ($0.46 \text{ nmol mol}^{-1}$), and CH₃COOH ($0.58 \text{ nmol mol}^{-1}$) were estimated following *Keene et al.* [1989].

3.2.3. Meteorological Conditions and Large-Scale Atmospheric Transport

Wind direction, wind speed, air temperature, and relative humidity (RH) were measured continuously by NOAA/ESRL instruments deployed at 10 m and 100 m AGL on the NOAA tower (Fig. 2 panels a and b; additional detail available at <http://www.esrl.noaa.gov/psd/technology/bao/>). Conditions at the level of the sampler intakes (22 m AGL) that are plotted in Figure 2 were based on linear interpolation between these two measurement heights. Five-day air mass back trajectories ending at 22 m AGL were calculated for one to four times during each impactor sampling interval using the NOAA Hybrid Single Particle Lagrangian Integrated Trajectory (HYSPLIT) model (Fig. 1) [*Draxler and Rolph*, 2012].

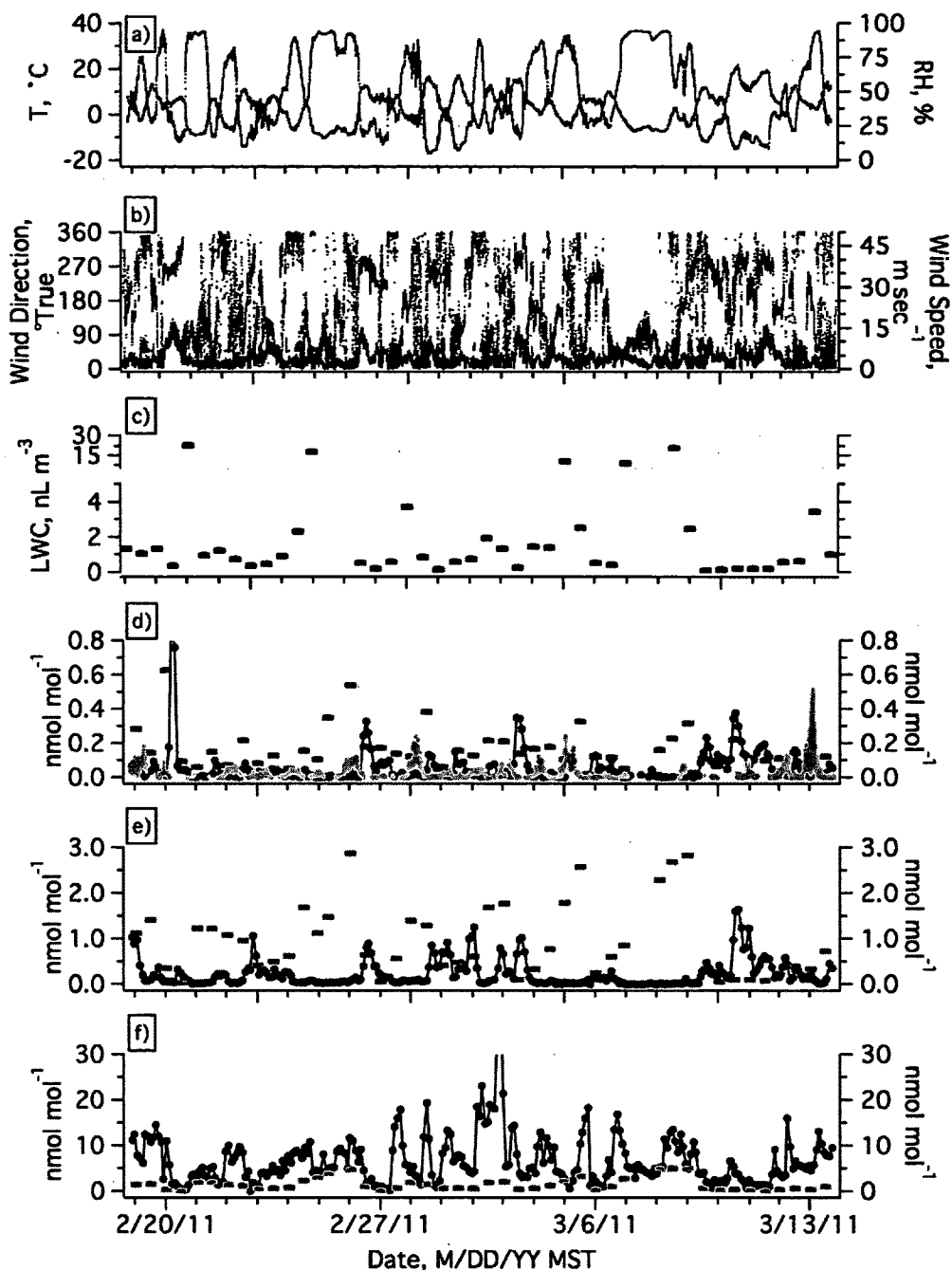
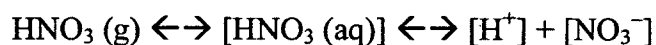


Figure 2. Time series of (a) temperature (red) and RH (blue); (b) Wind direction (blue) and wind speed (red); (c) aerosol LWC; (d) HCl (black trace), particulate Cl⁻ based on bulk aerosol (purple bars), and ClNO₂ within ±5 m of the platform (green trace); (e) HNO₃ (black trace) and NO₃⁻ summed over impactor size bins (blue bars); and (f) NH₃ (black trace) and particulate NH₄⁺ summed over impactor size bins (orange bars). Cl⁻, NO₃⁻, and NH₄⁺ are plotted in units of equivalent nmol mol⁻¹ to facilitate direct quantitative comparison with the corresponding gas-phase mixing ratios. The shaded background intervals depict nighttime (sunset to sunrise).

3.3. Calculations

3.3.1. Aerosol pH Inferred From Measured Phase Partitioning

Equilibrium hydrogen ion concentrations for individual aerosol size fractions were calculated based on the measured phase partitioning and associated thermodynamic properties of compounds with pH-dependent solubility (HCl, HNO₃, NH₃) following the approach of *Keene and Savoie* [1998]. Briefly, using HNO₃ as an example, the equilibrium



was evaluated on the basis of simultaneous measurements of gas-phase HNO₃ mixing ratios averaged over the aerosol sampling interval, size-resolved particulate NO₃⁻ concentrations in air, temperature-adjusted Henry's Law (K_H) and acidity (K_a) constants for HNO₃ (Table 1), aerosol LWC (liquid water content), and NO₃⁻ activity coefficients. The rationale for selecting among reported Henry's Law constants is discussed below. LWCs and activity coefficients were estimated using the Extended Aerosol Thermodynamic Model (E-AIM, [*Friese and Ebel*, 2010]) parameterized based on the measured chemical composition and the corresponding relative humidity (RH) and temperature averaged over each aerosol sampling interval [*Engelhart et al.*, 2011].

Table 1. Henry's Law (K_H) and Ionization Constants for Acids (K_a), NH_3 (K_b), and Water (K_w)

Species	K_H , M atm^{-1}	K_a or K_b , M
HCl	$1.1 \times 10^0 \exp [2300(1/T - 1/298)]^a$	$1.7 \times 10^6 \exp [6896(1/T - 1/298)]^a$
HNO_3	$2.46 \times 10^6 \exp [8700(1/T - 1/298)]^b$	$1.5 \times 10^1 \exp [8700(1/T - 1/298)]^c$
NH_3	$6.1 \times 10^1 \exp [4300(1/T - 1/298)]^b$	$1.7 \times 10^{-5} \exp [-4325(1/T - 1/298)]^d$
H_2O	-	$1.0 \times 10^{-14} \exp [-6870(1/T - 1/298)]^e$

^a*Marsh and McElroy* [1985]

^b*Clegg and Brimblecombe* [1989]

^c*Schwartz and White* [1981]

^d*Chameides* [1984]

^e*Bandura and Lvov* [2006]

E-AIM Model IV, which considers a multiphase system with aerosols comprised of SO_4^{2-} , NO_3^- , Cl^- , NH_4^+ , Na^+ , H^+ , and H_2O , was employed to estimate LWCs and activity coefficients for all samples for which the model yielded an aqueous phase (generally at RHs greater than about 60%). At lower RHs, Model IV is unstable [*S.L. Clegg, University of East Anglia, personal communication, 2012*]. In these cases, Model II was employed, which considers all of the above constituents except Cl^- and Na^+ . Because Cl^- is not considered in Model II, Cl^- activity coefficients under low RH conditions were based on Model IV at the lowest RH that yielded an aqueous phase. E-AIM requires initialization with input data that are charge balanced (i.e., sum of anions must equal sum of cations on an equivalent basis). Because (1) the model does not consider all ionic constituents associated with aerosols and (2) all analytical data are subject to random measurement error, the measured subset of constituents with which the model was initialized were not exactly charge balanced for any sample. The following procedure was employed to adjust the measured ionic composition for implementation in the model. Cation deficits (where a sample had a lower amounts of measured cations than anions) were balanced by adding equivalents of H^+ . Anion deficits (measured sample had

lower amounts of measured anions than cations) were balanced by increasing the equivalents of measured anions in proportion to their relative concentrations in ambient air. Because the ionic compositions of virtually all samples were dominated by NO_3^- , SO_4^{2-} , and NH_4^+ , the adjustments required to balance charges were generally small and, based on sensitivity runs (described below), had minor to negligible influences on resulting aerosol acidities.

3.3.2 Uncertainties in Estimated pH

Potential sources of error involving the approach described in Section 3.3.1 include: Measurement uncertainties, variability in composition and averaging over long sampling times, the reliability of aerosol LWCs and activity coefficients estimated by E-AIM parameterized as described above, uncertainties in the temperature-adjusted Henry's Law and dissociation constants, and the assumption that the multiphase system was at thermodynamic equilibrium [e.g., *Keene and Savoie*, 1998, 1999; *Keene et al.*, 2002; 2004; *Pszenny et al.*, 2004]. The sensitivity of results to several of these factors was evaluated explicitly. In addition to aerosol pH calculated based on the mixing ratios of gases averaged over each aerosol sampling interval, pH was also calculated based on the corresponding maximum and minimum values over each interval. Sensitivity of pH to variability in temperature and RH was evaluated over a range of $\pm 25\%$ for each. The sensitivity of results to the approach employed to charge balance the input data for E-AIM was evaluated by increasing NH_4^+ (rather than adding H^+) to account for cation deficits and by increasing only the anion present at the highest concentration (rather than all anions in proportion to their relative concentrations) to account for anion deficits.

Finally, aerosol pHs were calculated over a range of published Henry's Law constants for HCl. In this regard, we note that published Henry Law constants for HNO₃ and NH₃ fall within relatively narrow ranges (2.3×10^4 to 2.6×10^6 M atm⁻¹ and 1.0×10^1 to 7.8×10^1 M atm⁻¹, respectively) whereas those for HCl vary over a much greater range (1.1×10^0 to 2.5×10^3 M atm⁻¹) [e.g., see R. Sander, Compilation of Henry's law constants for inorganic and organic species of potential importance in environmental chemistry, version 3, <http://www.henrys-law.org>, 1999, hereafter referred to as *R. Sander, unpublished data*, 1999].

The large variability in K_{HS} for HCl may reflect the fact that HCl is a very strong acid and thus the undissociated fraction (i.e., the numerator in K_H) is difficult to quantify reliably. pHs inferred from the phase partitioning of HNO₃ and NH₃ based on the most commonly used K_{HS} (Table 1) provide useful constraints for evaluating pH values inferred from HCl over the range of reported Henry's Law constants. The reported values of K_H for HNO₃ and NH₃ were thoroughly evaluated by *Clegg and Brimblecombe* [1989] and result in size-resolved median calculated pHs that are very close in value (discussed below). The K_H value for NH₃ has been well established, and has been largely unchanged through several different studies and evaluations [e.g. *Clegg and Brimblecombe*, 1989; *Chameides*, 1984; and *Sander, et al.*, 2011].

CHAPTER 4

Results and Discussion

4.1 Chemical and Meteorological Characteristics

4.1.1 Meteorological Characteristics

During NACHTT sampling from 18 February to 12 March 2011, the median wind speed was 2.9 m s^{-1} and generally remained below 7 m s^{-1} during the campaign with only occasional spikes above 10 m s^{-1} . Median wind direction was 162° (SSE), but was highly variable over the campaign. Highest wind speeds were associated primarily with flow from the WNW. Back trajectories suggest that the sampled air masses were primarily influenced by conditions to the west and southwest of the sampling site, with the most prevalent flow over the far southwestern U.S. and northern Gulf of California or over northern California and the eastern North Pacific Ocean (Fig. 1). See *Brown et al.* [manuscript in preparation] for additional details regarding meteorological conditions and large-scale atmospheric flow during the campaign.

4.1.2 Aerosol Size Distributions

Although detectable in all size fractions, soluble Cl^- and Na^+ were both associated primarily with super- μm -diameter aerosol size fractions (Fig. 3a). In addition, virtually all particulate Cl was in the form of Cl^- , which was highly correlated with Na^+ [*Pszenny et al.*, manuscript in preparation]. These relationships suggest that soluble Cl^- and Na^+ originated from a similar primary source or sources. In contrast, most NO_3^- , NH_4^+ , and

SO_4^{2-} were associated with the sub- μm -diameter size fractions suggesting these particulate-phase species originated primarily from gas-phase precursors (Fig. 3b). Assuming that all Na^+ was produced in association with marine aerosol, virtually all SO_4^{2-} (97% based on median values summed over all size fractions and 88% based on median values summed over super- μm size fractions) originated from non-sea-salt sources.

NO_3^- , NH_4^+ , and SO_4^{2-} summed over the impactor size bins agreed well with concentrations in paired samples of bulk aerosol (not shown); slopes for Reduced Major Axis (RMA) regressions were 1.11, 0.86 and 0.96, respectively. The corresponding correlation coefficients (expressed as r^2) were 0.91, 0.93, and 0.98, respectively. Because these analytes (1) were associated primarily with sub- μm aerosols (Fig. 3b), and (2) SO_4^{2-} is conservative with respect to mixing chemically distinct aerosols, the good agreement in paired data, particularly for SO_4^{2-} , indicates that the impactor sampled sub- μm size fractions quantitatively.

In contrast, RMA regressions of Cl^- and Na^+ sampled with the impactor versus bulk sampler exhibited lower slopes (0.61 and 0.64 respectively) and greater scatter (r^2 of 0.82 and 0.80, respectively). Because (1) these analytes were associated primarily with super- μm aerosols (Fig. 3a), (2) Na^+ is conservative with respect to mixing chemically distinct aerosols, and (3) available evidence summarized above indicates that sub- μm size fractions were sampled quantitatively by the impactor, these relationships imply that larger size fractions were sampled at lower efficiencies by the impactor relative to the bulk sampler. It is likely that the slower flow rate through the impactor's inlet ($0.1 \text{ m}^3 \text{ min}^{-1}$) relative to the bulk sampler's ($\sim 1.3 \text{ m}^3 \text{ min}^{-1}$) resulted in greater wind- or

turbulence-induced, inertial segregation of larger particles at the impactor's inlet resulting in lower and somewhat more variable sampling efficiencies for the larger size fractions. The calculated passing efficiencies under quiescent conditions did not explicitly evaluate such effects. Consequently, concentrations of analytes associated with super- μm size fractions are considered lower limits.

In addition, compounds with pH dependent solubilities such as HCl, HNO₃, and NH₃ are subject to artifact phase changes when chemically distinct aerosol size fractions are sampled in bulk because the pH of the bulk mixture may diverge significantly from that of the size fractions with which individual gases preferentially partition. For example, in marine air, most particulate Cl⁻ and NO₃⁻ are typically associated with super- μm size fractions whereas most NH₄⁺ is associated with sub- μm size fractions because, on average, larger marine aerosol size fractions are less acidic than smaller size fractions [e.g., Keene *et al.*, 2004; Keene *et al.*, 2009]. When sampled in bulk, volatile losses may cause negative bias in analyte concentrations. The generally good agreement between slopes for conservative (SO₄²⁻) and non-conservative species (NO₃⁻ and NH₄⁺) associated primarily with sub- μm size fractions and for conservative and non-conservative species (Na⁺ and Cl⁻, respectively) associated primarily with super- μm size fractions indicates that the lower slopes for regressions of summed versus bulk Na⁺ and Cl⁻ are driven primarily by physical rather than chemical processes, as argued above. Unlike the situation in most marine regions, aerosol pH during NACHTT was relatively similar across the aerosol size distribution (discussed in detail below).

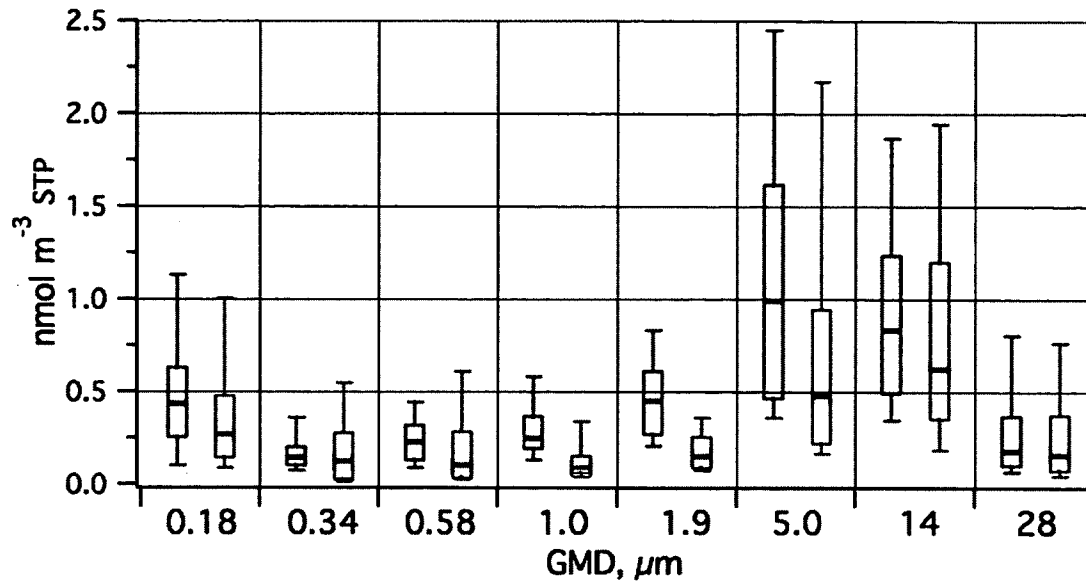


Figure 3a

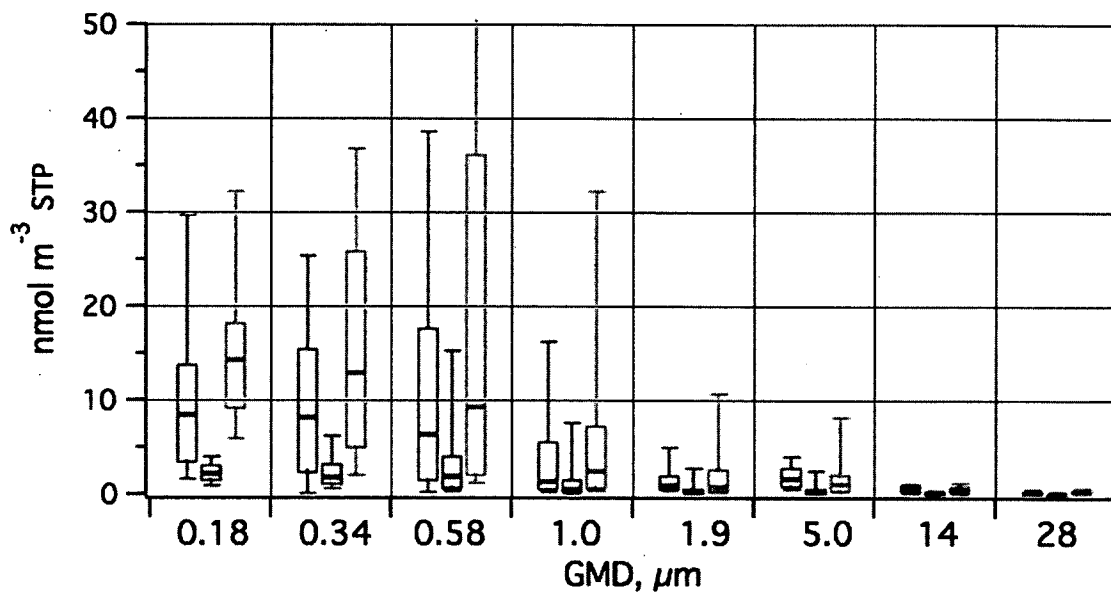


Figure 3b

Figure 3. Box and whisker plots depicting the 10th, 25th, 50th, 75th and 90th percentiles of size-resolved particulate (a) Na⁺ (left box and whisker for each size fraction, black) and Cl⁻ (right box, purple) and (b) NO₃⁻ (left box, blue), SO₄²⁻ (middle box, red), and NH₄⁺ (right box, orange) vs ambient geometric mean diameter (GMD).

4.1.3 Sources and Phase Partitioning of HCl, HNO₃, and NH₃

The production of marine aerosol via wind-waves at the ocean surface is the dominant global source for particulate Cl⁻ in the troposphere; volatilization from primary marine aerosols via acid displacement reactions is the largest global source for HCl [Keene *et al.*, 1999]. Other important sources for total Cl (particulate Cl⁻ + HCl) include emission of particulate Cl⁻ in association with crustal aerosols and emission of HCl during coal combustion, waste incineration, biomass burning, and evaporation of HCl from cooling towers at power plants. [Graedel and Keene, 1995; Keene *et al.*, 1999].

Large-scale atmospheric flow during the NACHTT campaign was predominantly from the west/southwest and transport times over land typically ranged from 2 to more than 5 days (Fig. 1). Although variable, the mean mass weighted lifetime of marine aerosol against deposition is of roughly similar duration (on the order of 1.5 to 2 days [Erickson *et al.*, 1999]). These times coupled with evidence for production via a mechanical process (discussed above) suggests that the long distance transport of marine aerosol from the eastern North Pacific Ocean may have contributed to particulate Cl⁻ (and its HCl displacement product) measured during the campaign. Observations of playa salts at altitude over Wyoming during November, 2007 [Pratt *et al.*, 2010] suggest that additional contributions from land surface sources may have been possible. Much of the land surface of the Great Basin is characterized by saline endorheic lakes (e.g., Great Salt Lake), playas (also known as dry lakes; e.g., Reynolds *et al.*, [2007]), and remnant deposits from pluvial lakes (e.g., Bonneville Salt Flats; e.g., Currey [1990]). A proximate source from road salt is also plausible, although only trace snowfalls occurred during the campaign and no active salting was observed to occur nearby. Sources of particulate Cl⁻

and Na^+ during NACHTT are discussed further by *Pszenny et al.* [manuscript in preparation].

In polluted regions, the combustion of fossil fuels and biomass is the dominant source for tropospheric NO_x , which is the primary precursor for HNO_3 and particulate NO_3^- . Direct emissions of NH_3 from agricultural activities (including animal waste and fertilized soils) and biomass burning are the primary sources for NH_3 and particulate NH_4^+ ; direct emissions of NH_3 from vegetation are also important during summer [Bouwman *et al.*, 1997]. NH_3 emissions from non-combustion sources are temperature dependent and thus vary seasonally and typically peak during daytime [Gilliland *et al.*, 2003].

Near-surface measurements of HCl [Graedel and Keene, 1995; Keene *et al.*, 2007; and references therein], HNO_3 [Fischer *et al.*, 2006], and NH_3 [Smith *et al.*, 2007] in polluted regions often reveal higher mixing ratios during daytime. The diel cycles and associated covariability in HCl and HNO_3 (e.g., Fig. 2 d and e) were driven in part by photochemical production of atmospheric acids during daytime that increased acidification of the multiphase system and drove HCl and HNO_3 phase partitioning towards the gas phase. The diel cycle in NH_3 during some intervals (Fig. 2f) was probably driven in part by the temperature dependence of proximate emissions sources. In addition, nocturnal inversions that isolate near-surface air from the deeper mixed layer may contribute to depletion of HCl , HNO_3 , and NH_3 in surface layers via dry deposition at night. Diel variability was not consistent day-to-day, and can depend on a variety of factors such as meteorology, transport, etc. Warming and associated vertical mixing following sunrise contribute to rising mixing ratios in the morning and associated diel

variability measured in near-surface air. During the NACHTT campaign, HCl and HNO₃ partitioned primarily in the particulate phase during most sampling intervals whereas NH₃ partitioning was primarily in the gas phase. HNO₃ mixing ratios were in the range of previous measurements near Boulder [Huey *et al.*, 1998].

4.2 Aerosol pH

All aerosol size fractions were acidic throughout the campaign (Fig. 4) and pHs inferred from HNO₃ and NH₃ partitioning agreed reasonably well, both in terms of absolute values and the overall pattern of increasing pH with increasing particle size (Fig. 5). Paired measurements of HCOOH and CH₃COOH phase partitioning (not shown) revealed particulate concentrations in all size fractions that were near or below analytical detection limits, which is consistent with the expectations based on the phase partitioning of these species with acidic aerosol [Keene and Pszenny, 2004]. The median difference in pHs inferred from HNO₃ and NH₃ was 0.2 pH units across all size fractions. Median pHs inferred from HNO₃ for the two largest size fractions (ambient geometric mean diameters, GMDs, of 28 and 14 μm) were less than those inferred from NH₃ by 0.1 and 0.2 pH units, respectively. The difference in median pHs for GMD 5-μm size fraction based on the two gas-aerosol couples were negligible. Corresponding differences for the smaller size fractions ranged from 0.2 to 0.5 pH unit.

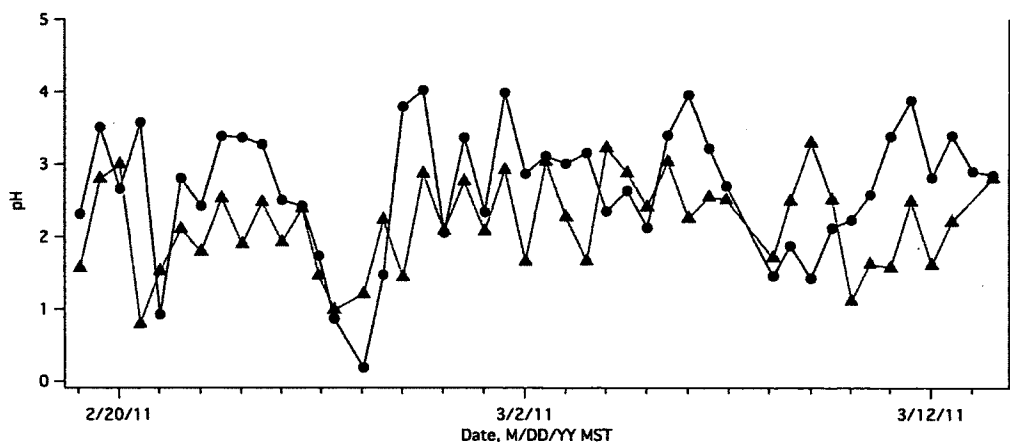


Figure 4. Aerosol pH based on HNO₃ phase partitioning in GMD 14 μm (black circles) and 0.58 μm (blue triangles).

The good agreement between pHs inferred from HNO₃ and NH₃ partitioning suggests that these results are reasonably representative and, thereby, provide useful context for evaluating pHs inferred from HCl partitioning over the range of reported Henry's Law constants. pHs based on the HCl K_H from *Marsh and McElroy* [1985] are systematically higher than those inferred from HNO₃ and NH₃ (Fig. 5). The applicable temperature range for the HCl K_H from *Marsh and McElroy* [1985] is 0° ≤ T ≤ 50° C, and average temperatures during the majority of impactor sampling intervals fell within this range. The pH calculations based on HCl display a similar overall trend in pH across all size fractions, with a small decrease from 0.18 μm to 0.34 μm and then an increase in pH from 0.34 to 14 μm, with a small decrease in the highest size fraction. However, as opposed to the difference in pH based on HNO₃ and NH₃ partitioning, the values based on HCl showed larger divergence in medians for the two largest size fractions (a difference of 1.7 to 1.9 pH units).

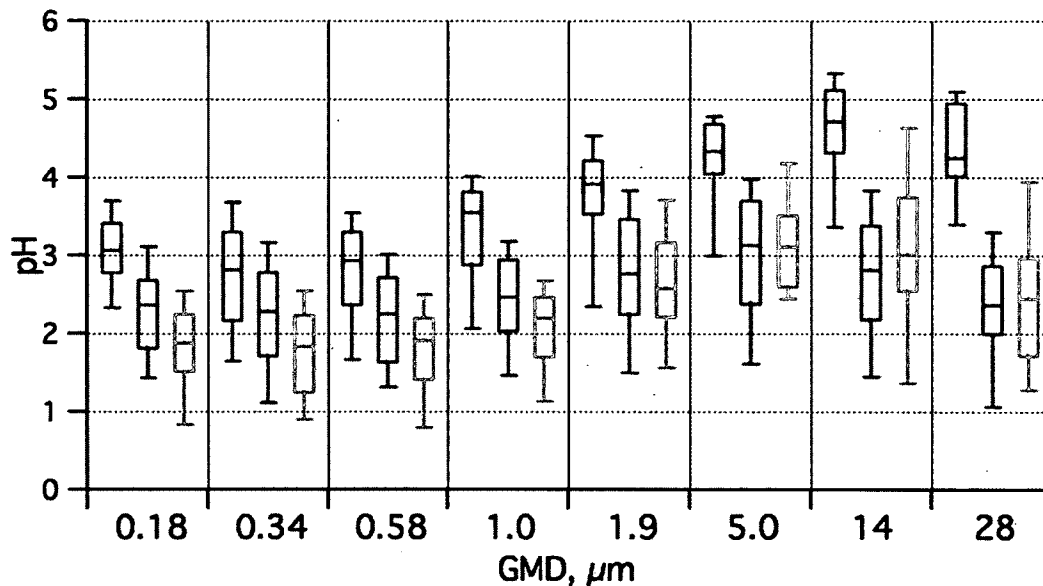


Figure 5. Box and whisker plots depicting the 10th, 25th, 50th, 75th and 90th percentiles of size-resolved aerosol pH based on HNO₃ (middle box and whisker for each size fraction, blue), NH₃ (right box and whisker, orange), and HCl (HCl K_H based on *Marsh and McElroy* [1985]) (left box and whisker, purple) vs ambient geometric mean diameter (GMD).

4.3 Sensitivity Calculations

The sensitivities of pHs inferred from the partition of HCl, HNO₃, and NH₃ to variability in major input parameters were evaluated as described in Chapter 3 with the results presented here. The parameters tested include: temperature, RH, concentrations of particulate-phase ions, approach for forcing ion balance (as described previously), and mixing ratios of gases. While it is not possible to unequivocally evaluate influences of changes in phase state (e.g., possible efflorescence at low RHs), the fact that systematic divergence in pHs based on the partitioning of HCl versus HNO₃ and NH₃ was evident for all size fractions over the entire range in RH implies that variability in phase state is probably not the primary explanation for these differences. Results were calculated for

four individual samples, two representing both high-RH conditions (86% and 78% RH) that were evaluated using E-AIM Model IV and two representing low-RH conditions (16% and 27%) that were evaluated using both E-AIM Model II and Model IV. The following summarizes results based on all three gas-aerosol couples. Relative variability in pH over the range of sensitivity evaluations represents the combined responses for all three sets of calculations.

Temperature influences activity coefficients, aerosol LWC, and density that were modeled by E-AIM as well as the Henry's Law and dissociation constants. To assess the potential influence of temperature variation on calculated pHs, the temperatures used in the calculations were increased and decreased by 25% relative to the average temperature over the sampling interval. pHs inferred over this temperature range generally varied by less than 0.25 pH unit. Higher temperature increased and lower temperature decreased the calculated pH.

RH impacts modeled aerosol LWC, particle density, and activity coefficients, and was similarly varied over a range of $\pm 25\%$ over each sampling interval, up to 100% RH. The relationship between RH and aerosol pH was in contrast to that for temperature; an increase in RH yielded lower solution pH. Similar relationships were reported by *von Glasow and Sander [2001]*. Briefly, the shift in equilibrium dissolution of HCl in aerosol liquid water with increasing RH exceeds the corresponding dilution factor and, consequently, for a given set of conditions, aerosol pH decreases with increasing RH. Relative to those at low RH, the pH of aerosols at higher RH were more sensitive to variability in RH. For the higher RH samples, $\pm 25\%$ variability resulted in pH changes of 1 to 2 units whereas, in the lower RH samples, a similar variability in RH yielded

changes of pH of only about 0.2 unit.

Particulate-phase concentrations of each analyte were adjusted individually by $\pm 25\%$ of the measured value and the E-AIM calculations were re-run for each sample and each analyte adjustment. The resulting changes in calculated pH were less than 0.6 pH unit with the largest difference associated with the smallest aerosol size fractions. pHs for the low-RH samples were relatively more sensitive to variability in ionic composition; pHs for the high-RH samples varied by less than 0.1 pH unit.

Forcing ion balance impacts both aerosol LWC and the calculated activity coefficients. To test the sensitivity of the pH approach to ion balancing, cation deficits were adjusted by increasing NH_4^+ rather than H^+ and anion deficits were adjusted by increasing only the anion present at the highest concentration rather than all anions in proportion to their relative concentrations. For most samples, NO_3^- was the anion present at the highest concentration. For the high-RH samples, pH was insensitive (difference of less than 0.15 unit across the full size distribution) to the ion-balancing approach but, for the low-RH samples, results were relatively more sensitive. Differences for sub- μm size fractions varied from negligible to 1.2 pH units. For size fractions greater than GMD 1.8 μm , which contained relatively little NH_4^+ and NO_3^- , differences ranged from 0.05 to 2.4 pH units.

Finally, pH was inferred from the maximum and minimum mixing ratio for the three gases measured over the corresponding aerosol sampling interval. The greatest change in aerosol pH was 0.6 pH unit.

The above results suggest that analytical errors, variability in the major analytes

and meteorological conditions over sampling intervals, and the ion balancing approach corresponded to relatively minor sources of systematic error in estimating aerosol pH based on this approach due to the larger effect on calculated aerosol pH that can occur by employing other reported values of Henry's Law for HCl. Therefore it is likely that the large uncertainty associated with the Henry's Law constant for HCl was probably the primary factor contributing to differences in pHs inferred from the measured phase partitioning of HCl, HNO₃, and NH₃. Specifically, these results suggest that the Henry's Law constant for HCl that was used in the calculations (Table 1) may be too low as the differences in calculated pH based on the reported values of K_H for HCl varied more widely than the above-discussed sensitivities. Results from varying the Henry's Law value for HCl (not shown) suggest that increasing the Henry's Law constant for HCl (Table 1, $K_H^o = 1.1 \times 10^0$) by roughly two orders of magnitude would bring the calculated aerosol pH based on HCl to within the range calculated using the HNO₃ and NH₃ couples.

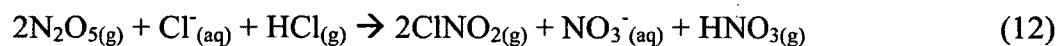
4.4 Implications

The above results have important implications for our understanding of Cl radical chemistry and related implications in continental air. Concentrations of particulate Cl⁻ measured during previous investigations were insufficient to sustain the production of ClNO₂ inferred from measured mixing ratios [e.g., *Osthoff et al.*, 2008; *Thornton et al.*, 2010], suggesting that particulate Cl⁻ consumed via reaction 4 is replenished. However, those measurements did not include 'refractory' molecular forms such as NaCl and also did not quantify aerosol size fractions greater than ~1 μm ambient diameter.

Consequently, particulate Cl^- concentrations limited to the sub- μm size range represent lower limits. During NACHTT, most particulate Cl^- was associated with super- μm size fractions and Na^+ and Cl^- were highly correlated suggesting that most Cl^- was associated with refractory salt (Fig. 3a).

In addition, HCl was not measured during previous experiments. Because HCl partitions with aerosols based on Henry's Law, losses of particulate Cl^- (due to ClNO_2 production) from particles that were previously in thermodynamic equilibrium with HCl vapor would undersaturate the aerosol and thereby drive HCl condensation. Sub- μm aerosol size fractions equilibrate rapidly (on the order of seconds to minutes) with the gas phase [Meng and Seinfeld, 1996] and, consequently, HCl vapor would serve as an effective reservoir for particulate Cl^- under these conditions.

Like HCl, HNO_3 and NO_3^- produced via reactions 3 and 4 subsequently partition between the vapor and aqueous phases based on Henry's Law and acid dissociation constants, LWC, and solution pH [Keene et al., 2004]. At night, the net result of the various multiphase pathways involved in ClNO_2 production that can be expressed as:

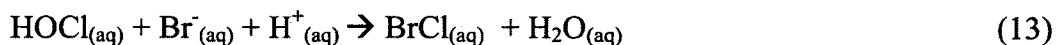


Because it regulates the equilibrium phase partitioning of HCl, solution pH is a key variable controlling the production of ClNO_2 via reaction 4 relative to HNO_3 via reaction 3. HCl, HNO_3 , and NH_3 are the major atmospheric constituents that partition significantly between the gas phase and acidic aerosols as a function of pH. During the NACHTT campaign, total Cl was generally found to be in excess of ClNO_2 (Fig. 2d), which implies that the availability of Cl^- did not limit the production of ClNO_2 under the conditions

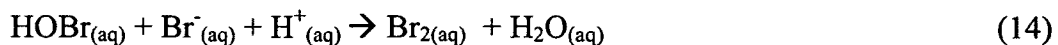
observed during the campaign.

The primary sources for total Cl in central Colorado during winter are uncertain. Given the predominant westerly flow and relatively short (few days) transport times (Fig. 1), the long distance transport of marine and/or soil-derived aerosols and associated reaction products from the west and southwest may represent a significant regional source for total Cl. In addition, available but limited measurements of HCl in polluted continental air [e.g., *Graedel and Keene, 1995*] indicate that non-marine sources (both primary and secondary), including fossil-fuel and biomass combustion, and industrial emissions [*Keene et al., 1999* and references therein], sustain mixing ratios typically ranging from 100 to 1000 pmol mol⁻¹. During NACHTT, high concentrations of HCl in association with other tracers of combustion were observed in discrete plumes that appeared to emanate from nearby power plants suggesting that fossil-fuel combustion was probably a significant regional source.

In addition to the Cl radical production and cycling pathways summarized above, the potential role of reactive bromine should also be considered. If sufficient Br⁻ is present, model calculations [e.g., *Keene et al., 2009*] indicate the following multiphase activation pathways may also be important:



and



HOBr in reaction 14 would be produced via pathways analogous to those for HOCl (5 through 7). Product BrCl, and Br₂ subsequently volatilize and, during daytime, photolyze yielding additional atomic Cl and atomic Br. Like reaction 11, these reactions proceed in

both the light and dark and would enhance halogen activation at night and sustain halogen-radical chemistry for longer periods during daytime relative to predictions based on the photolysis of ClNO₂ and the assumption that all atomic Cl reacts with hydrocarbons. Concentrations of particulate Br⁻ associated with bulk aerosol sampled during NACHTT varied from less than 0.02 to 0.06 nmol m⁻³. Br⁻ was present at concentrations above detection limits in only 27% of samples. This concentration range overlaps the lower portions of those reported for marine regions [*Sander et al.*, 2003; *Keene et al.*, 2009] and, although volatile Br species were not quantified during the campaign, implies that Br chemistry may have been occurring. In this regard, it is important to note that volatile inorganic Br has a longer atmospheric lifetime against deposition relative to the parent aerosol [e.g., *Keene et al.*, 2009], which suggests more efficient transport from marine regions relative to particles. Inorganic Br is also emitted over continents during biomass burning and from various industrial sources [*Sander et al.*, 2003]. To more fully evaluate the nature and potential importance of halogen radical chemistry in continental regions, it is recommended that volatile inorganic and particulate Br be measured during future field investigations of these processes. Within the context of the NACHTT campaign, a forthcoming manuscript will more fully evaluate the specific impacts of the Cl multiphase processing on tropospheric oxidation [*Kim et al.*, manuscript in preparation].

CHAPTER 5

Summary and Conclusions

Multiphase processing of reactive halogens impacts important, interrelated chemical processes in Earth's troposphere. During winter 2011, major water soluble trace gases (HCl, HNO₃, NH₃, HONO, HCOOH, and CH₃COOH), the ionic composition of size-resolved aerosols over the full relevant size distribution (ambient GMD from 0.18 to 28 μm), the ionic composition of bulk aerosol, and associated physical conditions in the continental troposphere were measured from the Boulder Atmospheric Observatory in Erie, Colorado. Aerosol acidities were inferred from the measured phase partitioning and associated thermodynamic properties of major analytes with pH-dependent solubilities (HCl, HNO₃, and NH₃). Cl⁻ and Na⁺ were associated primarily with super-μm diameter aerosol size fractions whereas NO₃⁻, SO₄²⁻, and NH₄⁺ were associated primarily with sub-μm size fractions. All aerosol size fractions were acidic throughout the campaign. pHs inferred from HNO₃ and NH₃ partitioning (most in the 2s and 3s) agreed reasonably well, both in terms of absolute values and the overall pattern of modest increases in pH with increasing aerosol size. Large uncertainties in the K_H for HCl contributed to systematically higher pHs inferred from HCl phase partitioning (approximately by 1 to 2 units based on median values) relative to HNO₃ and NH₃. Condensation of HCl sustained Cl⁻ in all size fractions thereby preventing the depletion of the particulate Cl⁻ via ClNO₂ production. These results imply that NO_x (the precursor to N₂O₅ formation), and not Cl⁻, was the limiting reagent in ClNO₂ production during this campaign.

LIST OF REFERENCES

- Ackerman, A. S., O. B. Toon, D. E. Stevens, A. J. Heymsfield, V. V. Ramanathan, and E. J. Welton (2000), Reduction of tropical cloudiness by soot, *Science*, *12*, 1042-1047.
- Alexander, B., M. G. Hastings, D. J. Allman, J. Dachs, J. A. Thornton, and S. A. Kunasek (2009), Quantifying atmospheric nitrate formation pathways based on a global model of the oxygen isotopic composition ($\Delta^{17}\text{O}$) of atmospheric nitrate, *Atmos. Chem. Phys.*, *9*, 5043-5046.
- Alicke, B., K. Hebestreit, J. Stutz, and U. Platt (1999), Iodine oxide in the marine boundary layer, *Nature*, *397*, 572-573.
- Bandura, A. V., and S. N. Lvov (2006), The ionization constant of water over wide ranges of temperature and density, *J. Phys. Chem. Ref. Data*, *35*, 15-30.
- Behnke, W., C. George, V. Scheer, and C. Zetzsch (1997), Production and decay of ClNO_2 from the reaction of gaseous N_2O_5 with NaCl solution: Bulk and aerosol experiments, *J. Geophys. Res.*, *102*, 3795-3804.
- Bouwman, A. F., D. S. Lee, A. H. Asman, F. J. Dentener, K. W. Van Der Hoek, and J. G. J. Oliver (1997), A global high resolution emission inventory for ammonia, *Global Biogeochem. Cycles*, *11*, 561-587.
- Brown, S., et al. (2012), Nitrogen, Aerosol Composition and Halogens on a Tall Tower: An overview of wintertime air chemistry measurements in Colorado's Front Range urban corridor, *J. Geophys. Res.*, manuscript in preparation.
- Chameides, W. L. (1984) The photochemistry of a remote stratiform cloud, *J. Geophys. Res.*, *89*, 4739-4755.
- Clegg, S. L. and P. Brimblecombe (1989), Solubility of ammonia in pure aqueous and multicomponent solutions, *J. Phys. Chem.*, *93*, 7237-7238.
- Crutzen, P.J. and M. O. Andreae (1990), Biomass burning in the tropics: impact on atmospheric chemistry and biogeochemical cycles, *Science*, *250*, 1669-1678.
- Currey, D. R. (1990), Quaternary palaeolakes in the evolution of semidesert basins, with special emphasis on Lake Bonneville and the Great Basin, U.S.A, *Palaeogeogr., Palaeoclim., Palaeoecol.*, *76* (3-4), 189-214, doi: 10.1016/0031-0182(90)90113-L.
- Draxler, R. R. and G. D. Rolph, 2012. HYSPLIT (HYbrid Single-Particle Lagrangian Integrated Trajectory) Model access via NOAA ARL READY Website (<http://ready.arl.noaa.gov/HYSPLIT.php>). NOAA Air Resources Laboratory, Silver Spring, MD.

- Engelhart, G. J., L. Hildebrandt, E. Kostenidou, N. Mihalopoulos, N. M. Donahue, and S. N. Pandis (2011), Water content of aged aerosol, *Atmos. Chem. Phys.*, *11*, 911-920.
- Erickson, D. J., C. Seuzaret, W. C. Keene, and S. L. Gong (1999), A general circulation model based calculation of HCl and ClNO₂ production from sea salt dechlorination: Reactive Chlorine Emissions Inventory, *J. Geophys. Res.*, *104*, 8347-8372.
- Finlayson-Pitts, B. J., M. J. Ezell, and J. N. Pitts (1989), Formation of chemically active chlorine compounds by reactions of atmospheric NaCl particles with gaseous N₂O₅ and ClONO₂, *Nature* *337*, 241-244.
- Finley, B. D., and E. S. Saltzman (2006), Measurement of Cl₂ in coastal urban air, *Geophys. Res. Lett.*, *33*, L11809, doi:10.1029/2006GL025799.
- Fischer, E., A. Pszenny, W. Keene, J. Maben, A. Smith, A. Stohl, and R. Talbot (2006), Nitric acid phase partitioning and cycling in the New England coastal atmosphere, *J. Geophys. Res.*, *111*, D23S09, doi:10.1029/2006JD007328.
- Forster, P., V. Ramaswamy, P. Artaxo, T. Berntsen, R. Betts, D. W. Fahey, J. Haywood, J. Lean, D. C. Lowe, G. Myhre, J. Nganga, R. Prinn, G. Raga, M. Schulz and R. Van Dorland, 2007: Changes in Atmospheric Constituents and in Radiative Forcing. In: *Climate Change 2007: The Physical Science Basis. Contribution of Working Group I to the Fourth Assessment Report of the Intergovernmental Panel on Climate Change* [Solomon, S., D. Qin, M. Manning, Z. Chen, M. Marquis, K.B. Averyt, M. Tignor and H.L. Miller (eds.)]. Cambridge University Press, Cambridge, United Kingdom and New York, NY, USA.
- Foster, K. L., R. A. Plastridge, J. W., Bottenheim, P. B. Shepson, B. J., Finlayson-Pitts, and C. W. Spicer (2001), The role of Br₂ and BrCl in surface ozone destruction at polar sunrise, *Science*, *291*, 471-474.
- Friese, E. and A. Ebel (2010) Temperature dependent thermodynamic model of the system H⁺ - NH₄⁺ - Na⁺ - SO₄²⁻ - NO₃⁻ - Cl⁻ - H₂O. *J. Phys. Chem. A*, *114*, 11595-11631.
- Gilliland, A. B., R. L. Dennis, S. J. Roselle, and T. E. Pierce (2003), Seasonal NH₃ emission estimates for the eastern United States based on ammonium wet concentrations and an inverse modeling method, *J. Geophys. Res.*, *108*, 4477-4488, doi:10.1029/2002JD003063.
- Graedel, T. E., and W. C. Keene (1995), The tropospheric budget of reactive chlorine, *Global Biogeochem. Cycles*, *9*, 47-78.
- Gwynn, R. C., R. T. Burnett, and G. D. Thurston (2000), A time-series analysis of acidic particulate matter and daily mortality and morbidity in the Buffalo, New York, region, *Environ. Health Perspect.*, *108*, 125-133.

- Huey, G. L., E. J. Dunlea, E. R. Lovejoy, D. R. Hanson, R. B. Norton, F. C. Fehsenfeld, and C. J. Howard (1998), Fast time response measurements of HNO₃ in air with a chemical ionization mass spectrometer, *J. Geophys. Res.*, *103*, 3355-3360.
- Keene, W. C., and A. A. P. Pszenny (2004), Comment on “Reactions at interfaces as a source of sulfate formation in sea-salt particles,” by A. Laskin, D. J. Gaspar, W. Wang, S. W. Hunt, J. P. Cowin, S. D. Colson, and B. J. Finlayson-Pitts, *Science*, *303*, 628.
- Keene, W. C., and D. L. Savoie (1998), The pH of deliquesced sea-salt aerosol in polluted marine air, *Geophys. Res. Lett.*, *25*, 2181-2184.
- Keene, W. C., and D. L. Savoie (1999), Correction to “The pH of deliquesced sea-salt aerosol in polluted marine air”, *Geophys. Res. Lett.*, *26*(9), 1315–1316, doi:10.1029/1999GL900221.
- Keene, W. C., R. W. Talbot, M. O. Andreae, K. Beecher, H. Berresheim, M. Castro, J. C. Farmer, J. N. Galloway, M. R. Hoffman, S.-M. Li, J. R. Maben, J. W. Munger, R. B. Norton, A. A. P. Pszenny, H. Puxbaum, H. Westberg, and W. Winiwarter (1989), An intercomparison of measurement systems for vapor- and particulate-phase concentrations of formic and acetic acids, *J. Geophys. Res.*, *94*, 6457-6471.
- Keene, W. C., J. R. Maben, A. A. P. Pszenny, and J. N. Galloway (1993), Measurement technique for inorganic chlorine gases in the marine boundary layer, *Environ. Sci. Technol.*, *27*, 866–874.
- Keene, W. C., R. Sander, A. A. P. Pszenny, R. Vogt, P. J. Crutzen, and J. N. Galloway (1998), Aerosol pH in the marine boundary layer: A review and model evaluation, *J. Aerosol Sci.*, *29*, 339–356.
- Keene, W. C., M. A. K. Khalil, D. J. Erickson, A. McCulloch, T. E. Graedel, J. M. Lobert, M. L. Aucott, S. L. Gong, D. B. Harper, G. Kleiman, P. Midgley, R. M. Moore, C. Seuzaret, W. T. Sturges, C. M. Benkovitz, V. Koropalov, L. A. Barrie, Y. F. Li (1999), Composite global emissions of reactive chlorine from anthropogenic and natural sources: Reactive Chlorine Emissions Inventory, *J. Geophys. Res.*, *107*, 8429-8440.
- Keene, W. C., A. A. P. Pszenny, J. R. Maben, and R. Sander (2002), Variation of marine aerosol acidity with particle size, *Geophys. Res. Lett.*, *29*(7), 1101, doi:10.1029/2001GL013881.
- Keene, W. C., A. A. P. Pszenny, J. R. Maben, E. Stevenson, and A. Wall (2004), Closure evaluation of size-resolved aerosol pH in the New England coastal atmosphere during summer, *J. Geophys. Res.*, *109*, D23307, doi:10.1029/2004JD004801.

- Keene, W. C., J. M. Lobert, P. J. Crutzen, J. R. Maben, D. H. Scharffe, T. Landmann, C. Hély, and C. Brain (2006), Emissions of major gaseous and particulate species during experimental burns of southern African biomass, *J. Geophys. Res.*, *111*, D04301, doi:10.1029/2005JD006319.
- Keene, W. C., J. Stutz, A. A. P. Pszenny, J. R. Maben, E. V. Fischer, A. M. Smith, R. von Glasow, S. Pechtl, B. C. Sive, R. K. Varner (2007), Inorganic chlorine and bromine in coastal New England air during summer, *J. Geophys. Res.*, *112*, D10S12, doi:10.1029/2006JD007689.
- Keene, W. C., M. S. Long, A. A. P. Pszenny, R. Sander, J. R. Maben, A. J. Wall, T. L. O'Halloran, A. Kerkweg, E. V. Fischer, and O. Schrems (2009), Latitudinal variation in the multiphase chemical processing of inorganic halogens and related species over the eastern North and South Atlantic Oceans, *Atmos. Chem. Phys.*, *9*, 7361-7385 (<http://www.atmos-chem-phys.net/9/7361/2009/acp-9-7361-2009.html>).
- Kim, S., T. VandenBoer, C. Young, J. Thornton, R. Swarthout, C. Warneke, J. Roberts, A. Guenther, S. Brown (2012), The primary and recycling sources of OH during the NACHTT 2011 Campaign, manuscript in preparation.
- Koren, I., Y. J. Kaufman, L. A. Remer, and J. V. Martins (2004), Measurement of the effect of Amazon smoke on inhibition of cloud formation, *Science*, *303*, 1342-1345.
- Laskin, A., D. J. Gaspar, W. Wang, S. W. Hunt, J. P. Cowin, S. D. Colson, and B. J. Finlayson-Pitts (2003), Reactions at interfaces as a source of sulfate formation in sea-salt particles, *Science*, *301*, 340-344.
- Lawler, M. J., B. D. Finley, W. C. Keene, A. A. P. Pszenny, K. A. Read, R. von Glasow, and E. S. Saltzman (2009), Pollution-enhanced reactive chlorine chemistry in the eastern tropical Atlantic boundary layer, *Geophys. Res. Lett.*, *36*, L08810, doi:10.1029/2008GL036666.
- Liu, B. Y. H., D. Y. H. Pui, X. Q. Wang, and C. W. Lewis (1983), Sampling of carbon fiber aerosols, *Aerosol Sci. Technol.*, *2*, 499-511.
- Ludwig, J., and O. Klemm (1990), Acidity of size-fractionated aerosol particles, *Water Air Soil Pollut.*, *49*, 35-50.
- Marple, V. A., K. L. Rubow, and S. M. Behm (1991), A microorifice uniform deposit impactor (MOUDI): Description, calibration, and use, *Aerosol Sci. Technol.*, *14*, 434-446.
- Marsh, A. R. W., and W. J. McElroy (1985), The dissociation constant and Henry's law constant of HCl in aqueous solution, *Atmos. Environ.*, *19*, 1075 - 1080.

- Matveev, V., M. Peleg, D. Rosen, D. S. Tov-Alper, K. Hebestreit, J. Stutz, U. Platt, D. Blake, and M. Luria (2001), Bromine oxide – ozone interactions over the Dead Sea, *J. Geophys. Res.*, *106*, 10,375-10,387.
- Meng, Z., and J. H. Seinfeld (1996), Time scales to achieve atmospheric gas-aerosol equilibrium for volatile species, *Atmos. Environ.*, *30*, 2889-2900.
- Mielke, L. H., A. Furgeson and H. D. Osthoff (2011) Observation of ClNO₂ in a mid-continental urban environment, *Environ. Sci. Technol.*, *45*, 8889–8896, dx.doi.org/10.1021/es201955u .
- Molina, M. J., and F. S. Rowland (1974), Stratospheric sink for chlorofluoromethanes: Chlorine atom-catalyzed destruction of ozone, *Nature*, *249*, 810-812.
- Munger, J. W., D. J. Jacob, B. C. Daube, L. W. Horowitz, W. C. Keene, and B. G. Heikes (1995), Formaldehyde, glyoxal, and methylglyoxal in air and cloud water at a rural mountain site in central Virginia, *J. Geophys. Res.*, *100*, 9325–9333.
- Osthoff, H. D., J. M. Roberts, A. R. Ravishankara, E. J. Williams, B. M. Lerner, R. Sommariva, T. M. Bates, D. Coffman, P. K. Quinn, J. E. Dibb, H. Stark, J. B. Burkholder, R. K. Talukdar, J. Meagher, F. C. Fehsenfeld, and S. S. Brown (2008), High levels of nitryl chloride in the polluted subtropical marine boundary layer, *Nature Geosci.*, *1*, 324-328, doi:10.1038/ngeo177.
- Pechtl, S., and R. von Glasow (2007), Reactive chlorine in the marine boundary layer in the outflow of polluted continental air: A model study, *Geophys. Res. Lett.*, *34*, L11813, doi:10.1029/2007GL029761.
- Phillips, G. J., M. Tang, J. Thieser, B. Brickwedde, G. Schuster, B. Bohn, J. Lelieveld, and J. N. Crowley (2012), Significant concentrations of nitryl chloride observed in rural continental Europe associated with the influence of sea salt chloride and anthropogenic emissions, *Geophys. Res. Lett.*, doi:10.1029/2012GL051912.
- Platt, U., W. Allan, and D. C. Lowe (2004), Hemispheric average Cl concentrations from ¹³C/¹²C ratios in atmospheric methane, *Atmos. Chem. Phys.*, *4*, 1-7.
- Pratt, K. A., C. H. Twohy, S. M. Murphy, R. C. Moffet, A. J. Heymsfield, C. J. Gaston, P. J. Demott, P. R. Field, T. R. Henn, D. C. Rogers, M. K. Gilles, J. H. Seinfeld, and K. A. Prather (2010), Observation of playa salts as nuclei in orographic wave clouds, *J. Geophys. Res.*, *115*, D15301, doi:10.1029/2009JD013606.
- Pszenny, A. A. P., J. Moldanová, W. C. Keene, R. Sander, J. R. Maben, M. Martinez, P. J. Crutzen, D. Perner, and R. G. Prinn (2004), Halogen cycling and aerosol pH in the Hawaiian marine boundary layer, *Atmos. Chem. Phys.*, *4*, 147–168.

- Pszenny, A. A. P., E. V. Fischer, R. S. Russo, B. C. Sive, and R. K. Varner (2007), Estimates of Cl atom concentrations and hydrocarbon kinetic reactivity in surface air at Appledore Island, Maine (USA), during International Consortium for Atmospheric Research on Transport and Transformation/Chemistry of Halogens at the Isles of Shoals, *J. Geophys. Res.*, *112*, D10S13, doi:10.1029/2006JD007725.
- Pszenny, A. A. P., et al. (2012), Origins of aerosol chlorine during winter over north central Colorado, USA, *J. Geophys. Res.*, manuscript in preparation.
- Read, K. A., A. S. Mahajan, L. J. Carpenter, M. J. Evans, B. V. E. Faria, D. E. Heard, J. R. Hopkins, J. D. Lee, S. J. Moller, A. C. Lewis, L. Mendes, J. B. McQuaid, H. Oetjen, A. Saiz-Lopez, M. J. Pilling, and J. M. C. Plane (2008), Extensive halogen-mediated ozone destruction over the tropical Atlantic Ocean, *Nature*, *453*, 1232-1235.
- Reynolds, R. L., J. C. Yount, M. Reheis, H. Goldstein, P. Chavez, Jr., R. Fulton, J. Whitney, C. Fuller and R. M. Forester (2007), Dust emission from wet and dry playas in the Mojave Desert, USA, *Earth Surf. Process. Landforms*, *32*, 1811–1827 doi: 10.1002/esp.1515.
- Riedel, T. P., T. H. Bertram, T. A. Crisp, E. J. Williams, B. M. Lerner, A. Vlasenko, S.-M. Li, J. Gilman, J. de Gouw, D. M. Bon, N. L. Wagner, S. S. Brown, and J. A. Thornton (2012), Nitryl chloride and molecular chloride in the coastal marine boundary layer, *Environ. Sci. Technol.*, In Press, doi: 10.1021/es204632r.
- Russell, K. M., W. C. Keene, J. R. Maben, J. N. Galloway, and J. L. Moody (2003), Phase-partitioning and dry deposition of atmospheric nitrogen at the mid-Atlantic U.S. coast, *J. Geophys. Res.*, *108*(D21), 4656, doi:10.1029/2003JD003736.
- Sander, R., Y. Rudich, R. von Glasow, and P. J. Crutzen (1999), The role of BrNO₃ in marine tropospheric chemistry: A model study, *Geophys. Res. Lett.*, *26*, 2858–2860.
- Sander, R., W. C. Keene, A. A. P. Pszenny, R. Arimoto, G. P. Ayers, V. Baboukas, J. M. Chainey, P. J. Crutzen, R. A. Duce, G. Hönninger, B. J. Huebert, W. Maenhaut, N. Mihalopoulos, V. C. Turekian, and R. van Dingenen (2003), Inorganic bromine in the marine boundary layer: A critical review, *Atmos. Chem. Phys.*, *3*, 1301-1336.
- Sander, R., P. J. Crutzen, and R. von Glasow (2004), Comment on “Reactions at interfaces as a source of sulfate formation in sea-salt particles,” by A. Laskin, D. J. Gaspar, W. Wang, S. W. Hunt, J. P. Cowin, S. D. Colson, and B. J. Finlayson-Pitts, *Science*, *303*, 628.

- Sander, S. P., J. Abbatt, J. R. Barker, J. B. Burkholder, R. R. Friedl, D. M. Golden, R. E. Huie, C. E. Kolb, M. J. Kurylo, G. K. Moortgat, V. L. Orkin and P. H. Wine. "Chemical Kinetics and Photochemical Data for Use in Atmospheric Studies, Evaluation No. 17," JPL Publication 10-6, Jet Propulsion Laboratory, Pasadena, 2011 <http://jpldataeval.jpl.nasa.gov>.
- Schwartz, S. E., and W. H. White (1981), Solubility equilibria of the nitrogen oxides and oxyacids in dilute aqueous solution, in: *Advances in Environmental Science and Engineering*, edited by J. R. Pfafflin and E. N. Ziegler, vol. 4, pp. 1–45, Gordon and Breach Science Publishers, NY.
- Seinfeld, J. H., and Pandis, S. N. (1998), *Atmospheric Chemistry and Physics: From Air Pollution to Climate Change*, 1st edition, J. Wiley, New York.
- Simpson, W. R., R. von Glasow, K. Riedel, P. Anderson, P. Ariya, J. Bottenheim, J. Burrows, L. J. Carpenter, U. Frieß, M. E. Goodsite, D. Heard, M. Hutterli, H.-W. Jacobi, L. Kaleschke, B. Neff, J. Plane, U. Platt, A. Richter, H. Roscoe, R. Sander, P. Shepson, J. Sodeau, A. Steffen, T. Wagner, and E. Wolff (2007), Halogens and their role in polar boundary-layer ozone depletion, *Atmos. Chem. Phys.*, 7, 4375-4418, 2007.
- Smith, A. M., W. C. Keene, J. R. Maben, A. A. P. Pszenny, E. Fischer, and A. Stohl (2007), Ammonia sources, transport, transformation, and deposition in coastal New England during summer, *J. Geophys. Res.*, 112, D10S08, doi:10.1029/2006JD007574.
- Tanner, R. L., and R. M. Harrison (1992), Acid-base equilibria of aerosols and gases in the atmosphere, in *Environmental Particles, Environ. Anal. Phys. Chem. Ser.*, vol. 1, edited by J. Buffle and H. P. van Leeuwen, pp. 75–106, Lewis, Boca Raton, Fla.
- Thornton, J. A., J. P. Kercher, T. P. Riedel, N. L. Wagner, J. Cozic, J. S. Halloway, W. P. Dubé, G. M. Wolfe, P. K. Quinn, A. M. Middlebrook, B. Alexander, and S. S. Brown (2010), A large atomic chlorine source inferred from mid-continental reaction nitrogen chemistry, *Nature*, 464, 271-274, doi:10.1038/nature08905.
- Twomey, S. (1977), The Influence of pollution on the shortwave albedo of clouds, *J. Atmos. Sci.*, 34, 1149-1152, doi: 10.1175/1520-0469(1977)034<1149:TIOPOT>2.0.CO;2
- Uematsu, M., R. A. Duce, J. M. Prospero, L. Chen, J. T. Merrill and R. L. McDonald (1983), Transport of mineral aerosol from Asia over the North Pacific Ocean, *J. Geophys. Res.*, 88(C9), 5343-5352.
- von Glasow, R. (2010), Wider role of airborne chlorine, *Nature*, 464, 168-169.
- von Glasow, R., and R. Sander, Variation of sea salt aerosol pH with relative humidity (2001), *Geophys. Res. Lett.*, 28, 247-250.

- von Glasow, R., R. Sander, A. Bott, and P. J. Crutzen (2002a), Modeling halogen chemistry in the marine boundary layer. 1. Cloud-free MBL, *J. Geophys. Res.*, *107*, 4341, doi:10.1029/2001JD000942.
- von Glasow, R., R. Sander, A. Bott, A., and P. J. Crutzen (2002b), Modeling halogen chemistry in the marine boundary layer. 2. Interactions with sulfur and cloud-covered MBL, *J. Geophys. Res.*, *107*, 4323, doi:10.1029/2001JD000943.
- Wennberg, P. O., R. C. Cohen, R. M. Stimpfle, J. P. Koplow, J. G. Anderson, R. J. Salawitch, D. W. Fahey, E. L. Woodbridge, E. R. Keim, R. S. Gao, C. R. Webster, R. D. May, D. W. Toohey, L. M. Avallone, M. H. Proffitt, M. Loewenstein, J. R. Podolske, K. R. Chan, and S. C. Wofsy (1994), Removal of stratospheric O₃ by radicals: In situ measurements of OH, HO₂, NO, NO₂, ClO, and BrO, *Science*, *266*, 398-404.
- Zhou, X., Y. He, H. Huang, T. D. Thorberry, M. A. Carroll, and S. B. Bertman (2002), Photochemical production of nitrous acid on glass sample manifold surface, *Geophys. Res. Lett.*, *29*, 1681, doi: 10.1029/2002GL015080

Appendices

Appendix I

Impactor Sample Start and End Times

SampNo	Day/Night	Start Date MM/DD/YYYY local	Start Time HH:MM local	Stop Date MM/DD/YYYY local	Stop Time HH:MM local
2	N	02/18/2011	18:05	02/19/2011	06:48
3	D	02/19/2011	07:21	02/19/2011	17:41
4	N	02/19/2011	17:57	02/20/2011	06:47
5	D	02/20/2011	07:00	02/20/2011	17:42
6	N	02/20/2011	18:08	02/21/2011	06:45
7	D	02/21/2011	07:02	02/21/2011	17:43
8	N	02/21/2011	18:00	02/22/2011	06:43
10	D	02/22/2011	06:55	02/22/2011	17:44
11	N	02/22/2011	18:06	02/23/2011	06:42
12	D	02/23/2011	06:59	02/23/2011	17:45
13	N	02/23/2011	18:02	02/24/2011	06:42
14	D	02/24/2011	06:53	02/24/2011	17:46
15	N	02/24/2011	18:00	02/25/2011	02:50
16	D	02/25/2011	07:00	02/25/2011	07:32
18	N	02/25/2011	18:18	02/26/2011	06:38
19	D	02/26/2011	06:58	02/26/2011	17:49
20	N	02/26/2011	18:10	02/27/2011	06:36
21	D	02/27/2011	06:49	02/27/2011	17:50
22	N	02/27/2011	18:06	02/28/2011	06:36
23	D	02/28/2011	06:48	02/28/2011	17:51
24	N	02/28/2011	18:04	03/01/2011	06:33
25	D	03/01/2011	06:45	03/01/2011	17:53
26	N	03/01/2011	18:06	03/02/2011	06:32
27	D	03/02/2011	06:43	03/02/2011	17:53
28	N	03/02/2011	18:09	03/03/2011	06:30
29	D	03/03/2011	06:42	03/03/2011	17:54
30	N	03/03/2011	18:06	03/04/2011	06:30
32	D	03/04/2011	06:43	03/04/2011	17:55
33	N	03/04/2011	18:09	03/05/2011	06:26
34	D	03/05/2011	06:37	03/05/2011	17:56
35	N	03/05/2011	18:09	03/06/2011	06:26
36	D	03/06/2011	06:38	03/06/2011	17:57
38	N	03/06/2011	18:08	03/07/2011	03:17

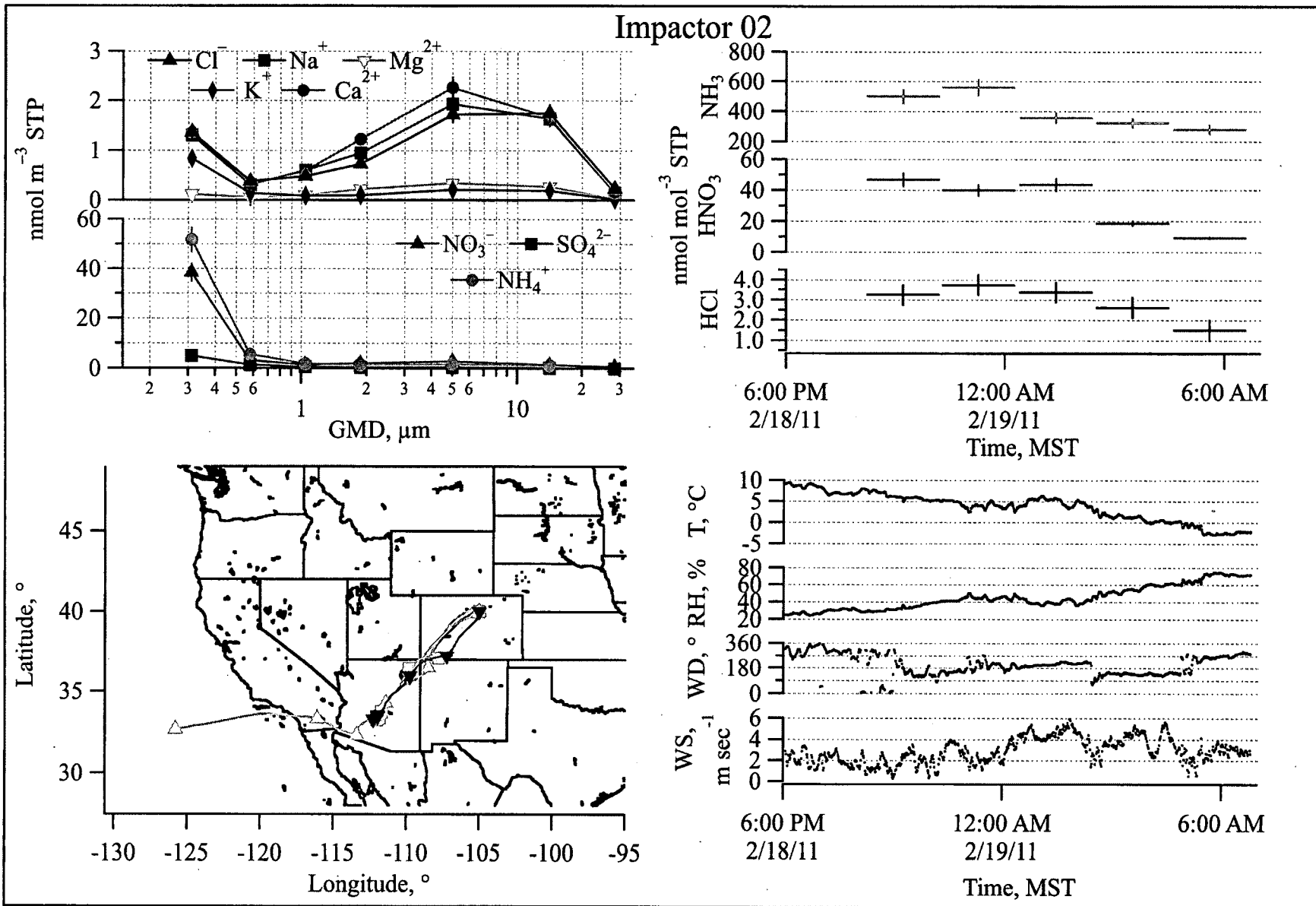
Impactor Sample Start and End Times (cont.)

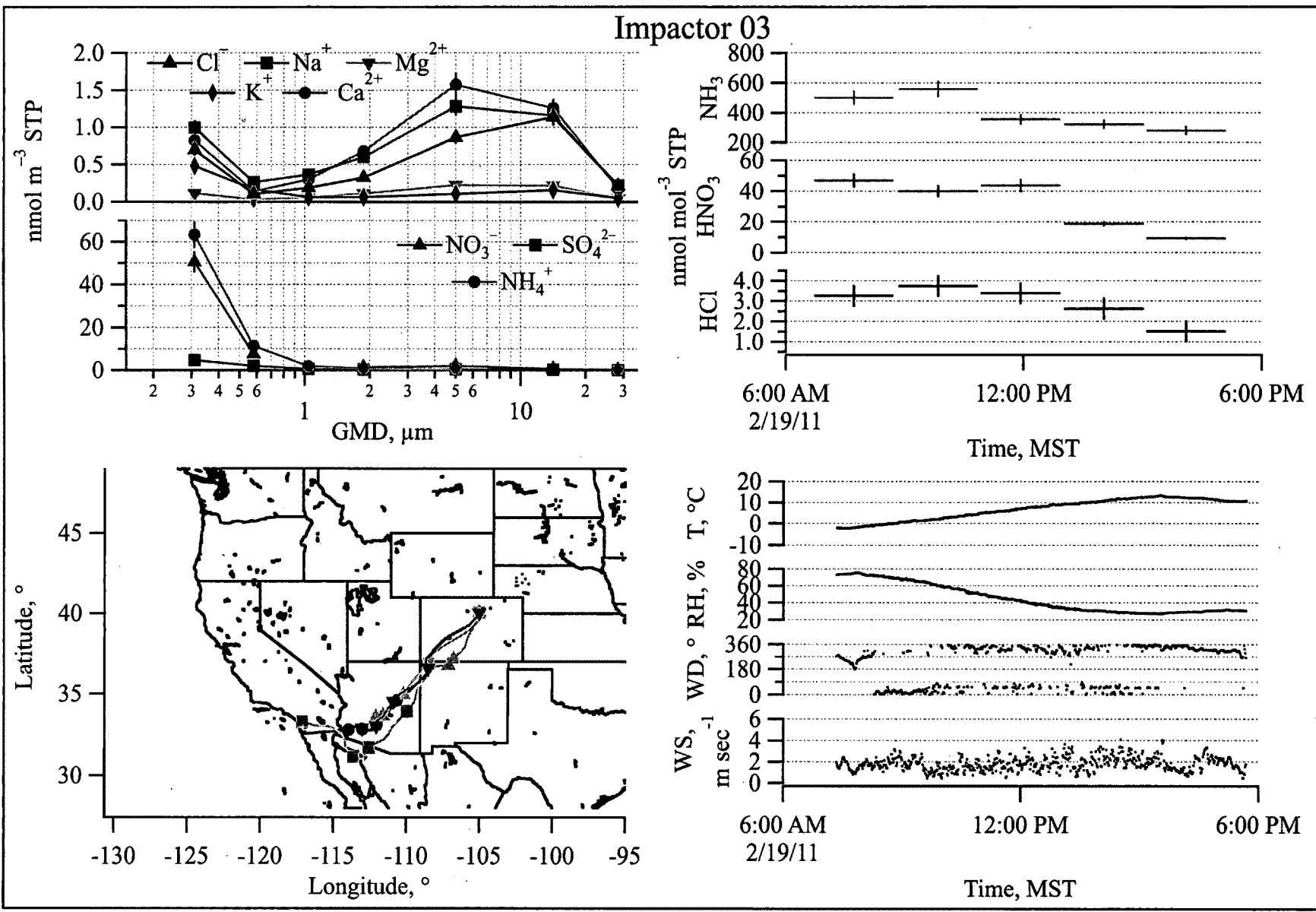
SampNo	Day/Night	Start Date MM/DD/YYYY local	Start Time HH:MM local	Stop Date MM/DD/YYYY local	Stop Time HH:MM local
39	N	03/08/2011	01:10	03/08/2011	03:17
40	D	03/08/2011	06:34	03/08/2011	17:59
41	N	03/08/2011	18:13	03/09/2011	06:21
42	D	03/09/2011	06:32	03/09/2011	18:00
43	N	03/09/2011	18:13	03/10/2011	06:20
44	D	03/10/2011	06:31	03/10/2011	18:01
45	N	03/10/2011	18:14	03/11/2011	06:18
46	D	03/11/2011	06:30	03/11/2011	18:03
48	N	03/11/2011	18:13	03/12/2011	06:17
49	D	03/12/2011	06:27	03/12/2011	18:04
50	N	03/12/2011	18:14	03/13/2011	06:15
52	D	03/13/2011	06:27	03/13/2011	18:05

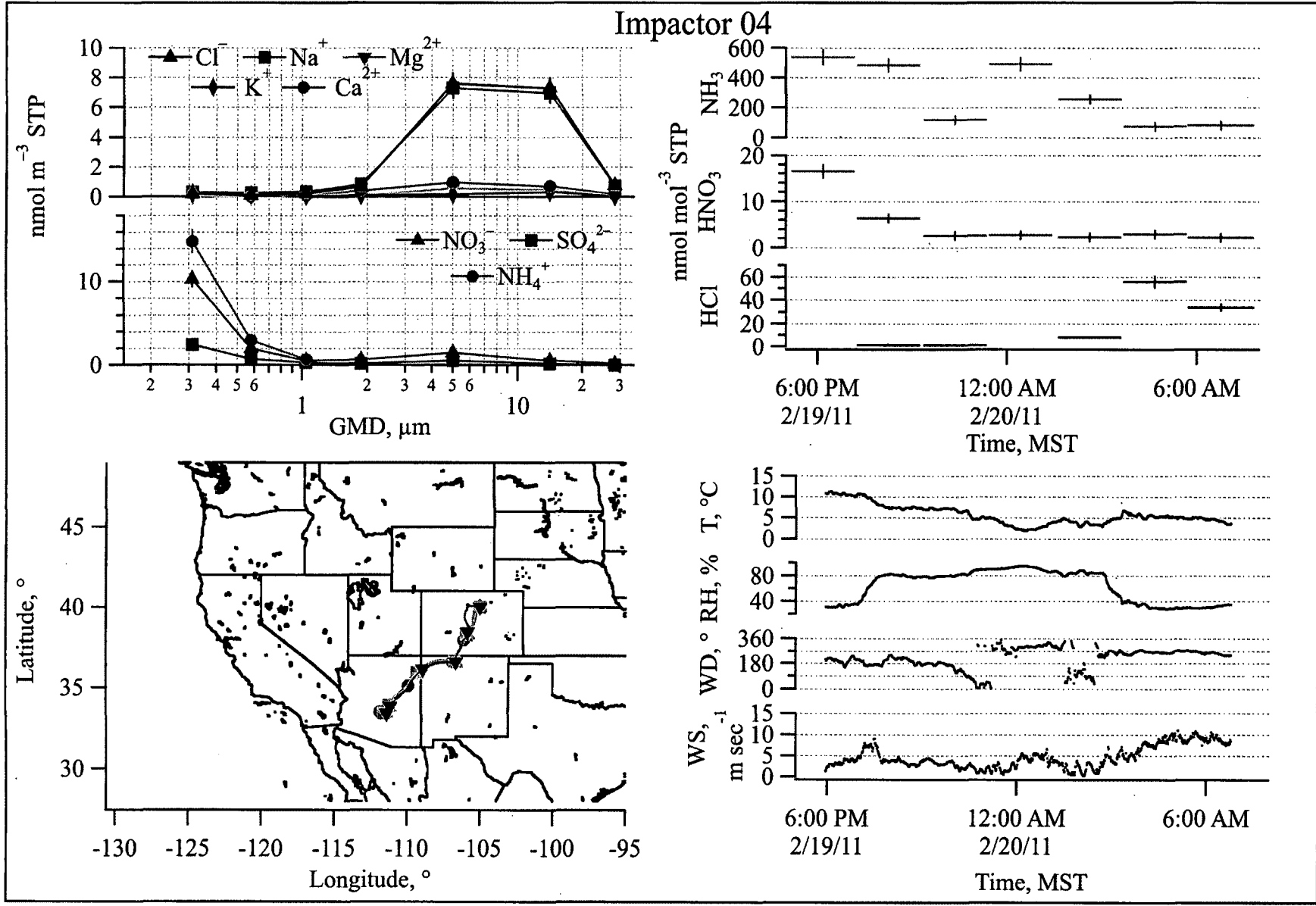
Appendix II

Impactor Sample Data

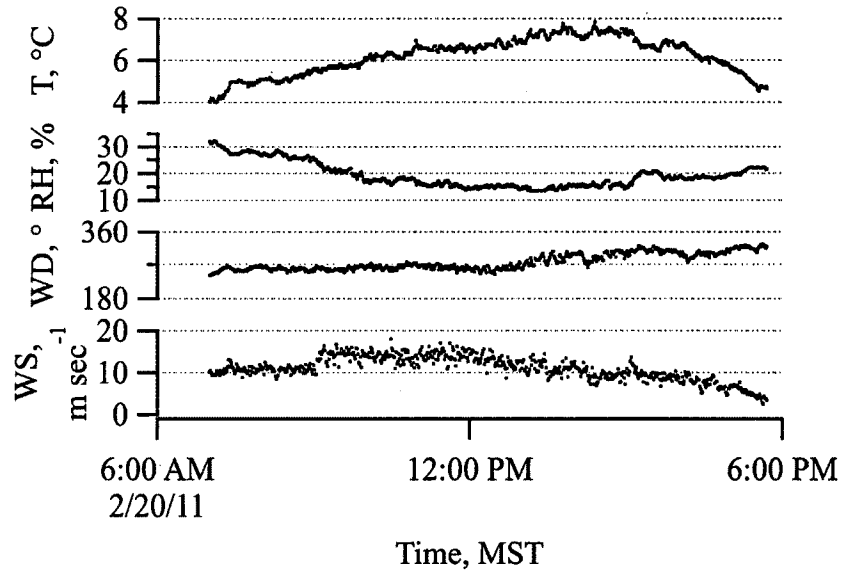
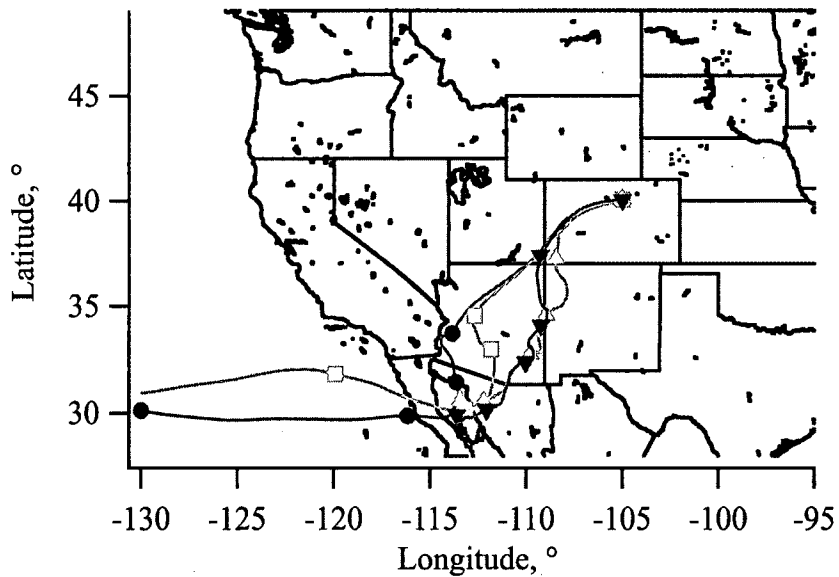
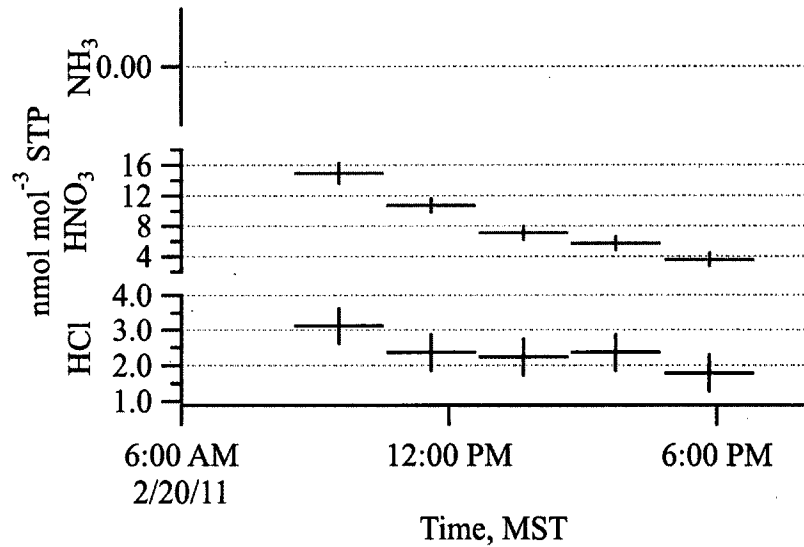
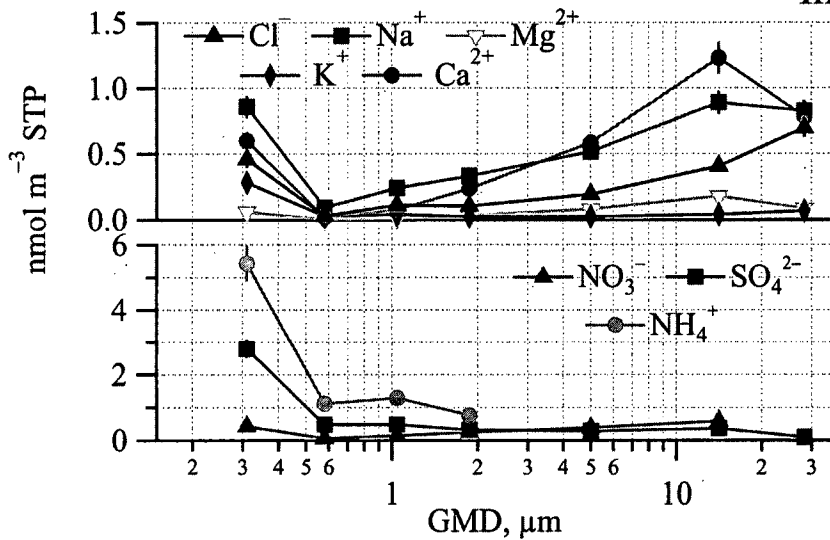
Size-resolved ionic composition of aerosol sample (top left panel); soluble trace gases sampled during impactor sample (top right panel); 5 day HYSPLIT back trajectories in 3-h intervals during sampling period (bottom left panel); Temperature, Relative Humidity (RH), Wind Direction (WD), and Wind Speed (WS) during impactor sampling period (bottom right panel).



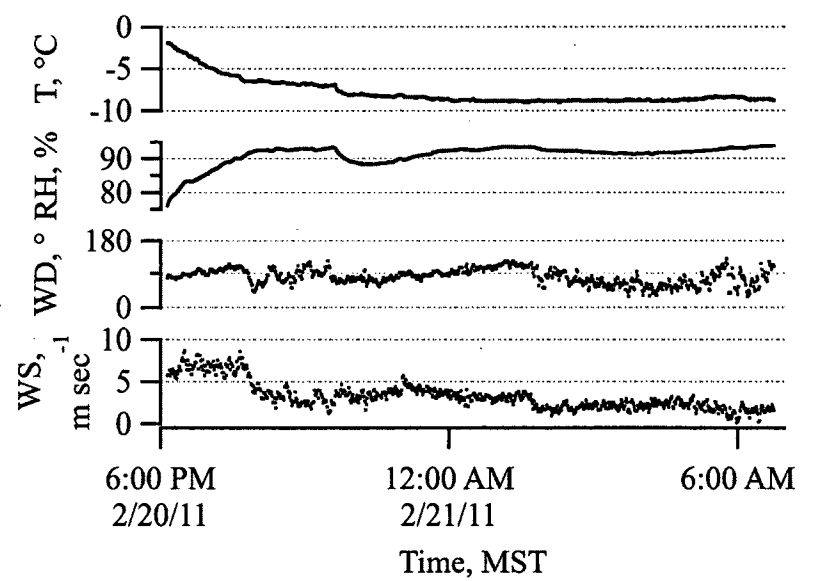
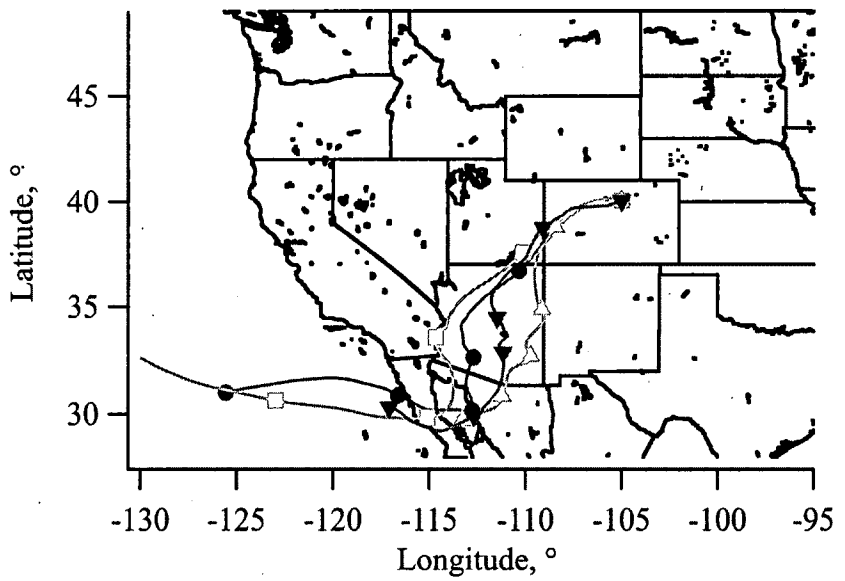
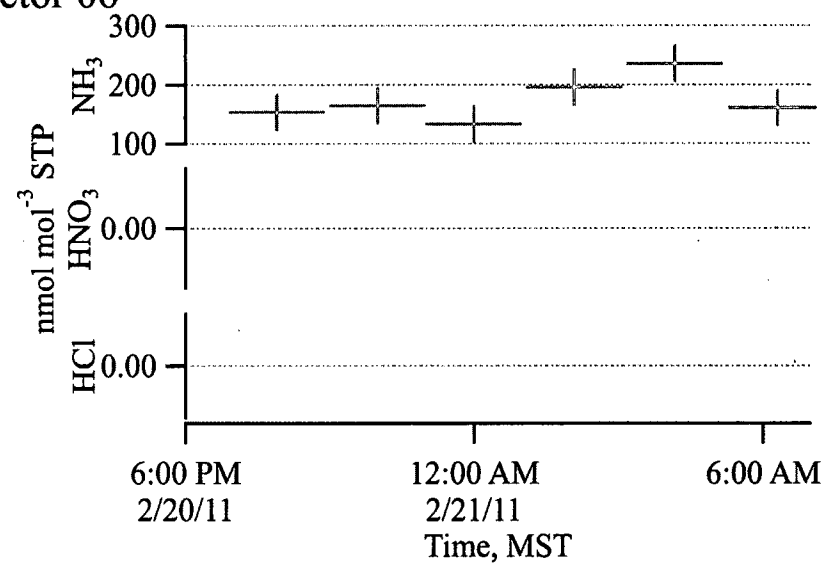
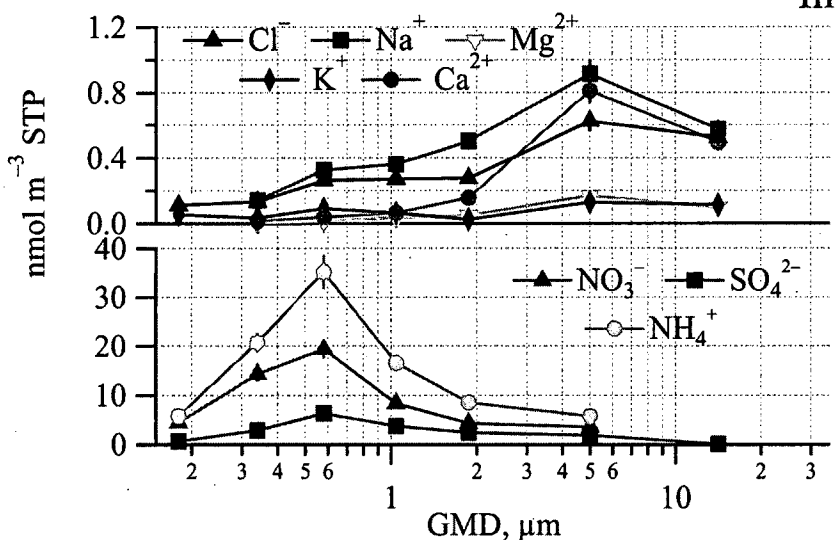


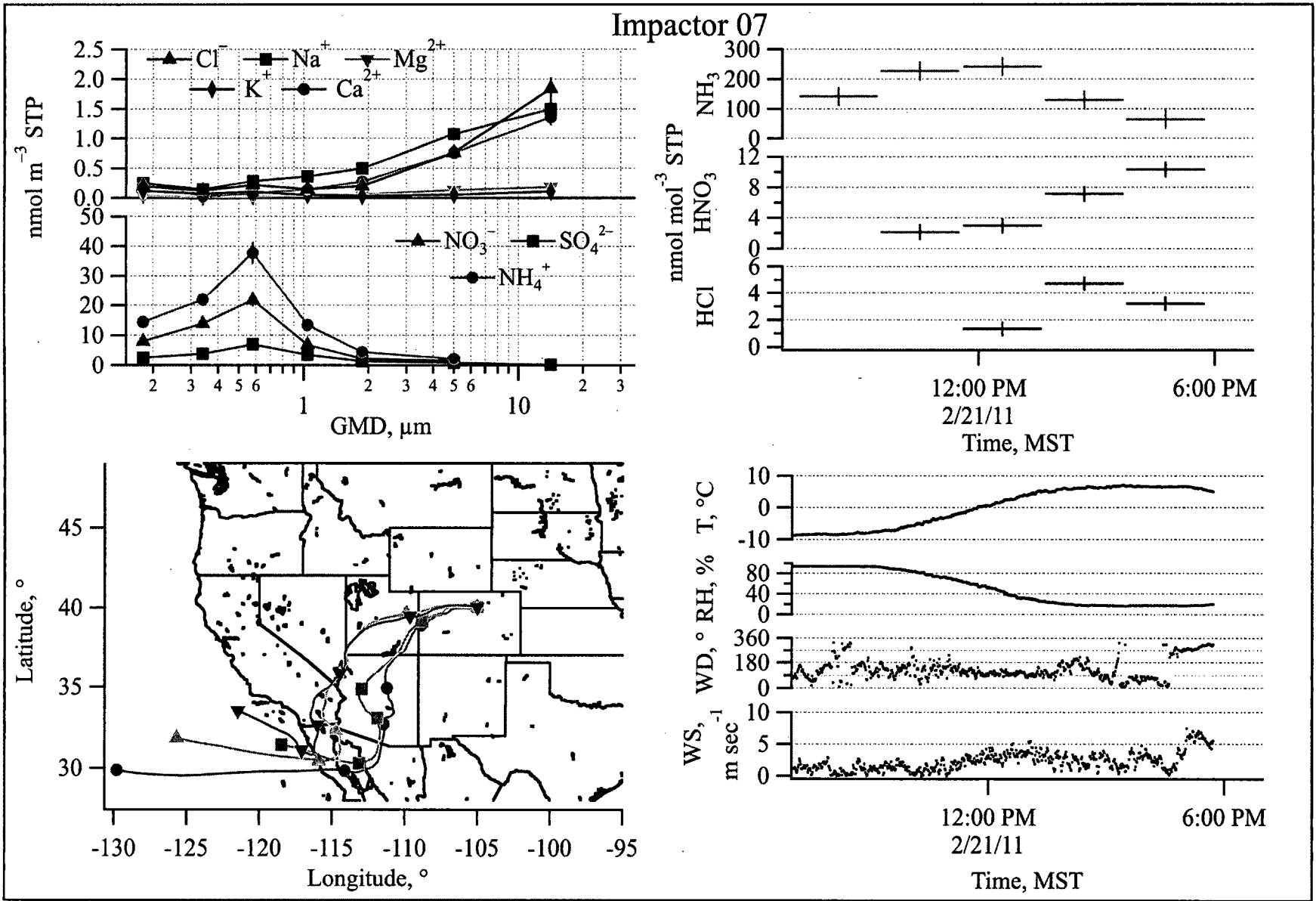


Impactor 05

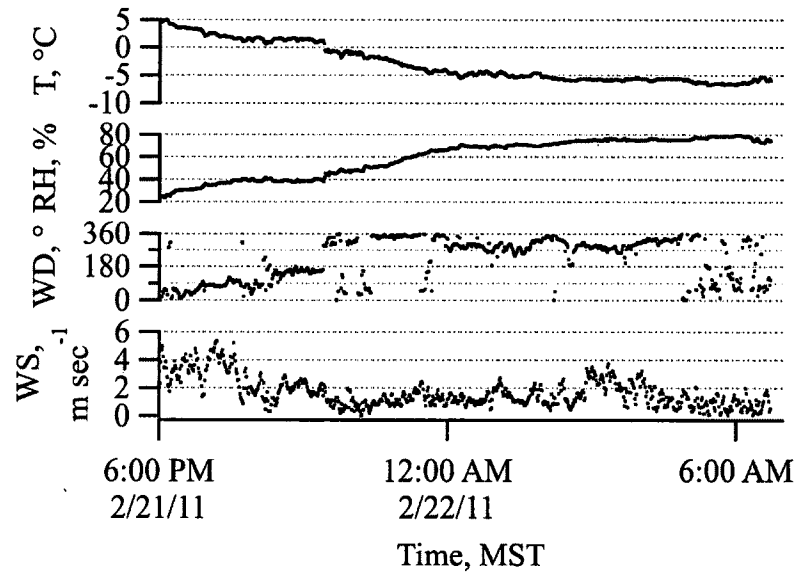
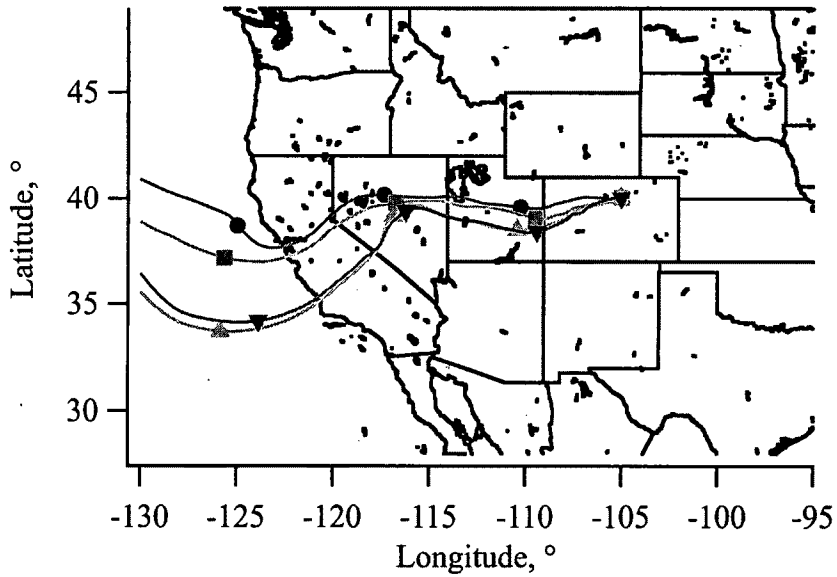
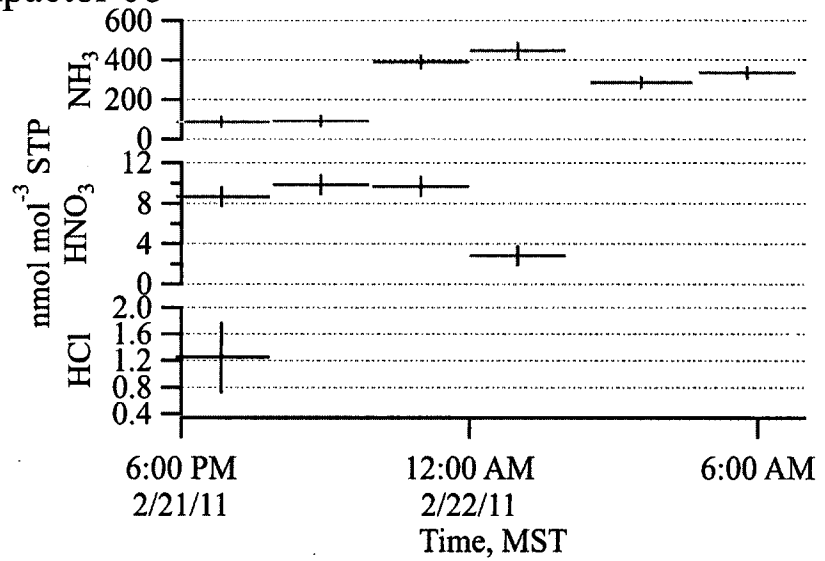
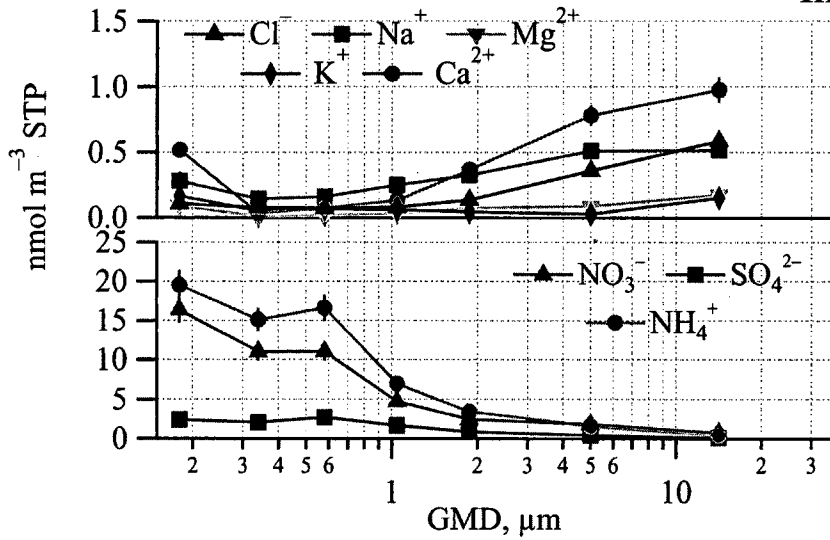


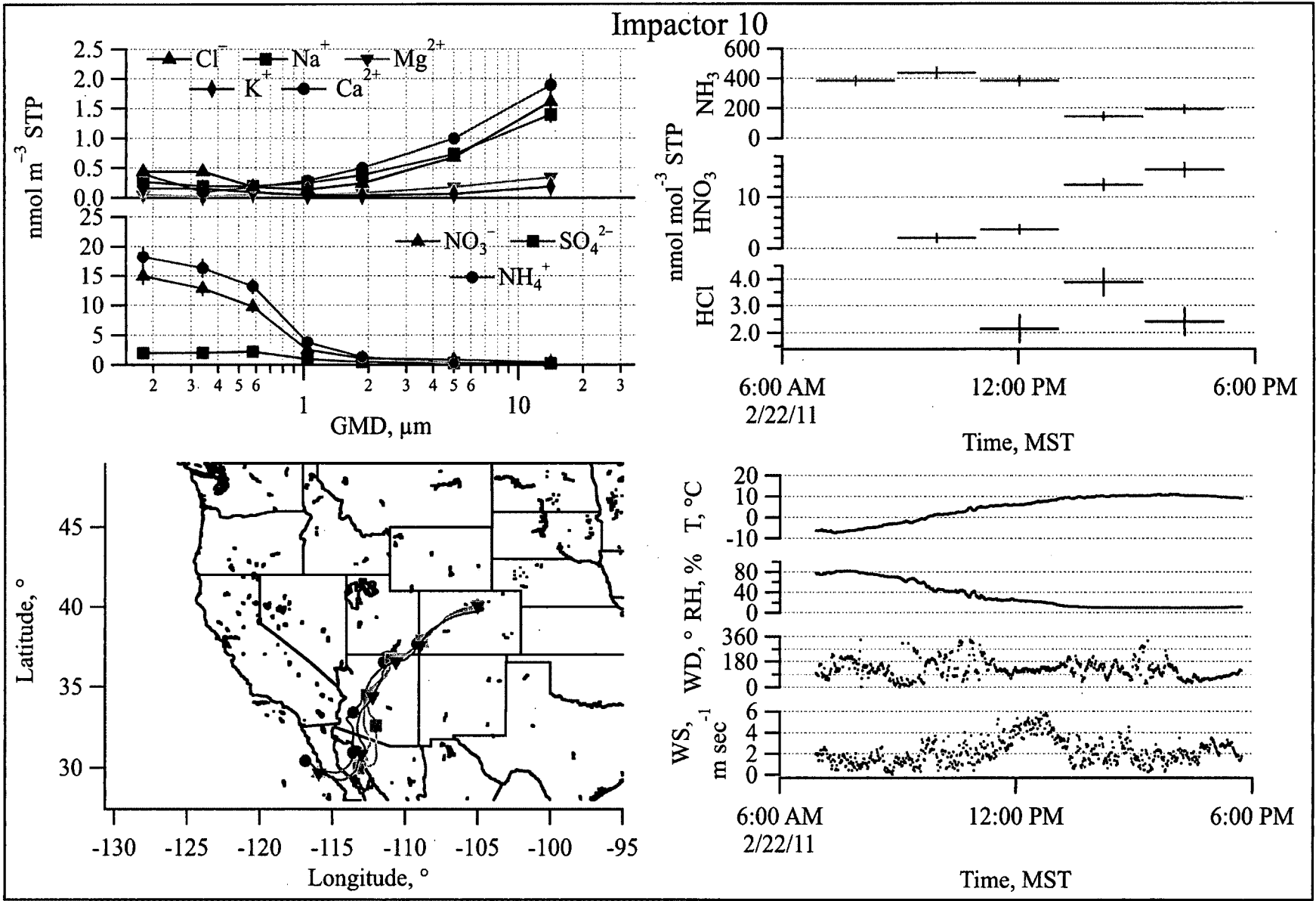
Impactor O6



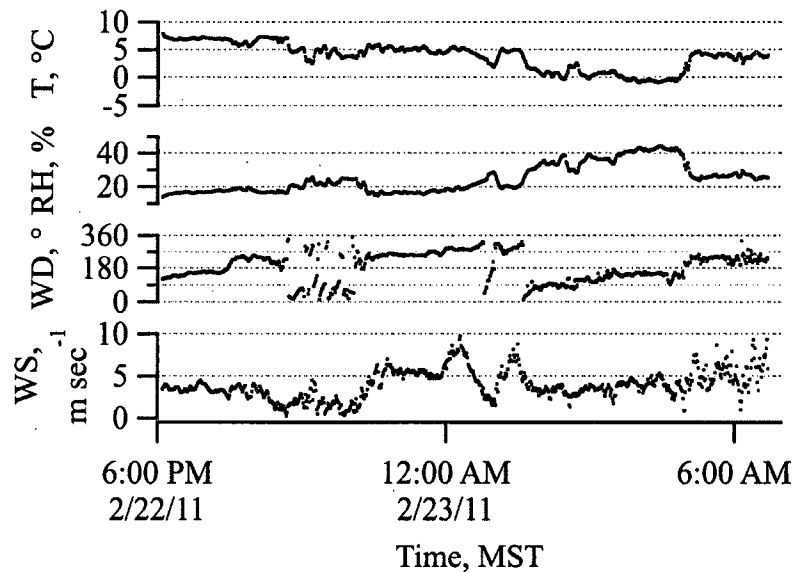
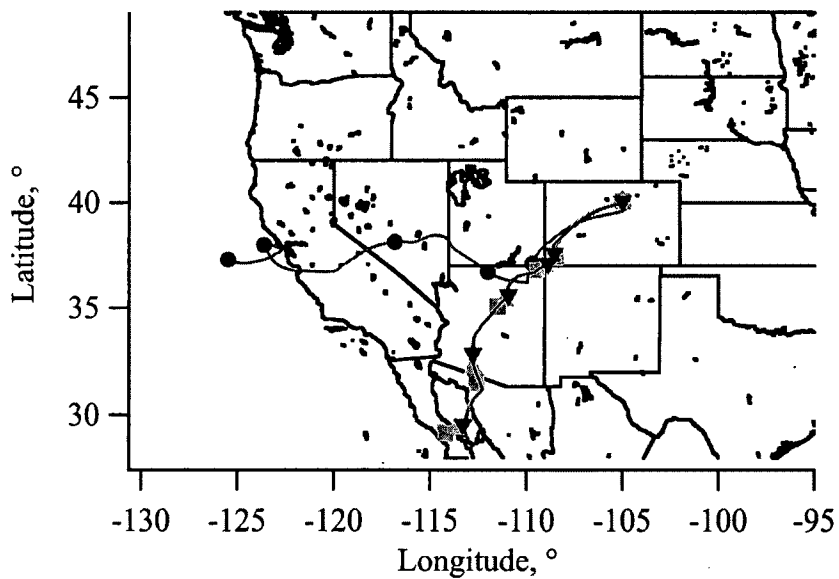
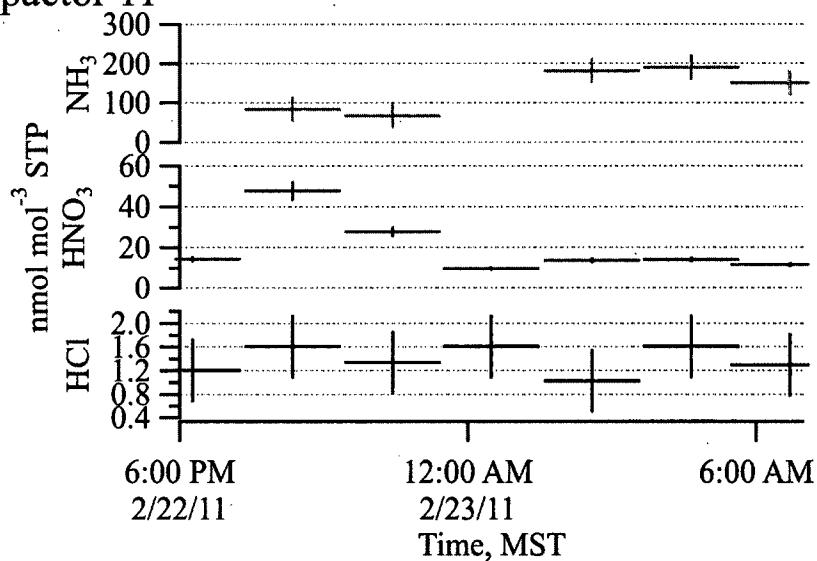
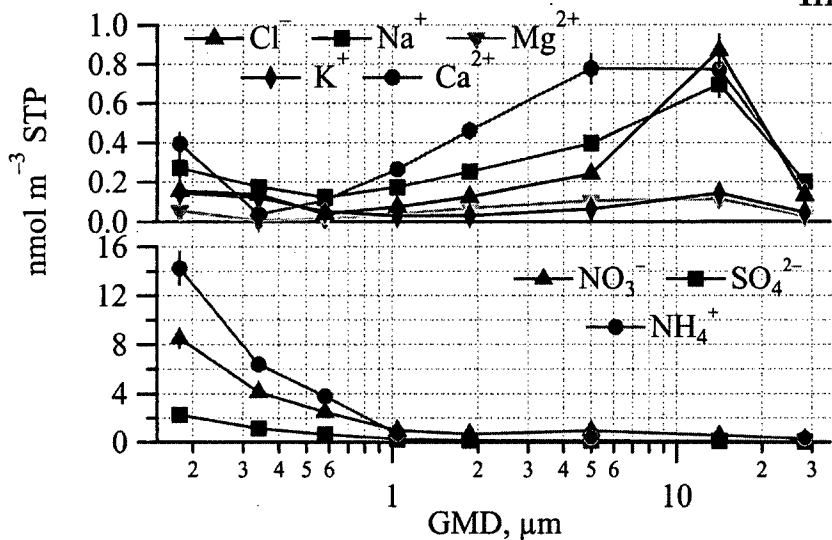


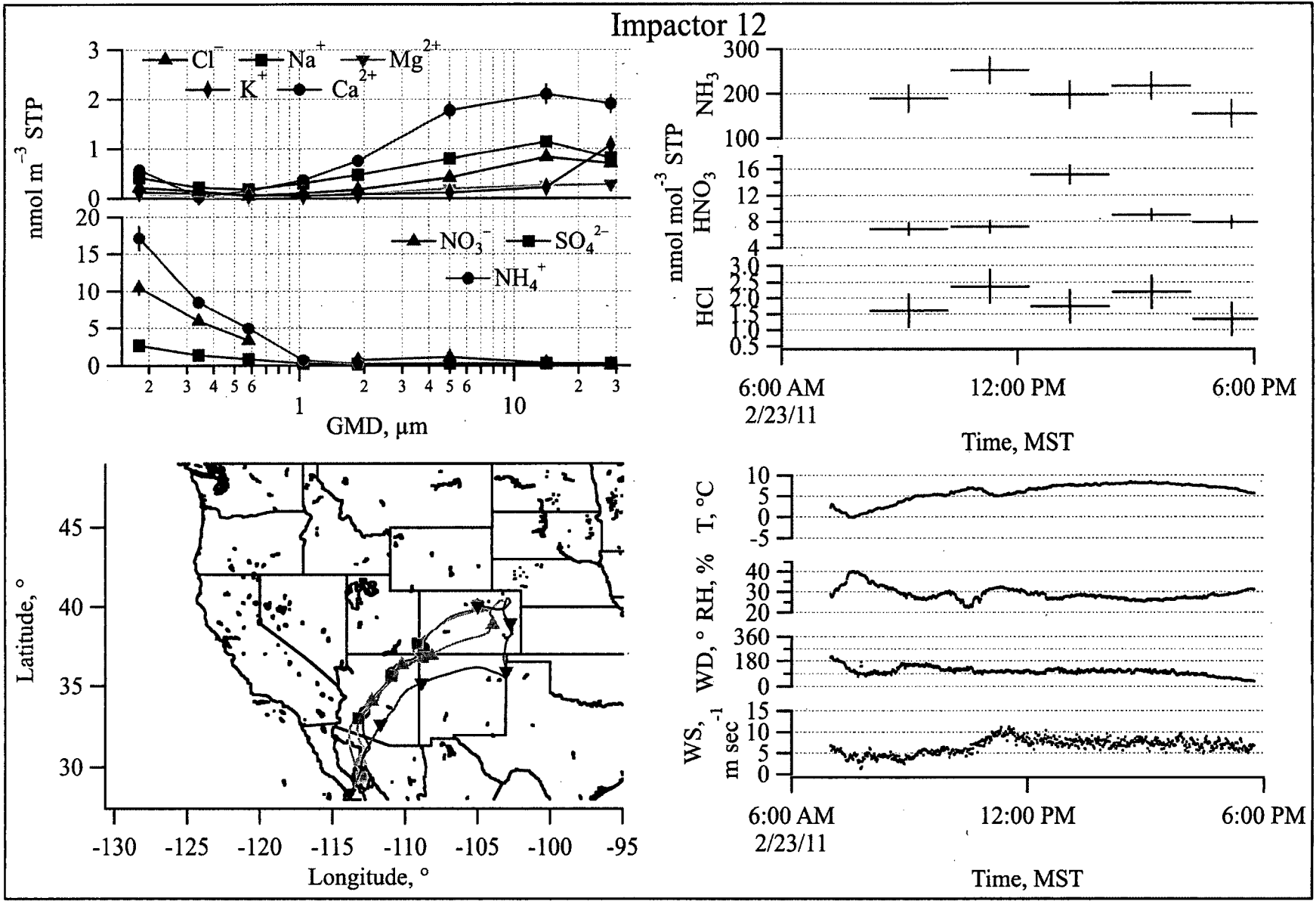
Impactor 08



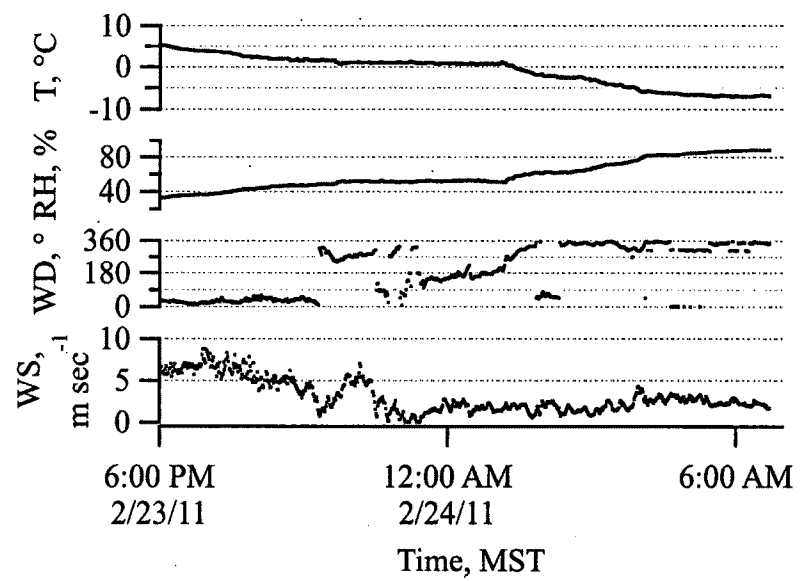
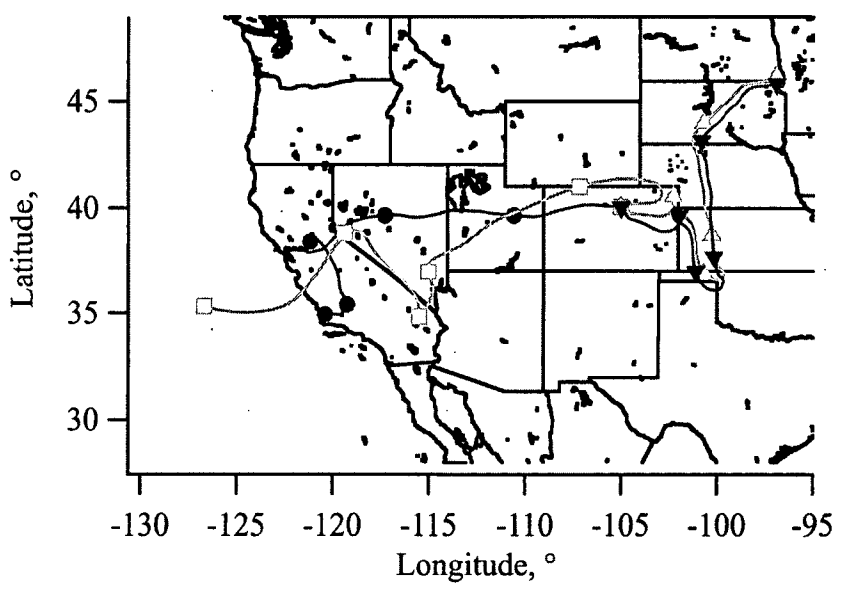
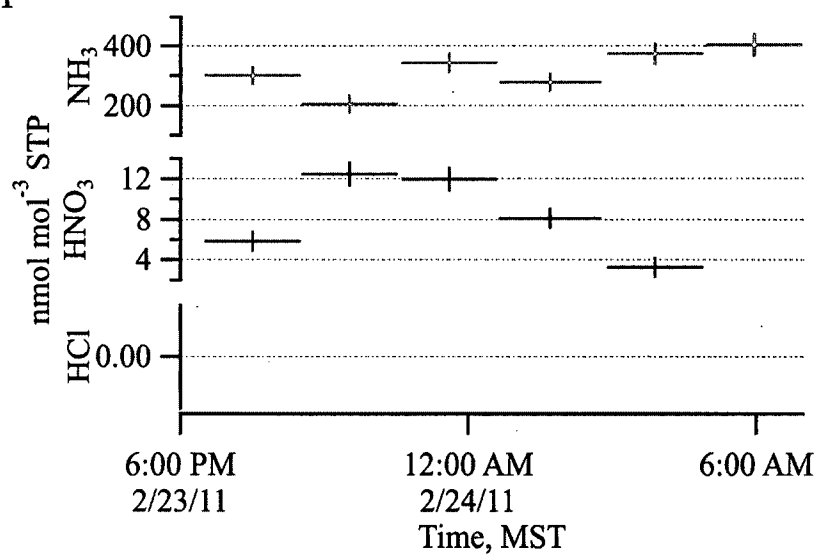
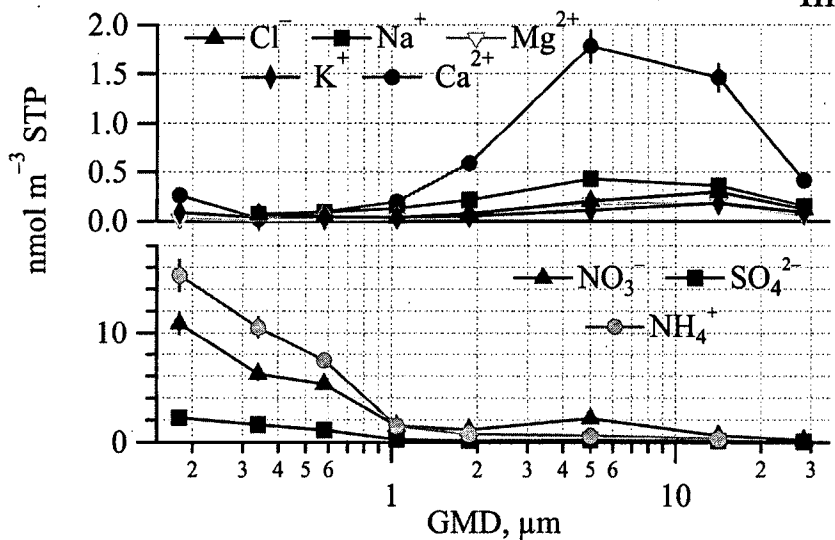


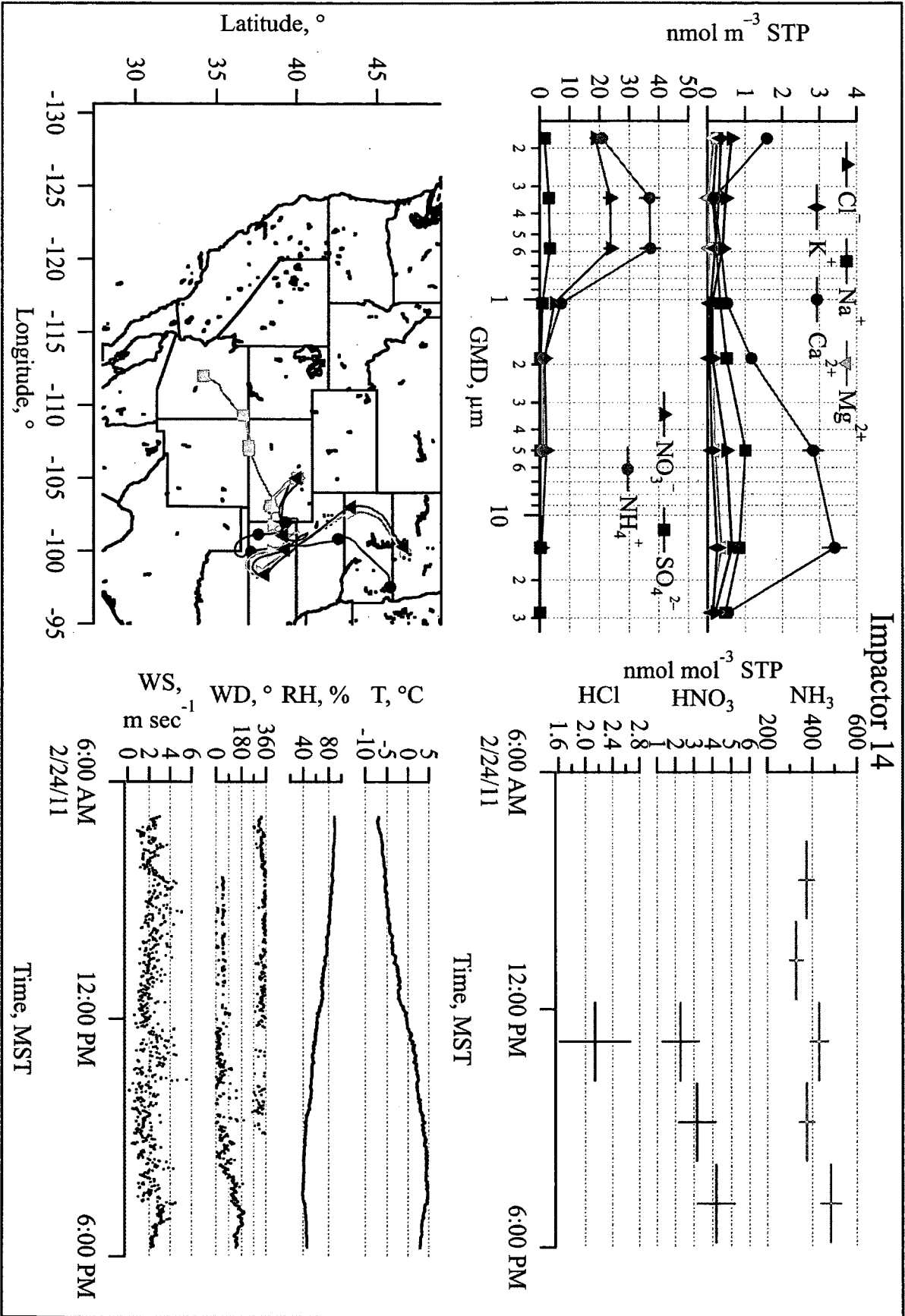
Impactor 11



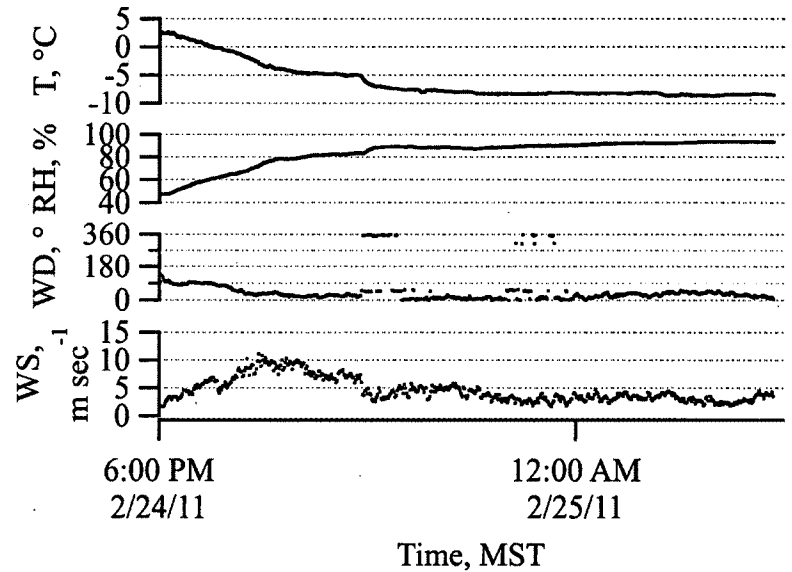
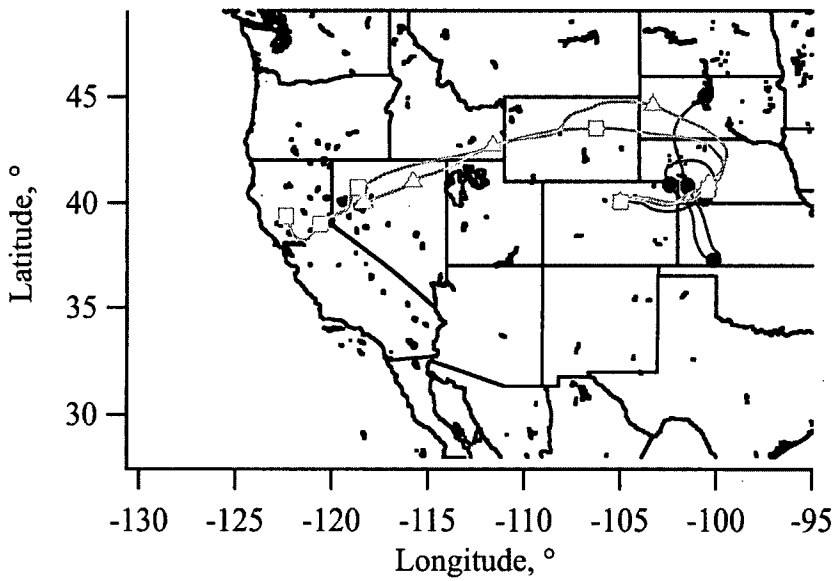
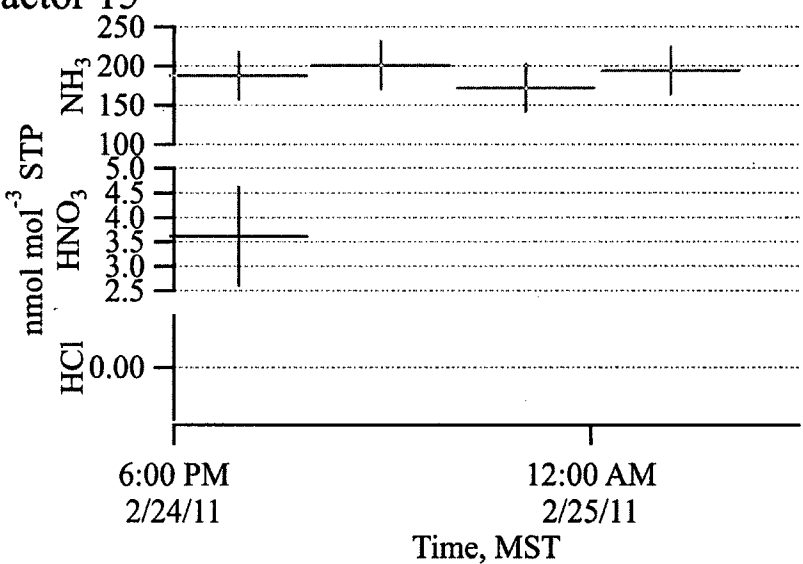
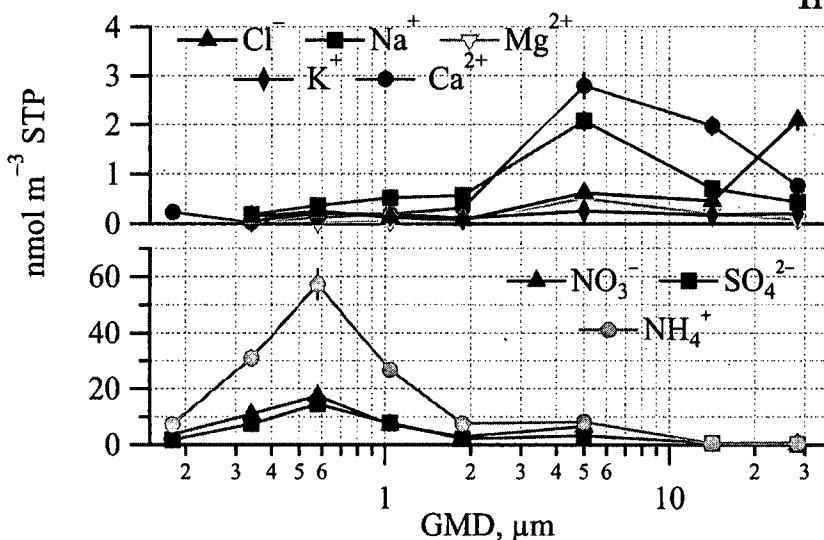


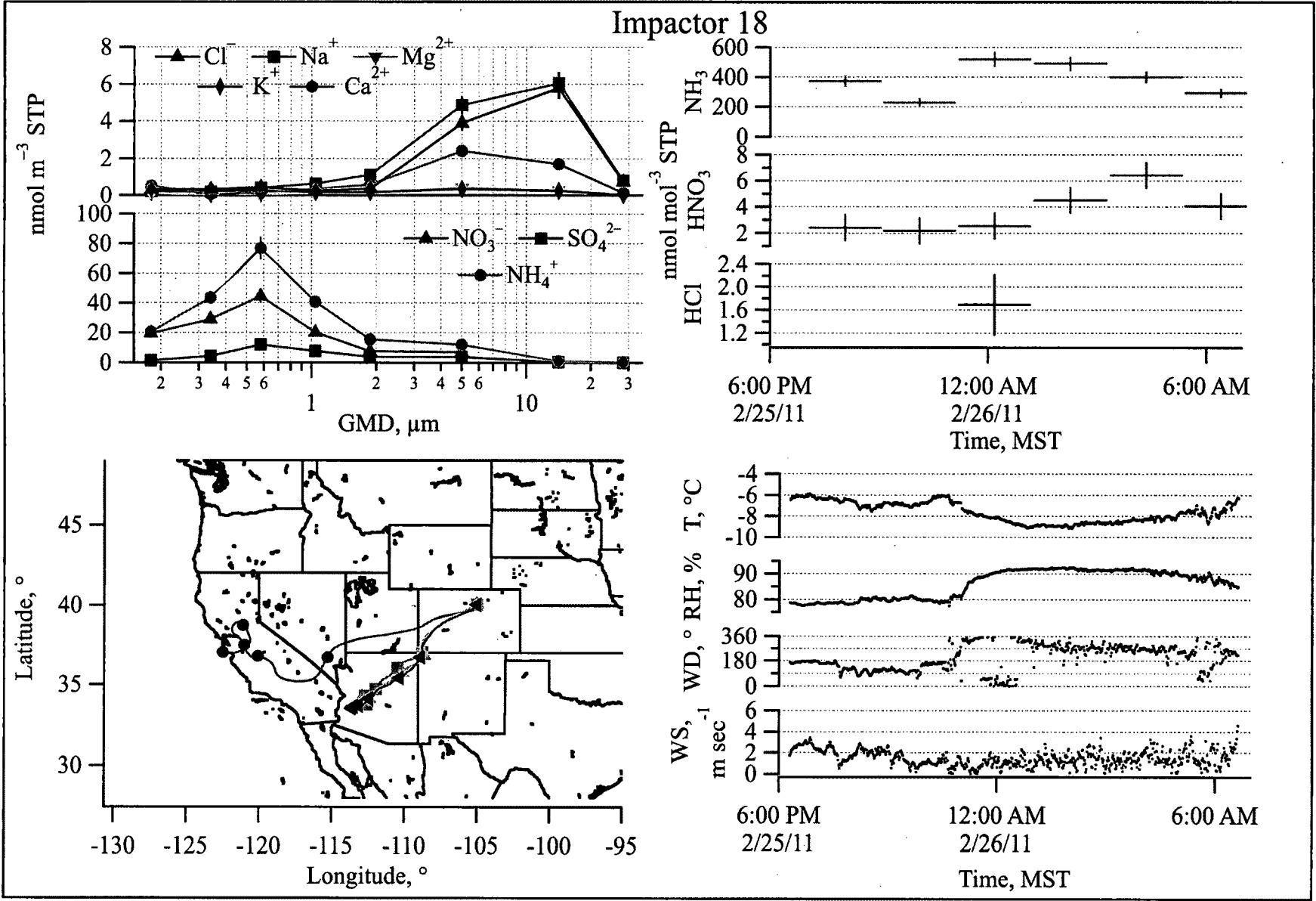
Impactor 13

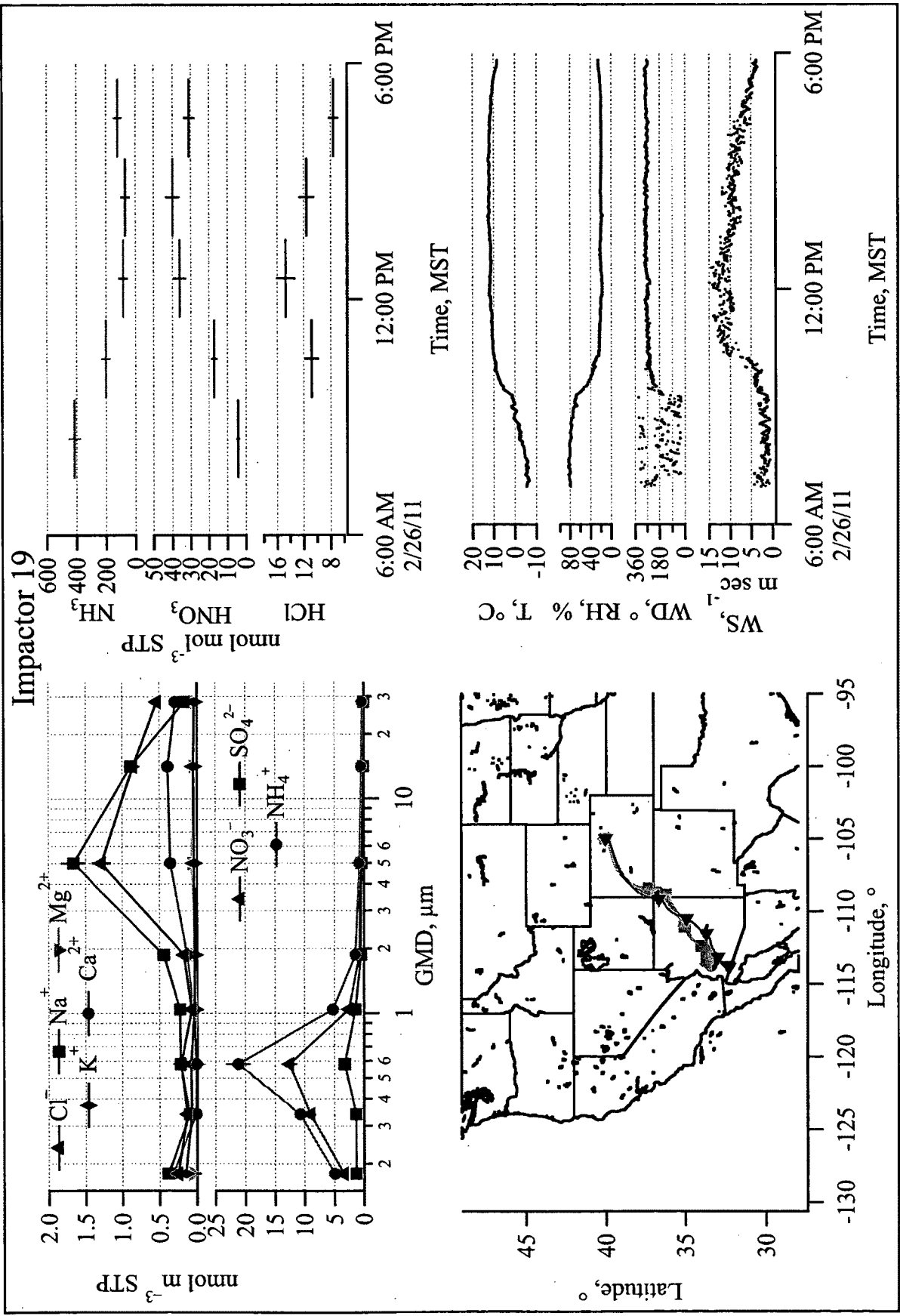




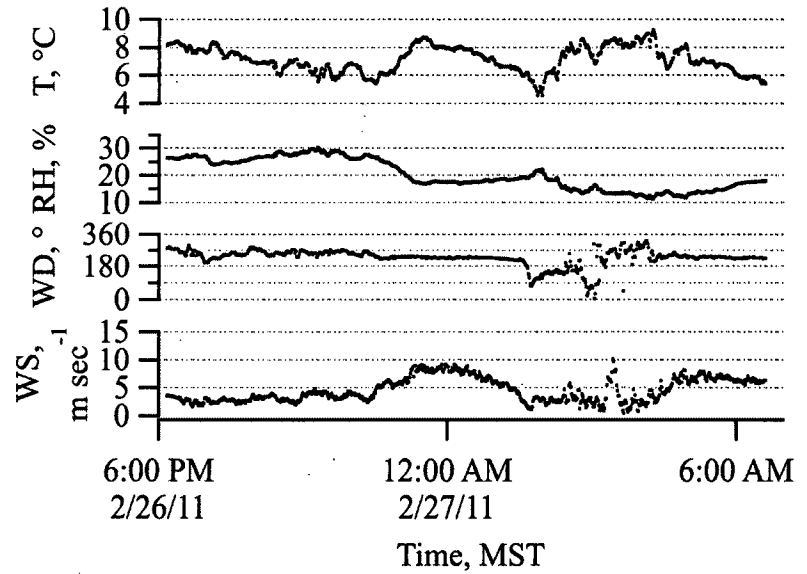
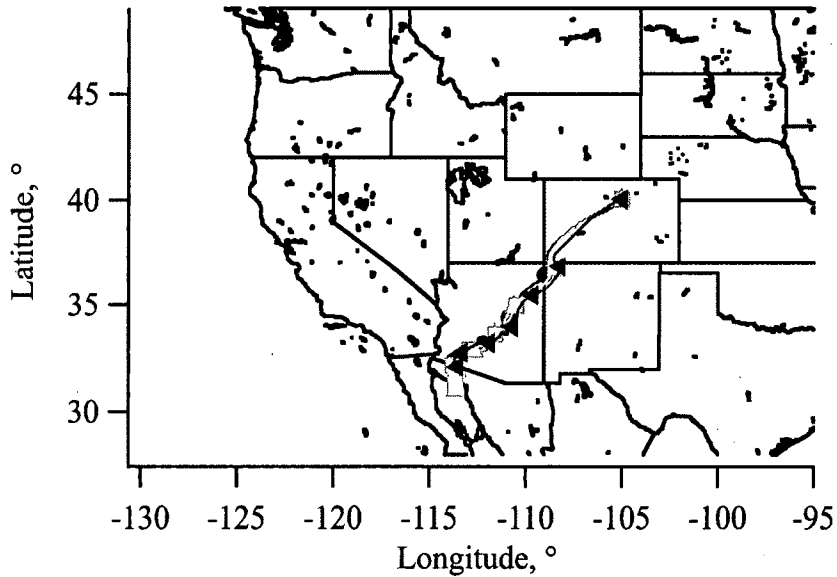
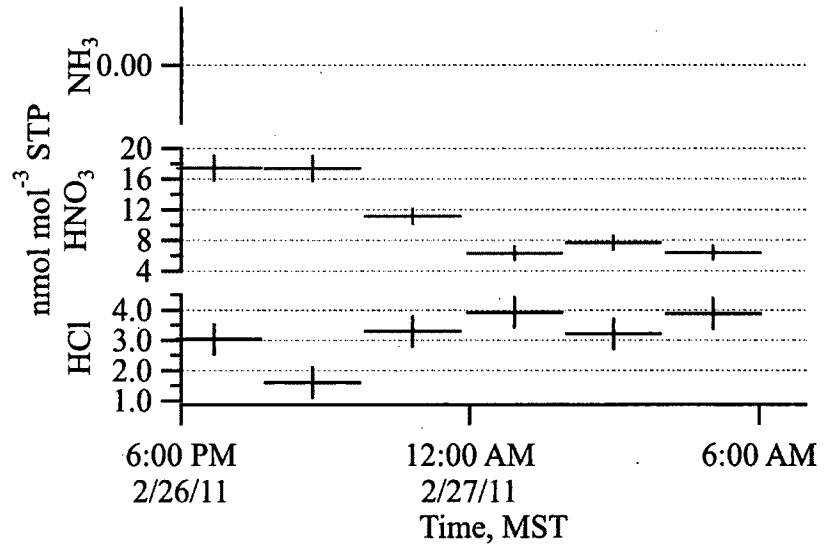
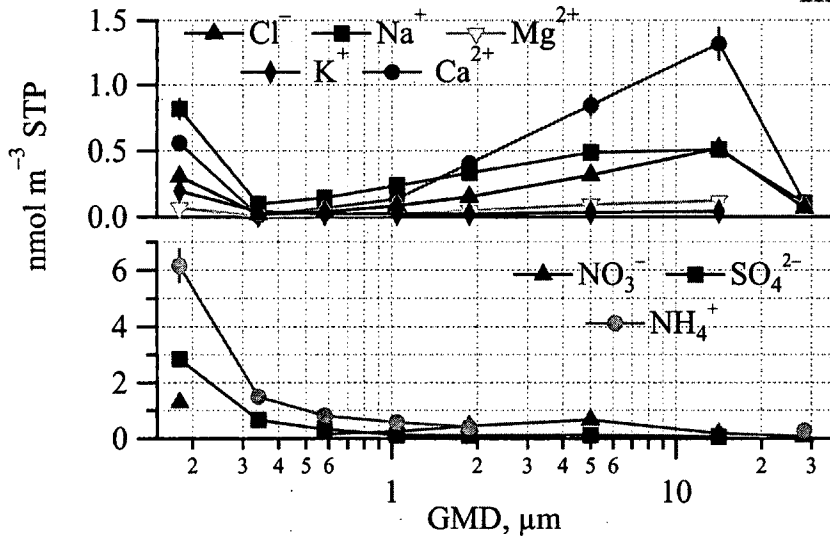
Impactor 15

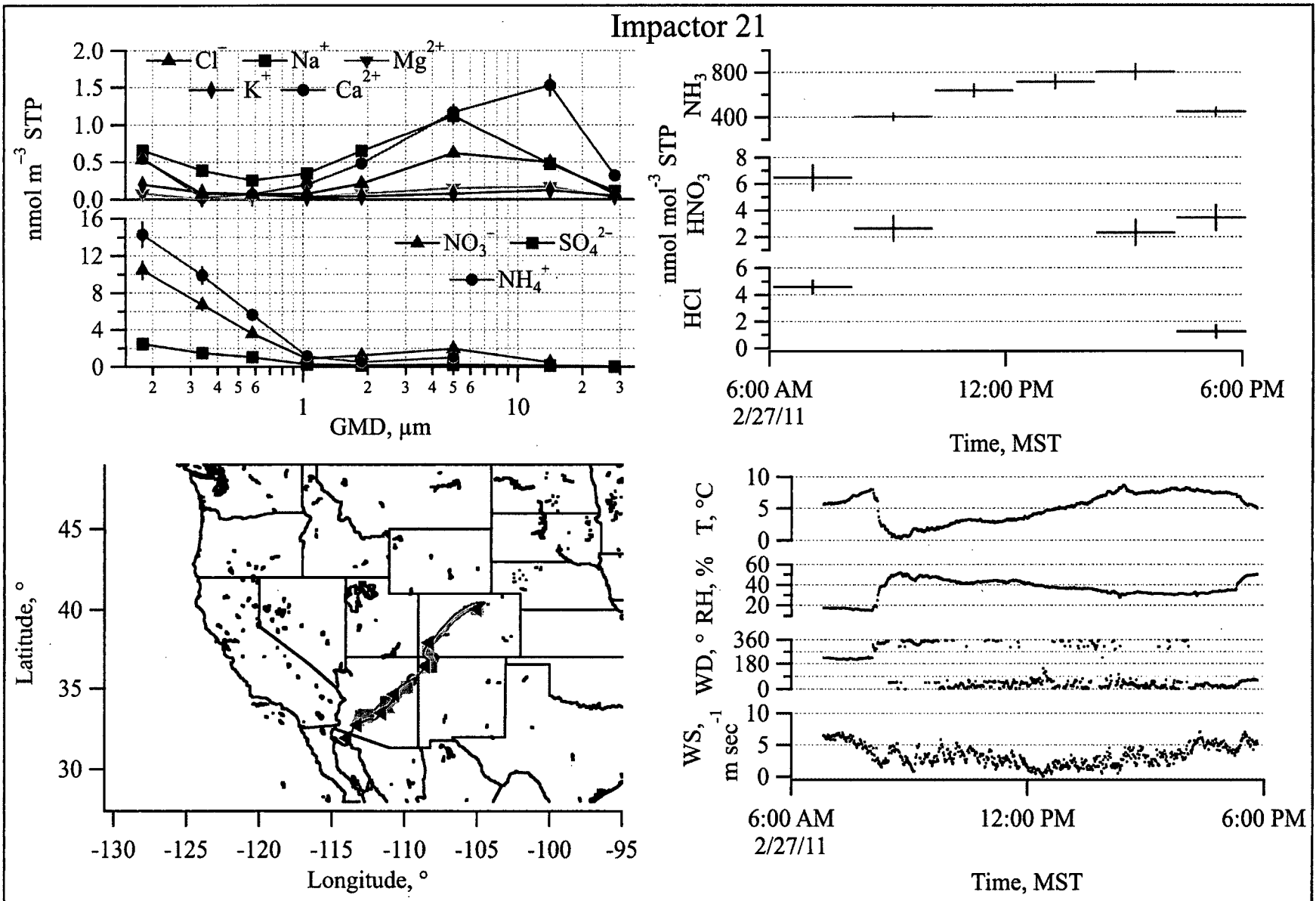


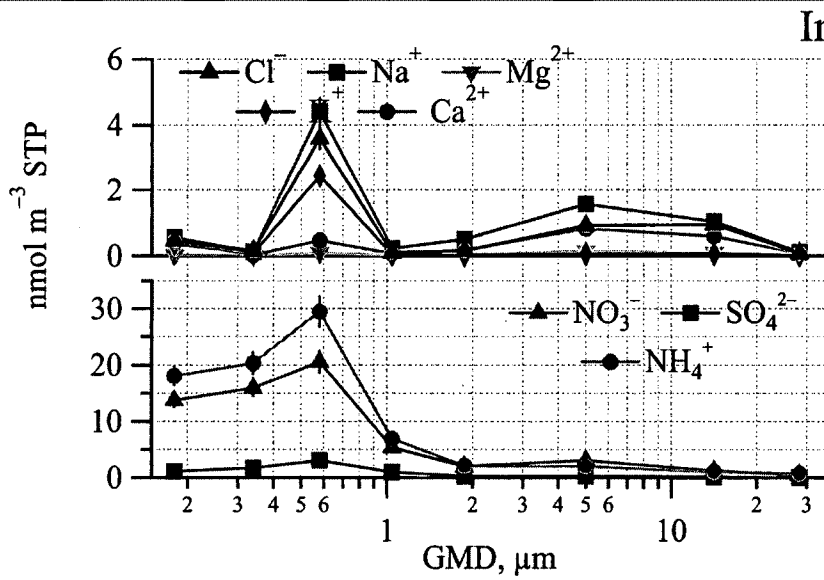




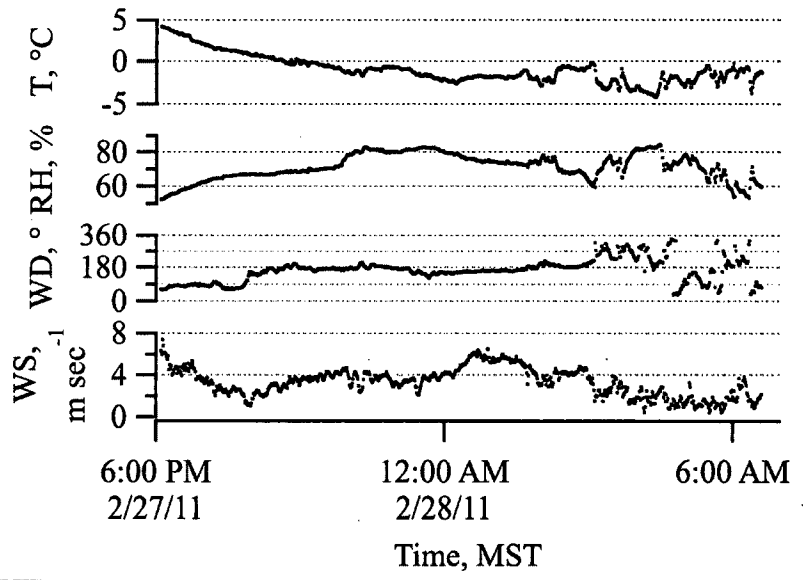
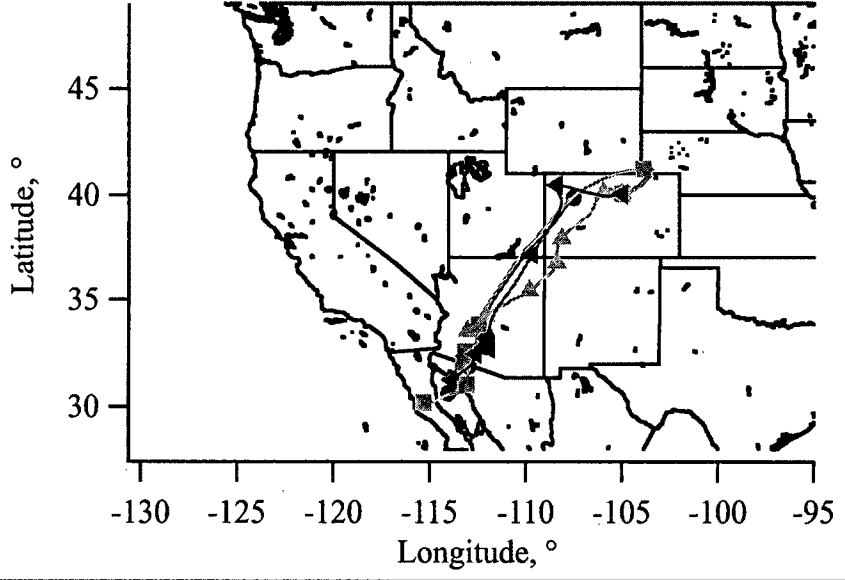
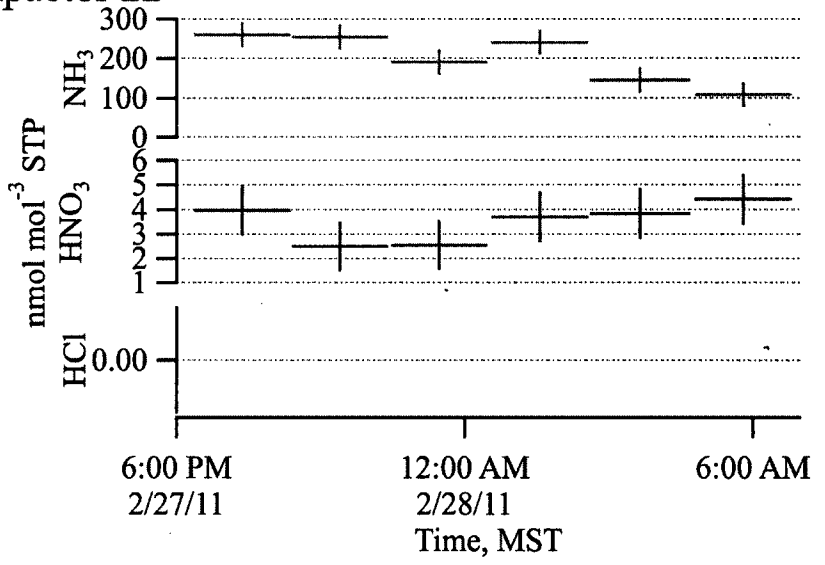
Impactor 20



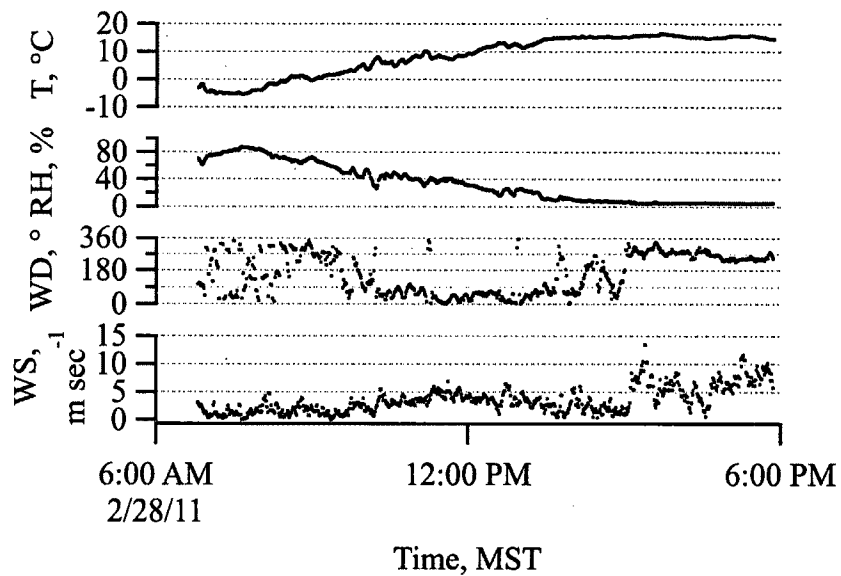
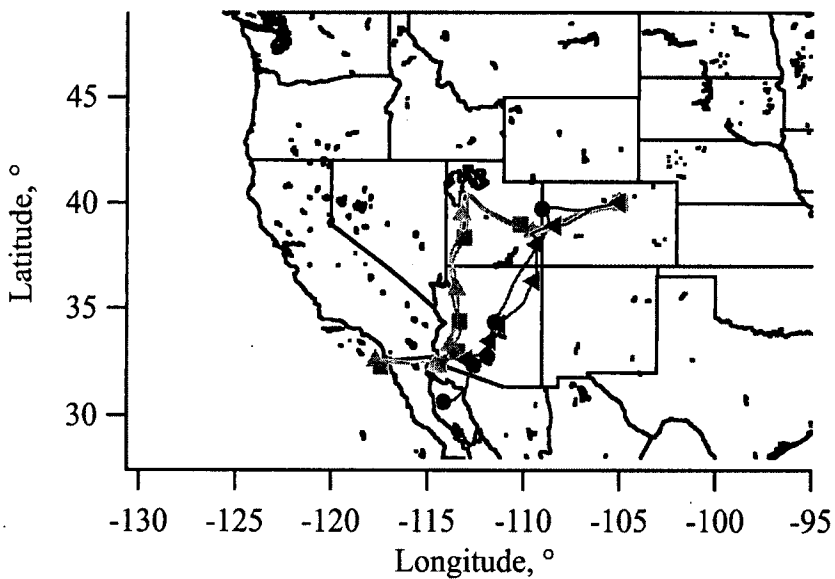
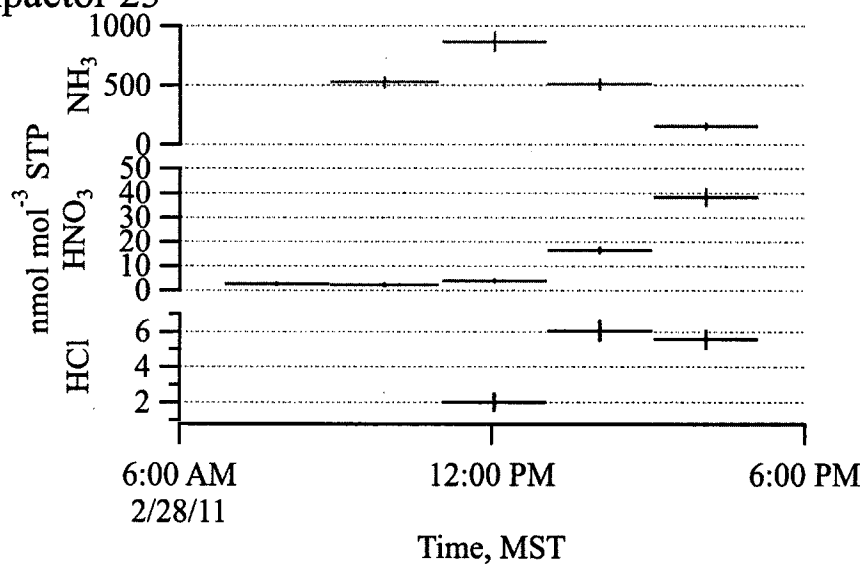
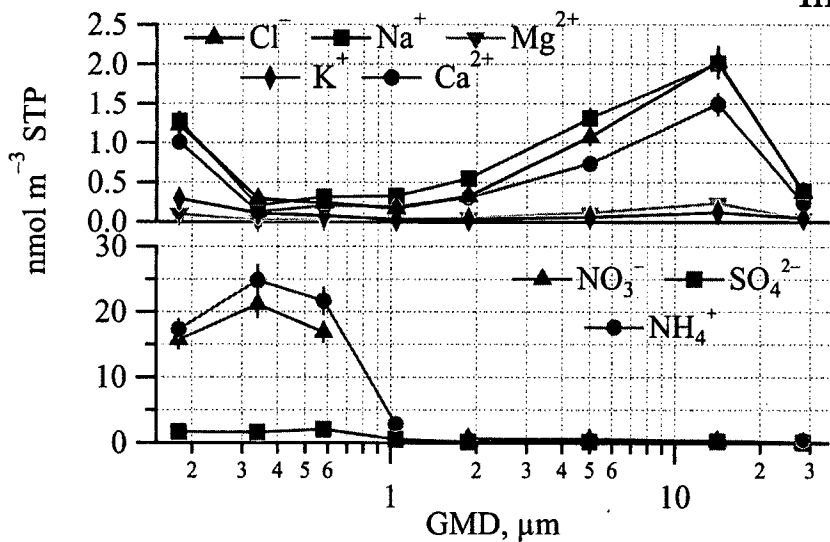




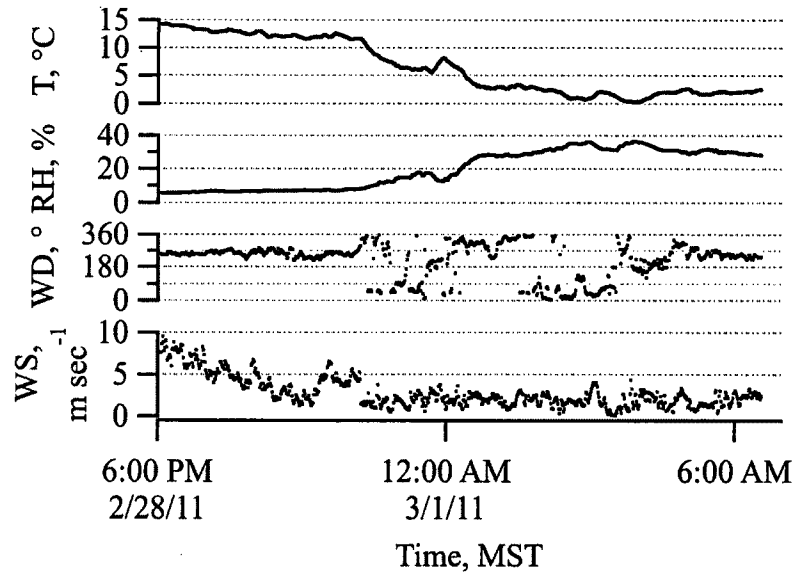
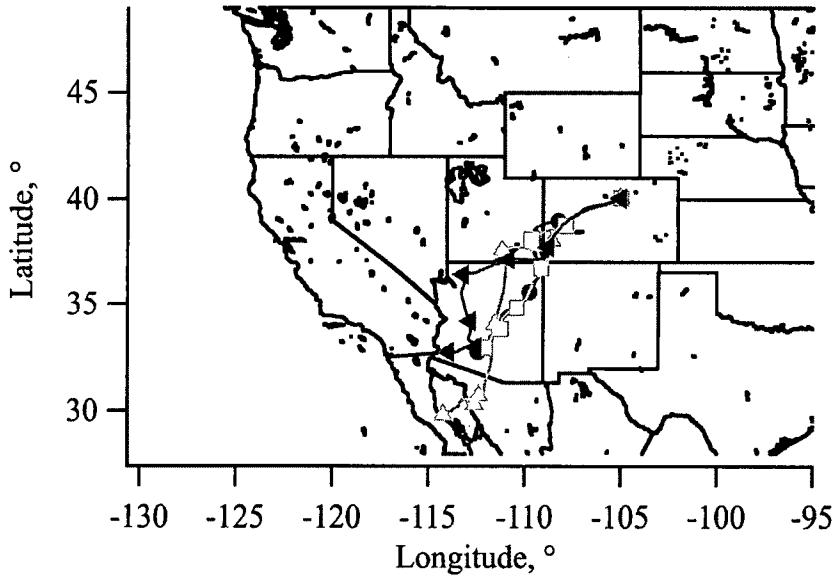
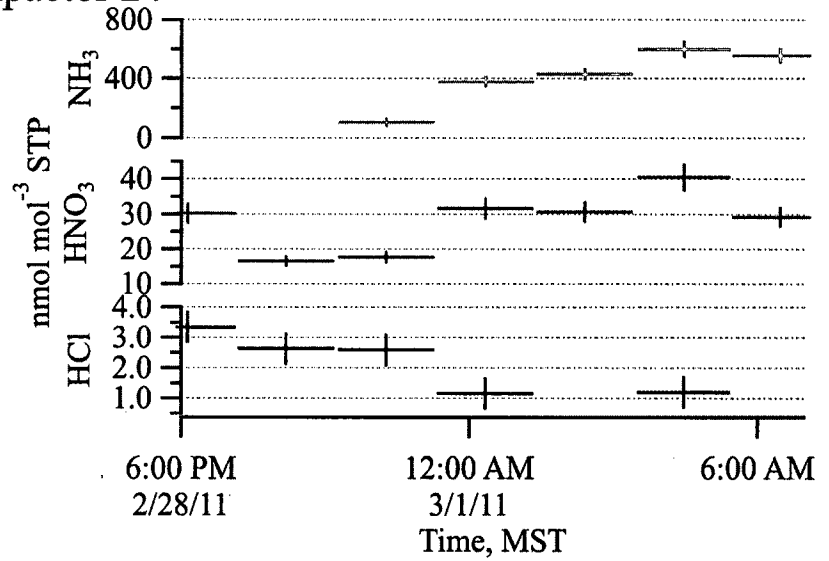
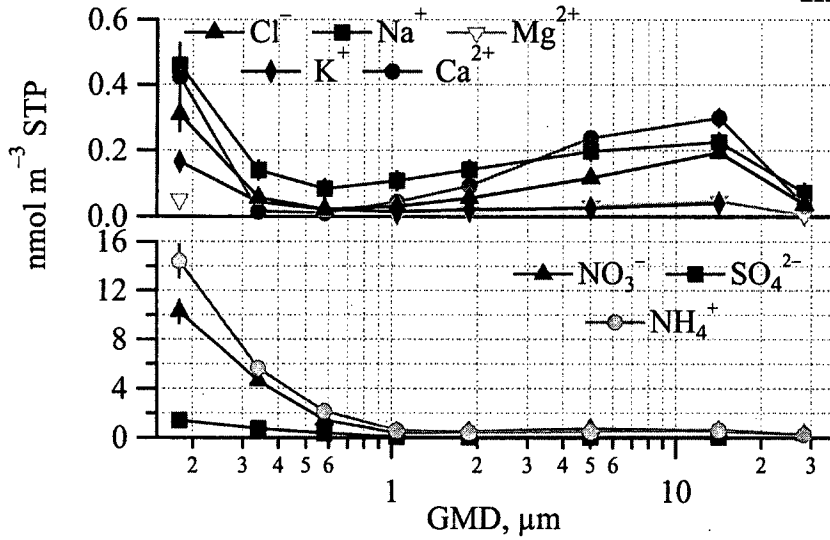
Impactor 22

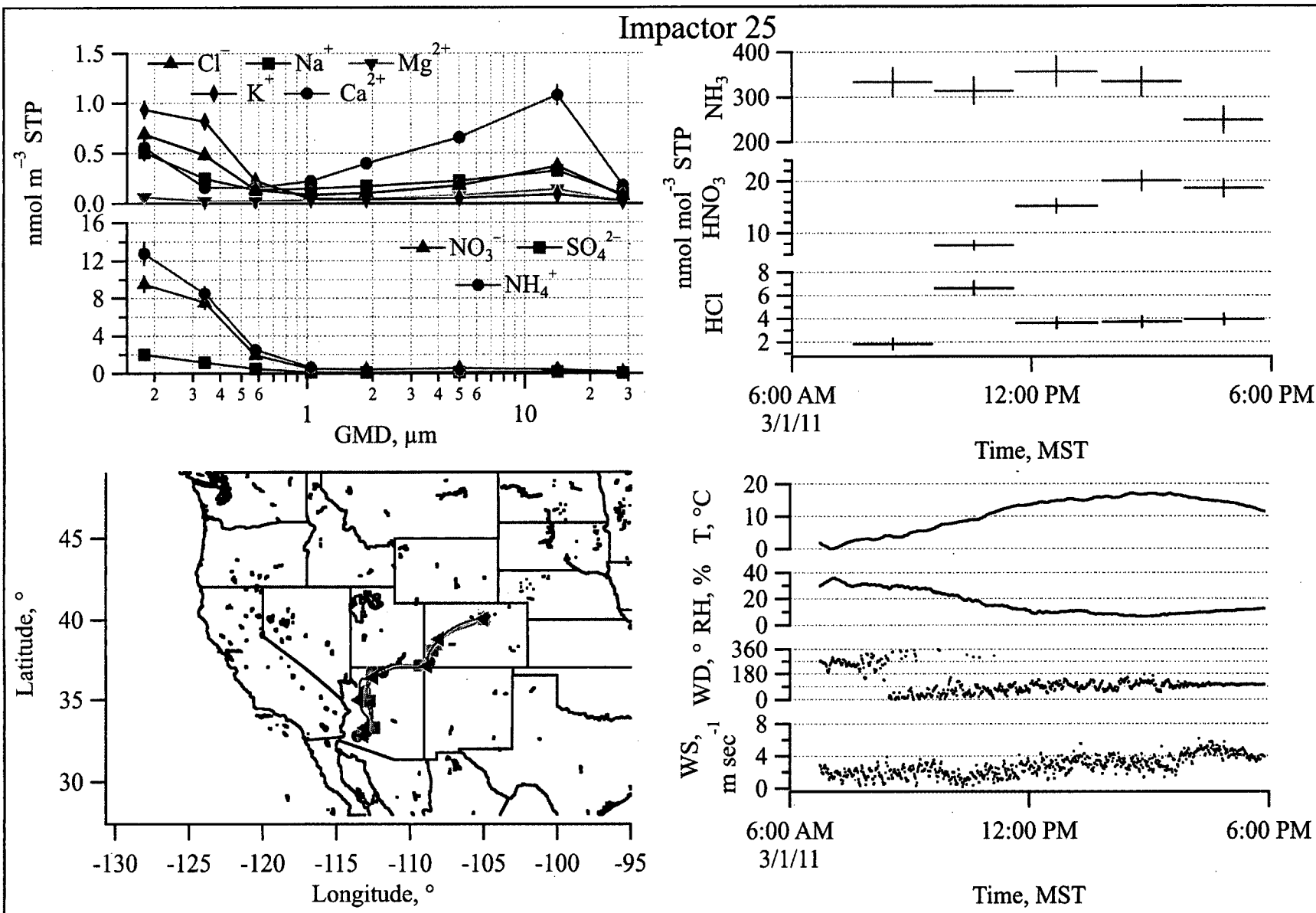


Impactor 23

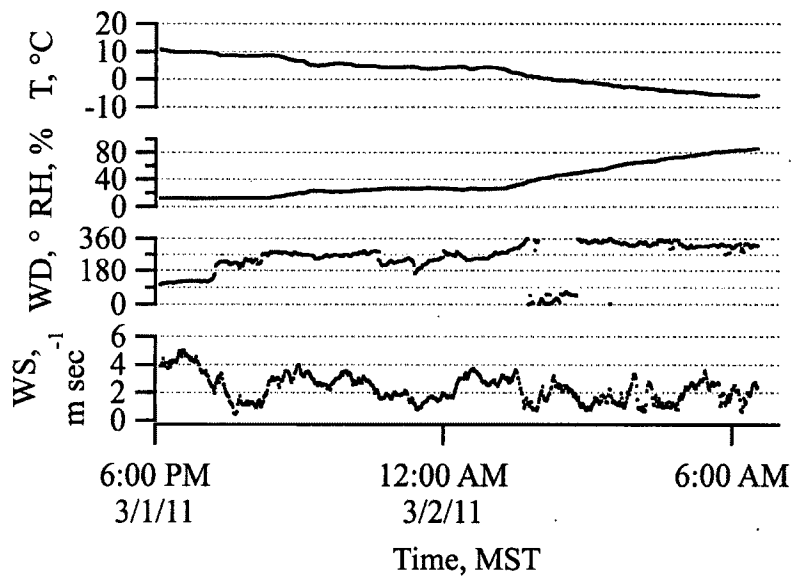
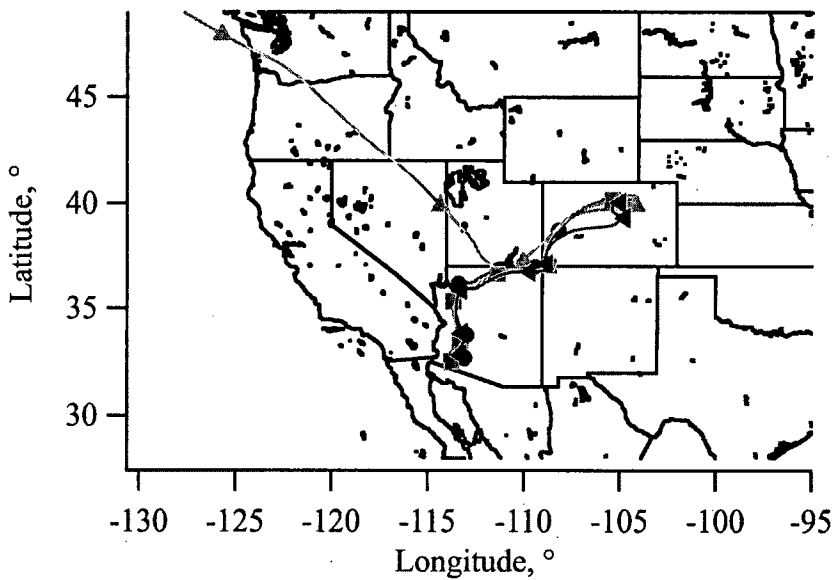
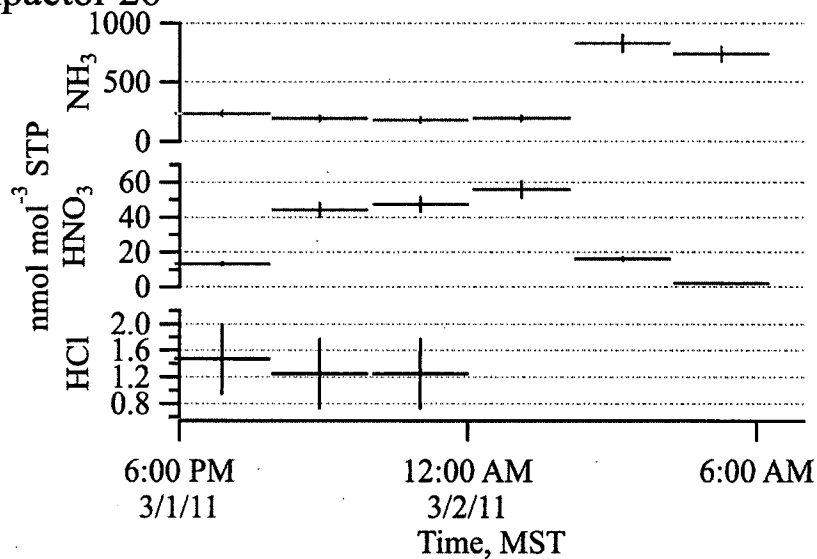
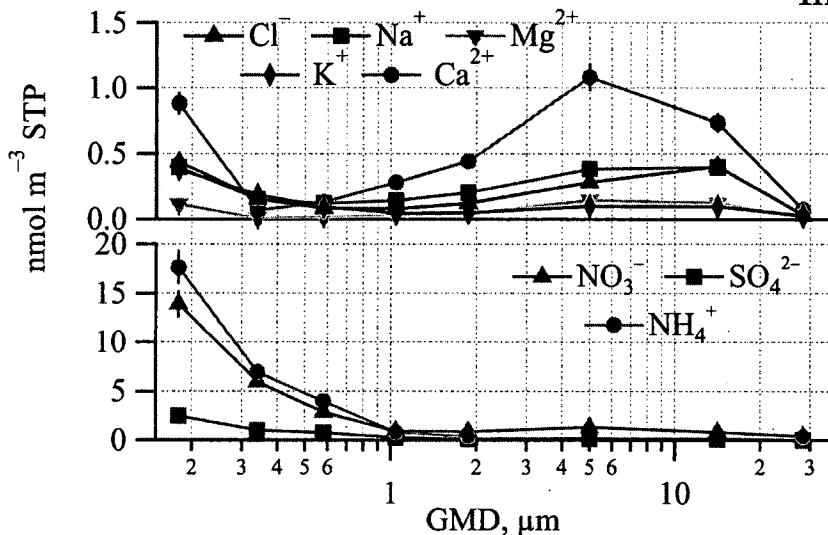


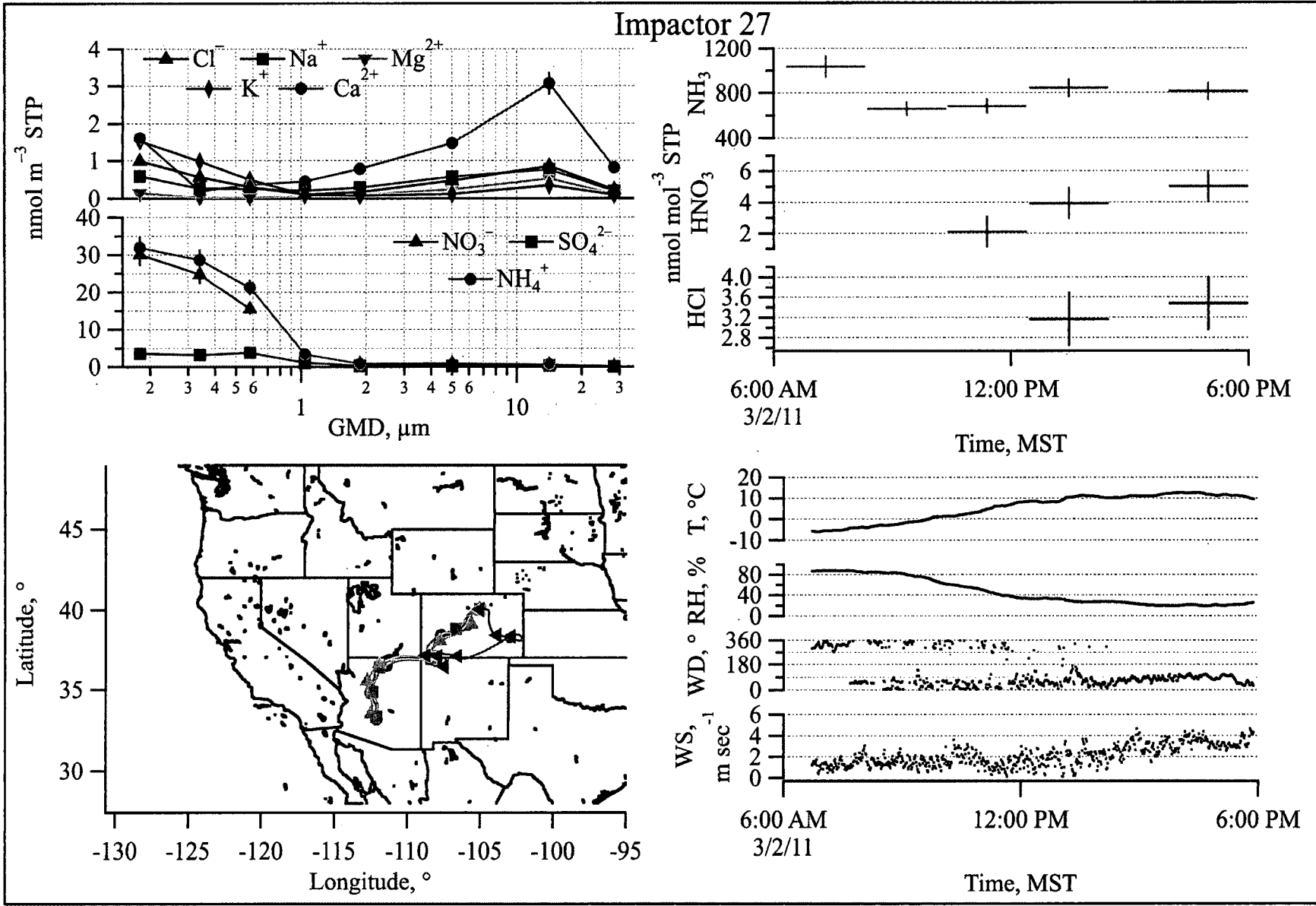
Impactor 24

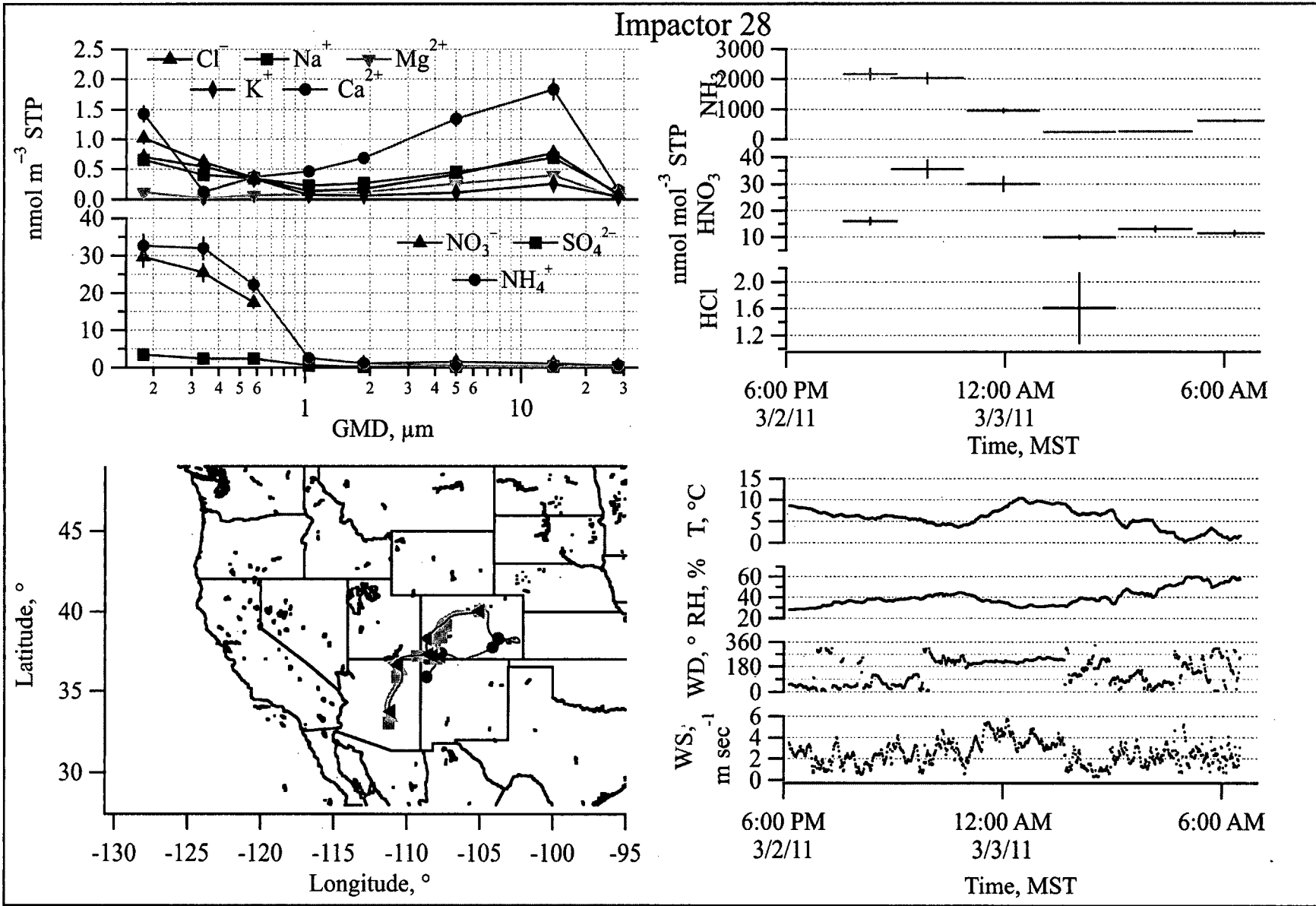


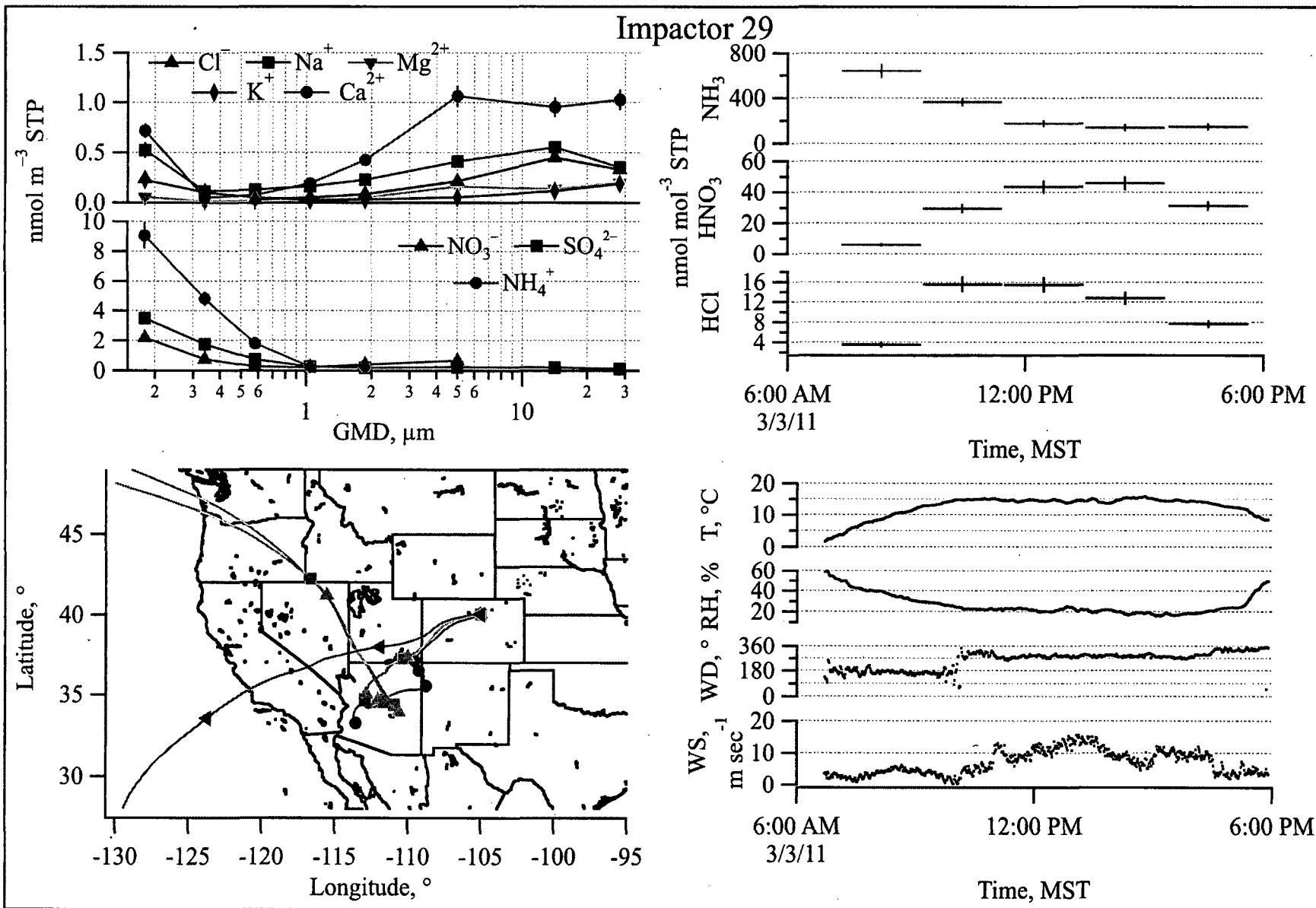


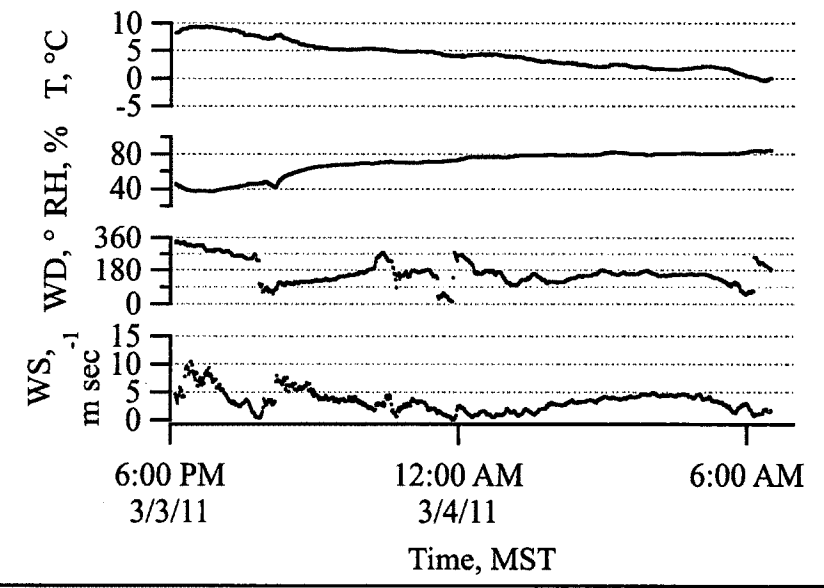
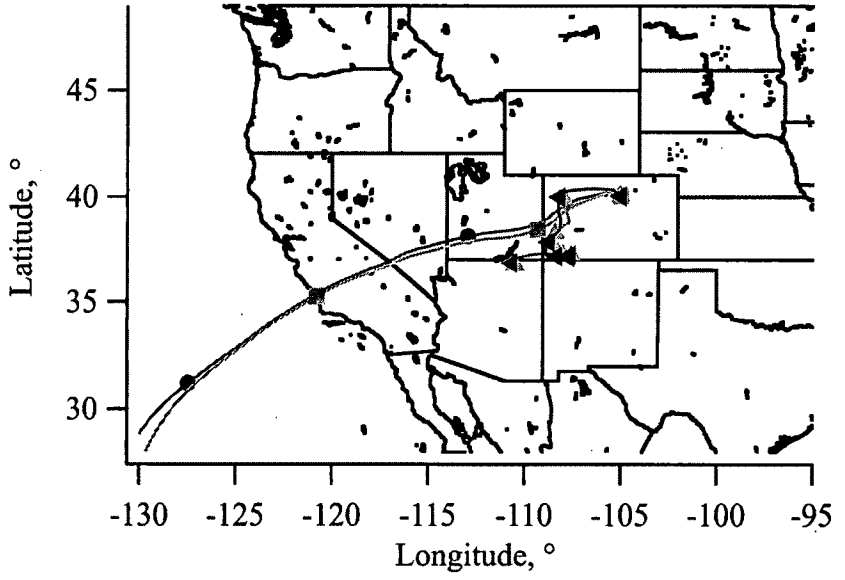
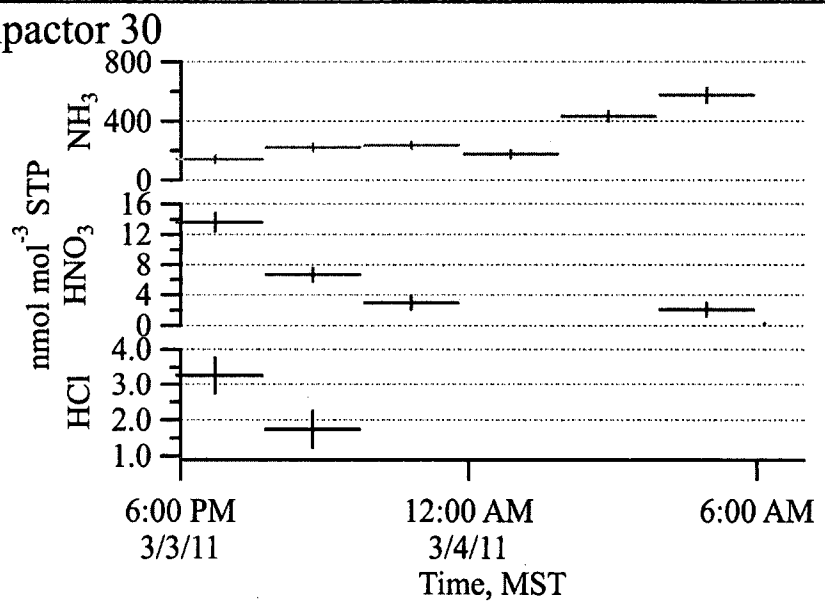
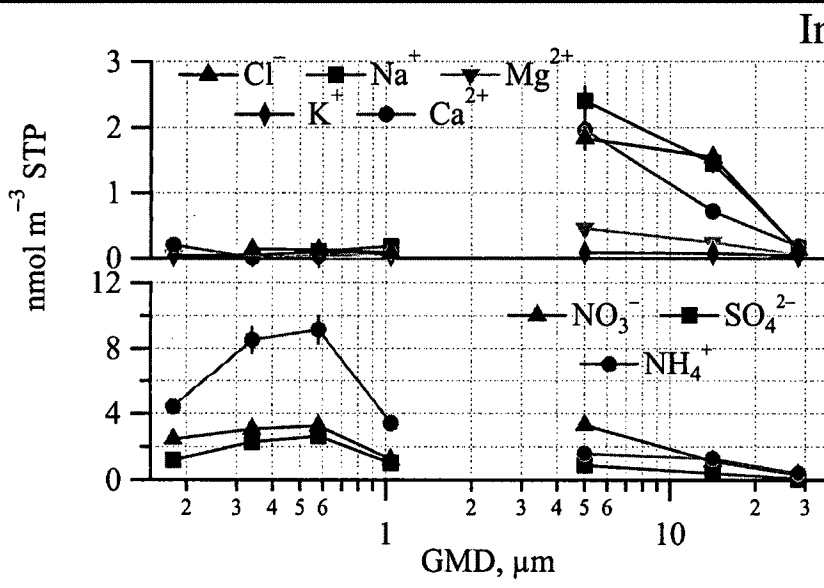
Impactor 26

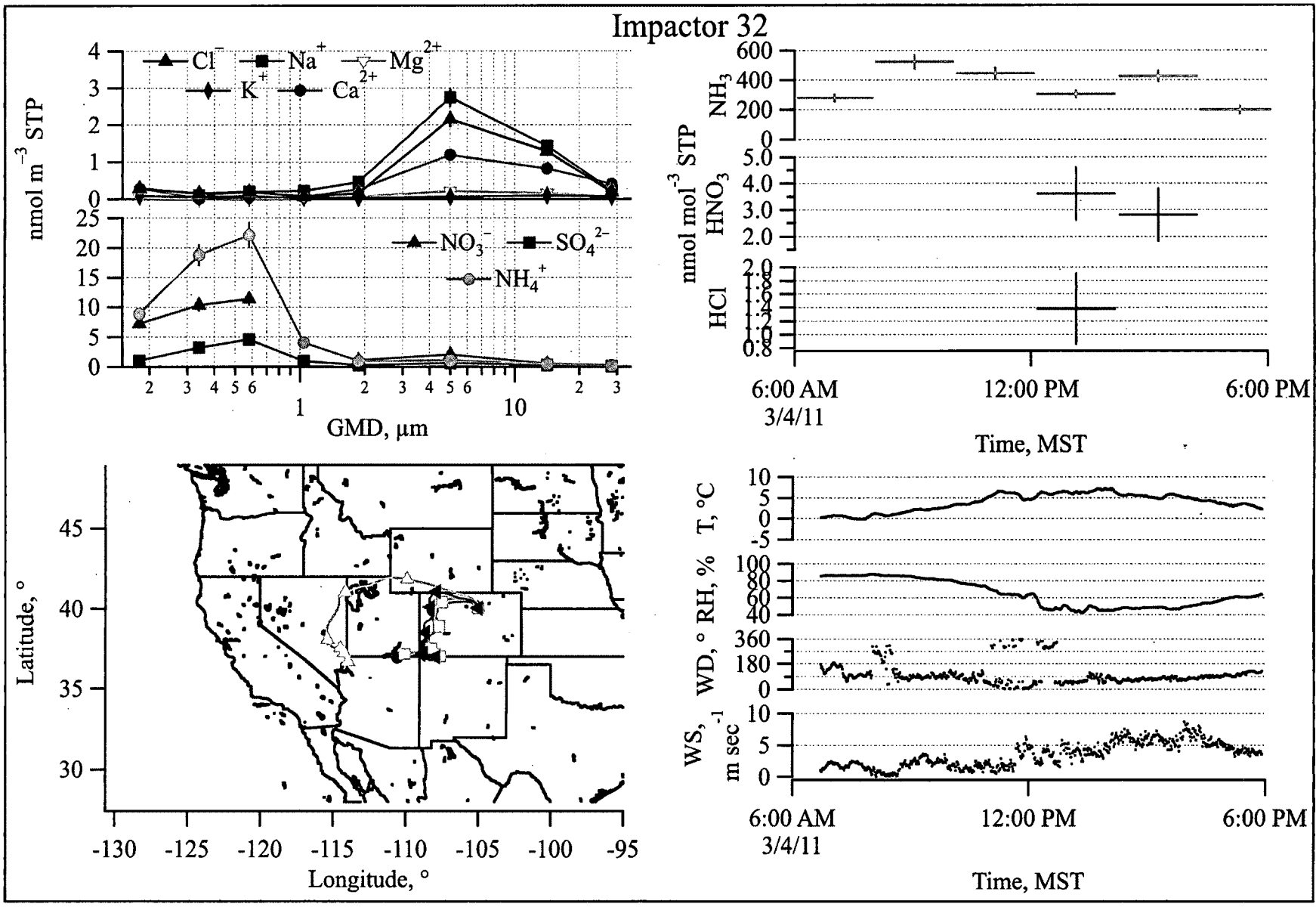




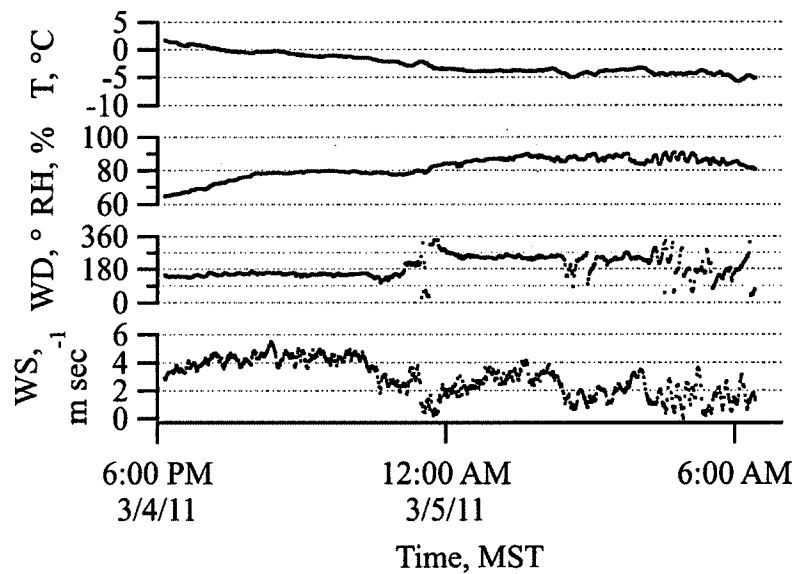
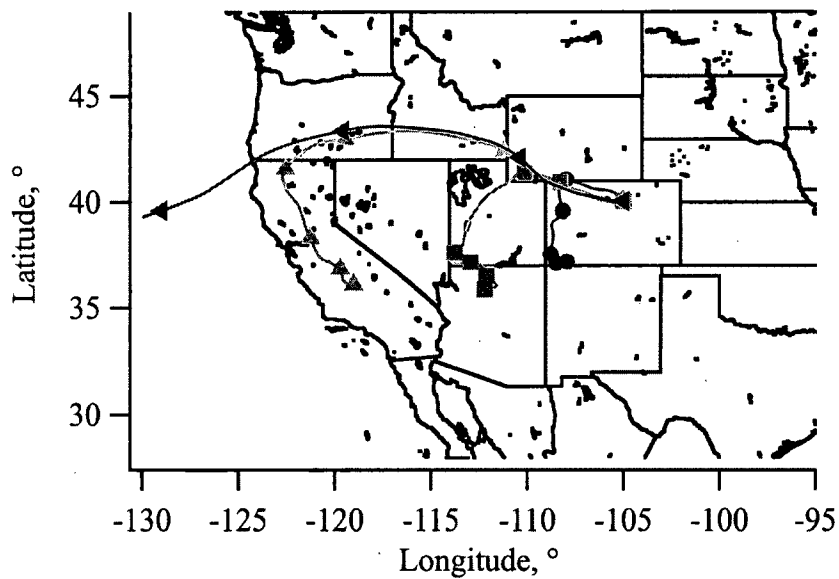
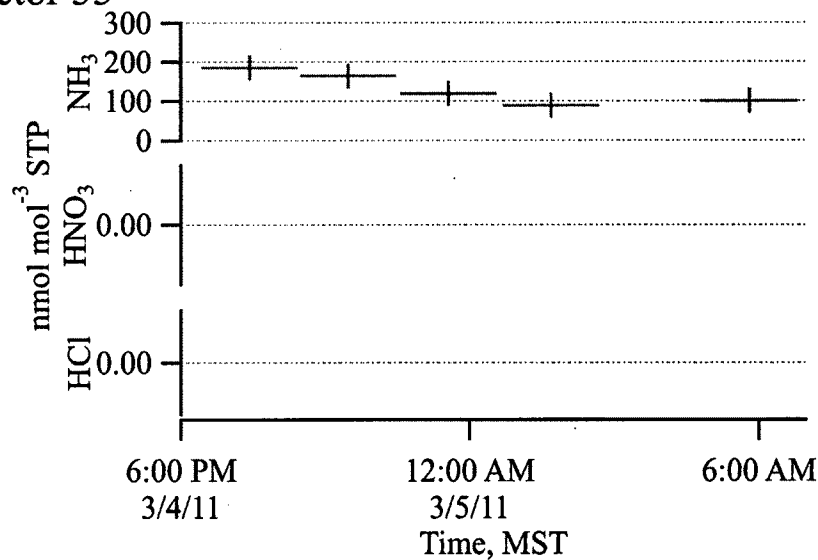
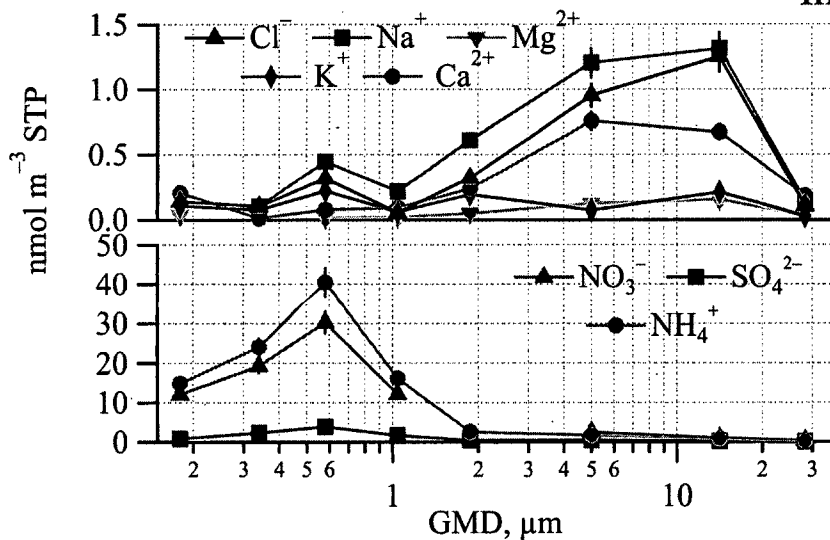




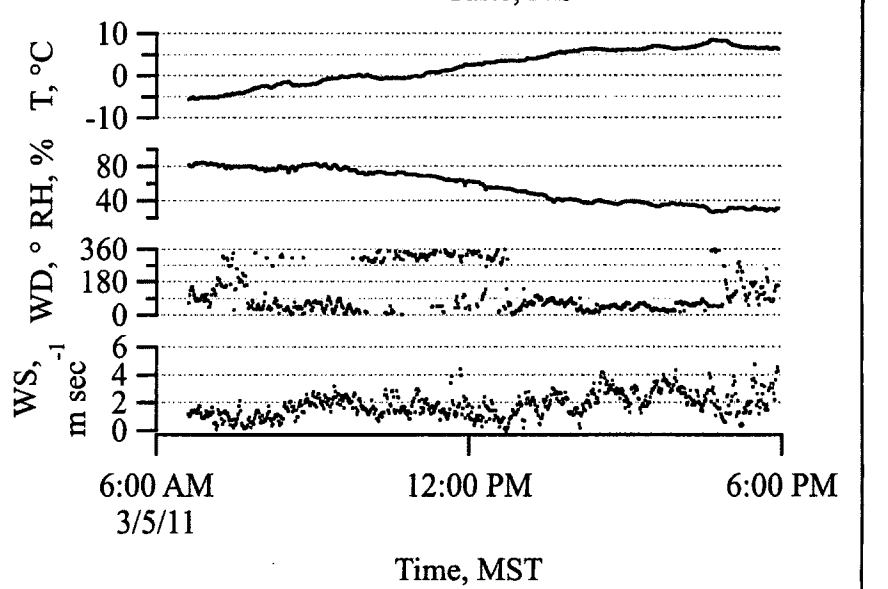
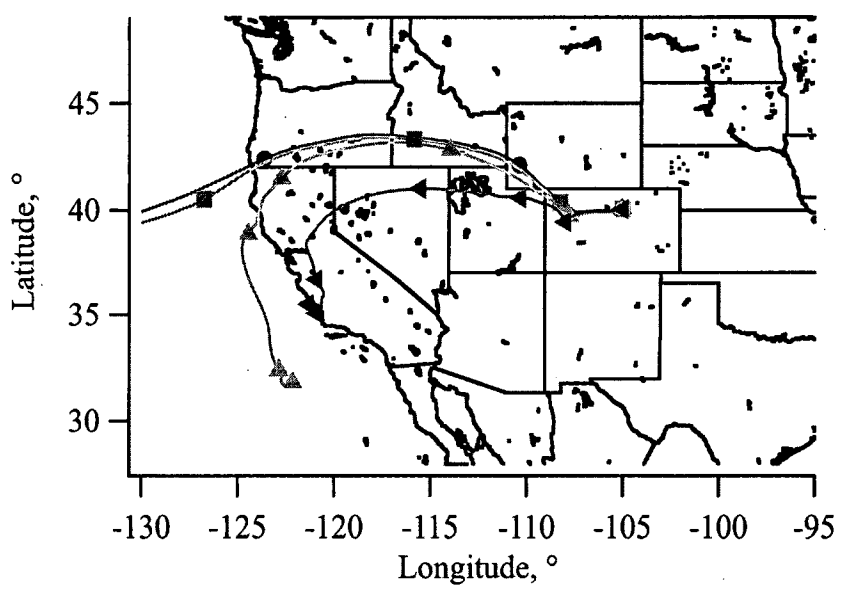
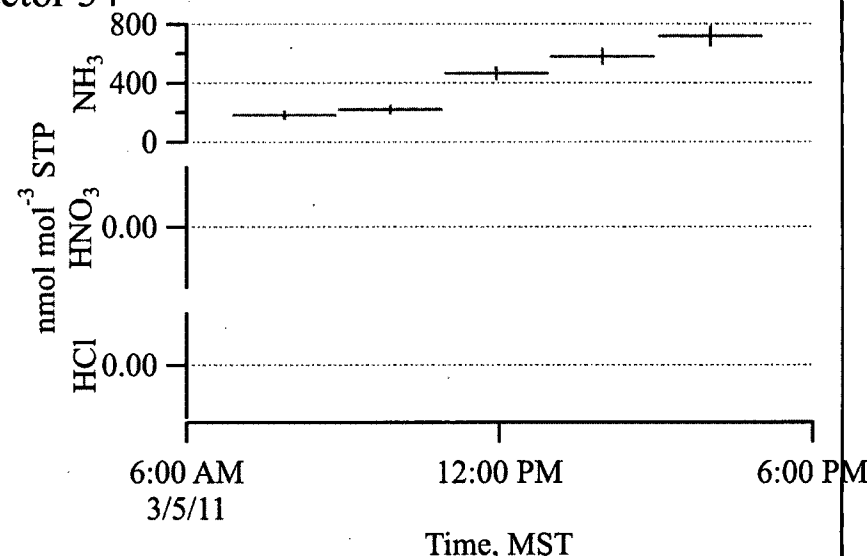
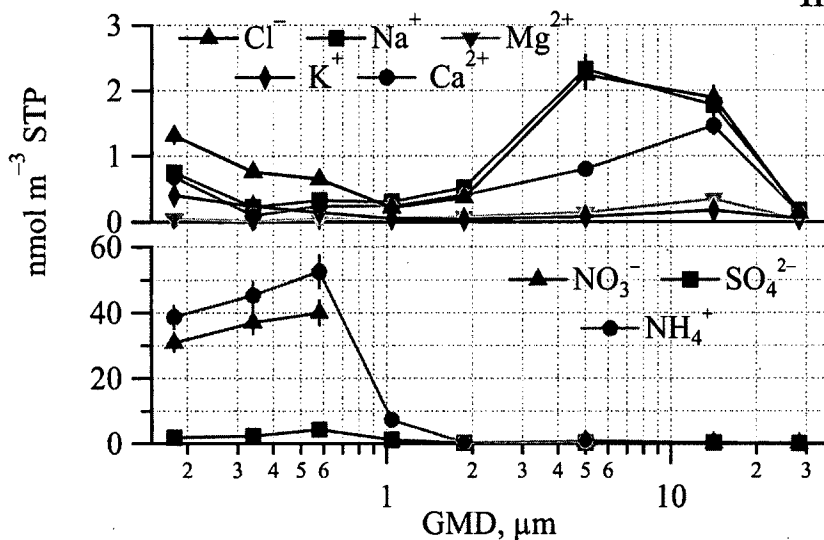


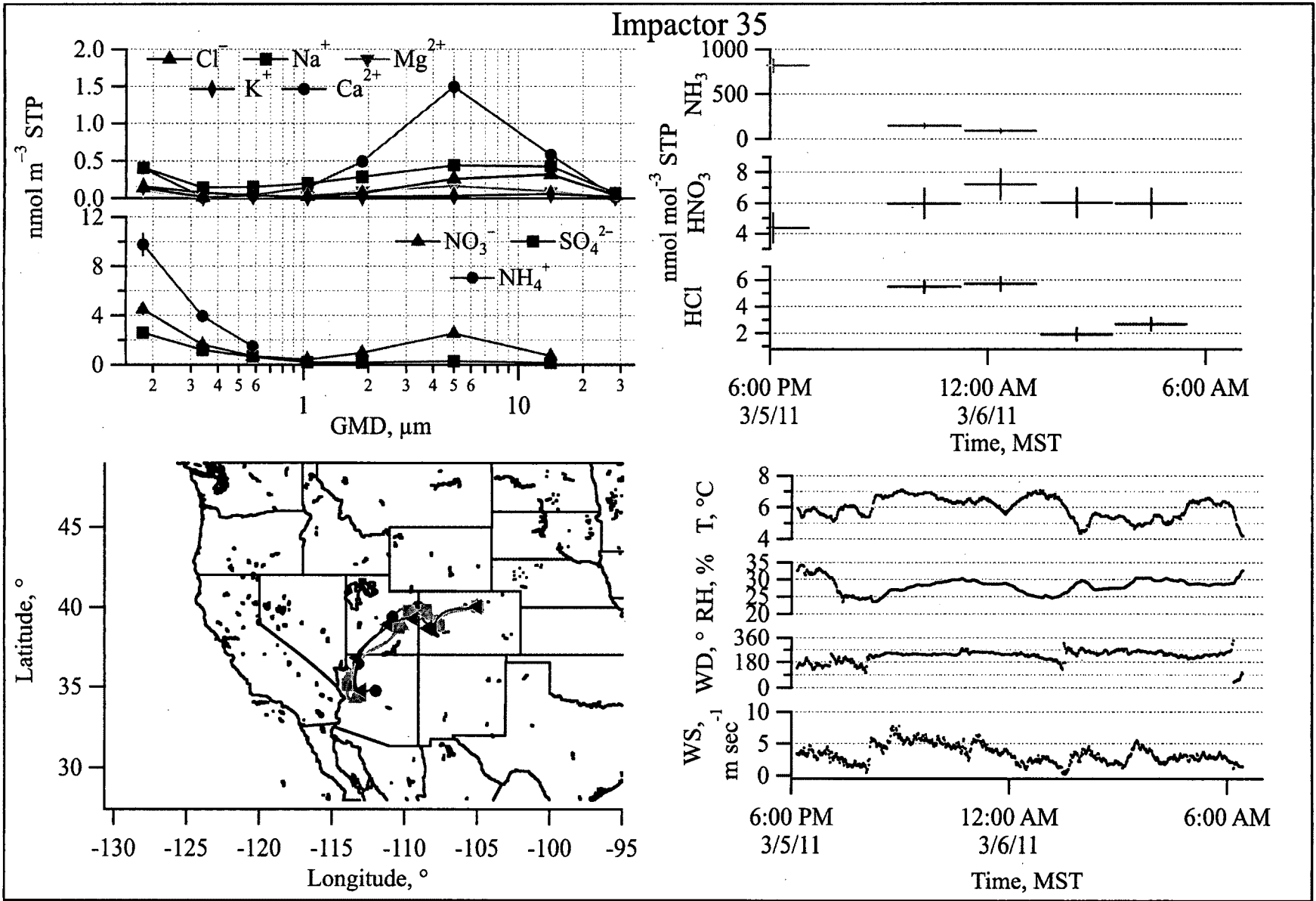


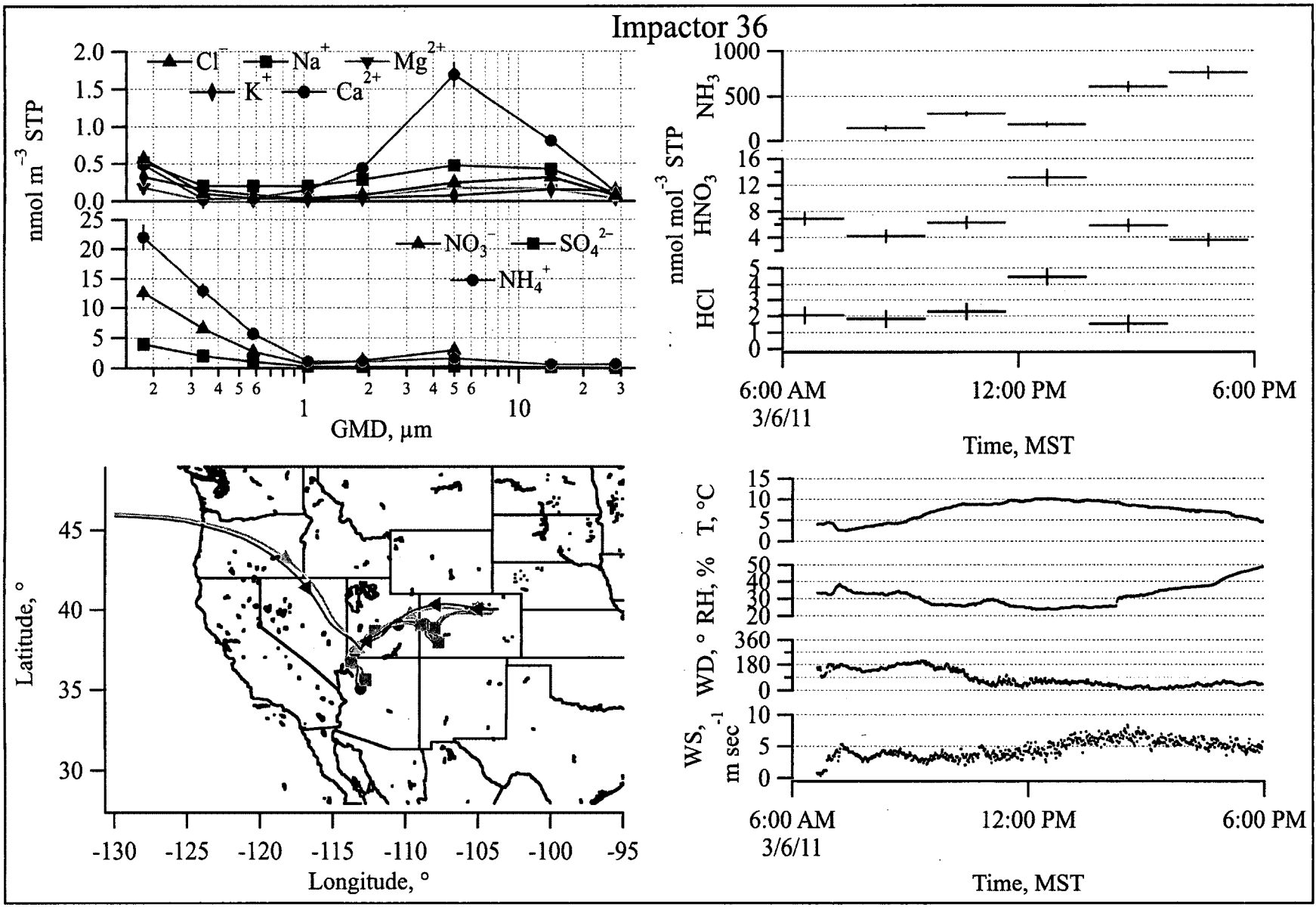
Impactor 33



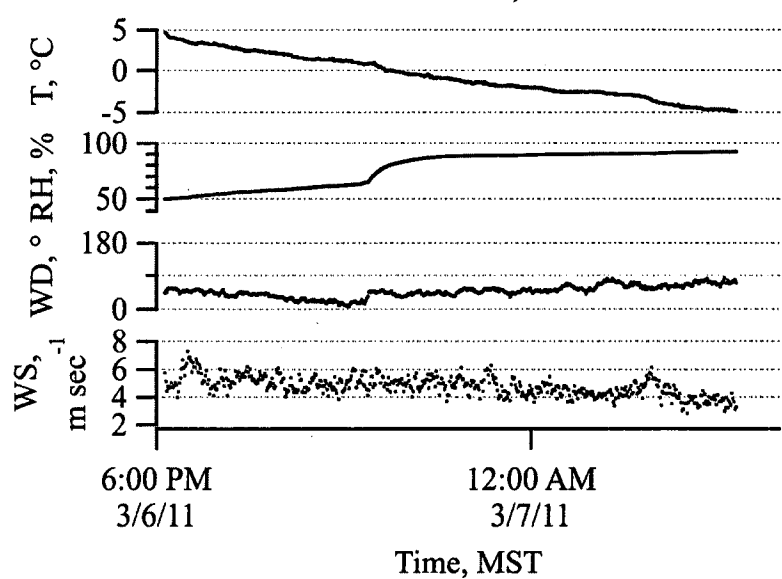
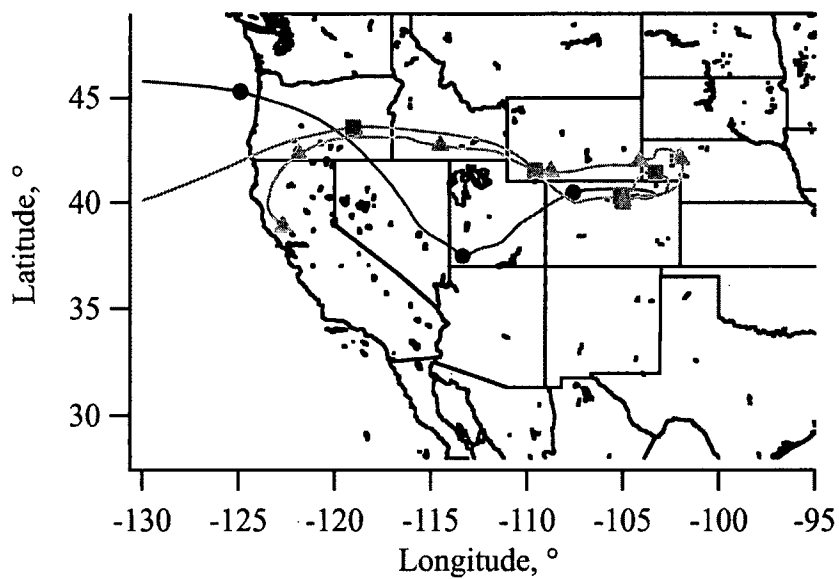
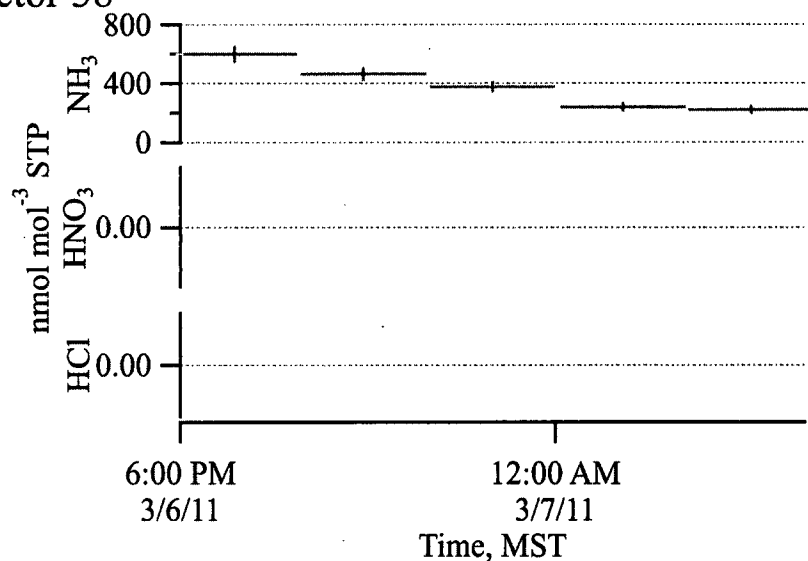
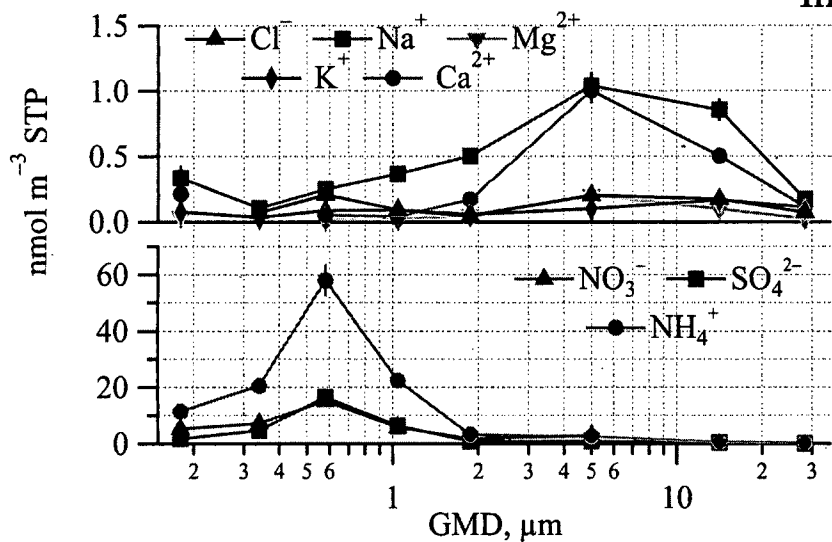
Impactor 34



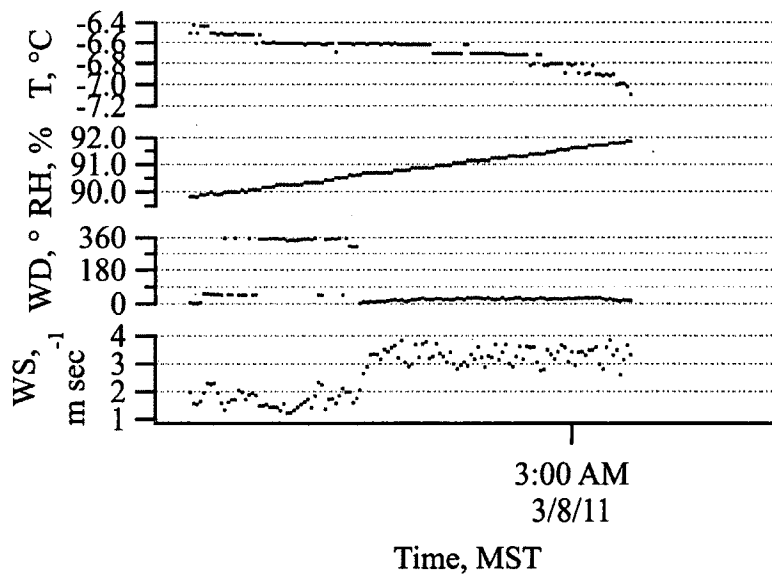
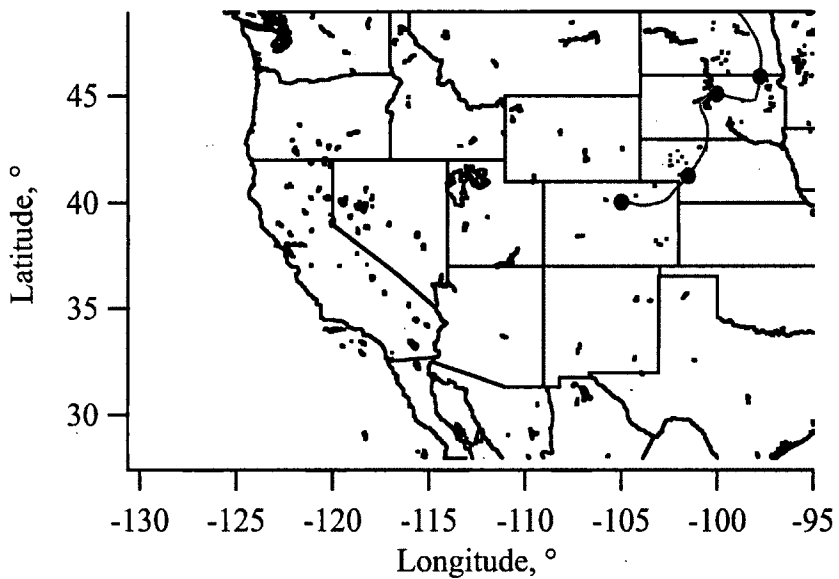
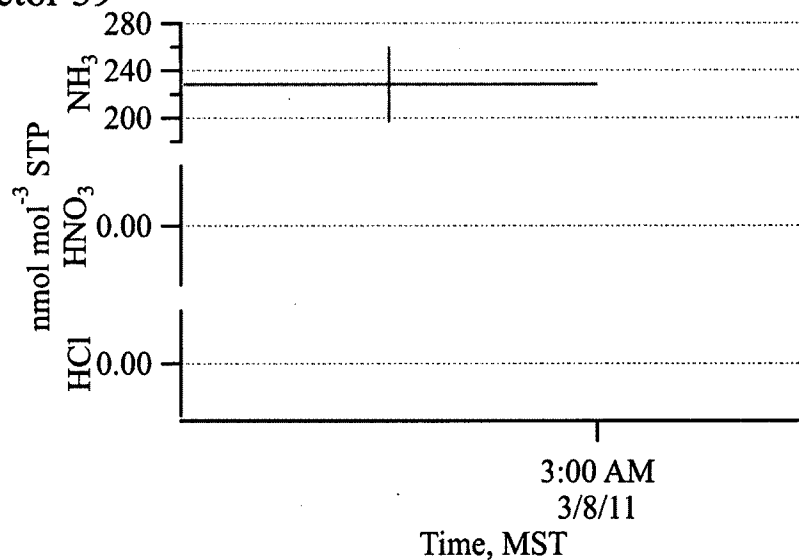
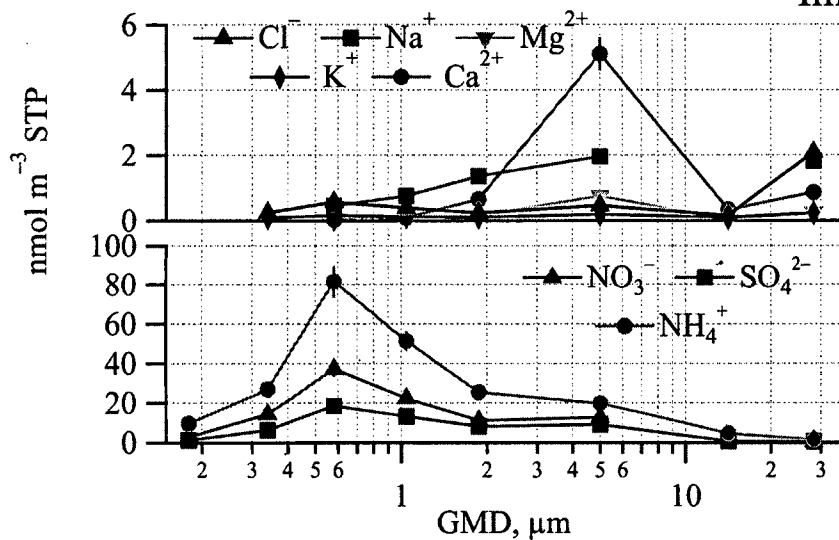




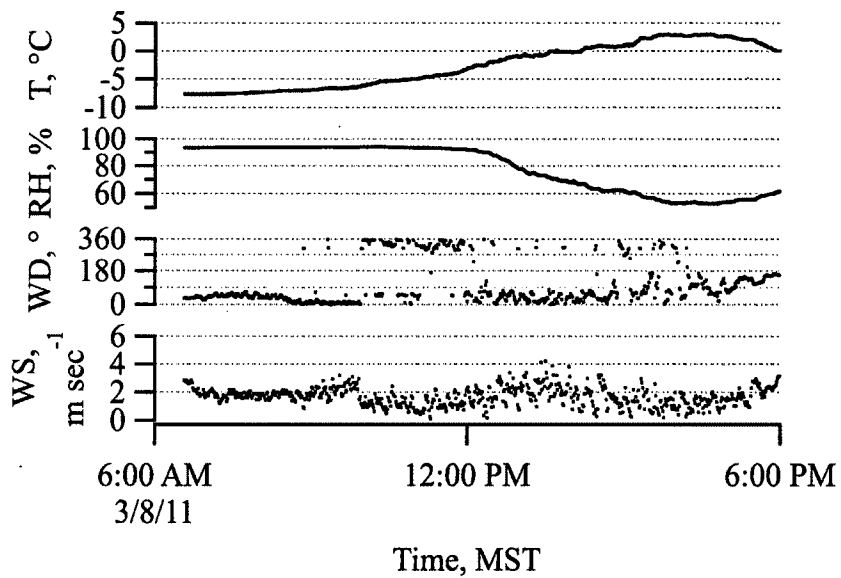
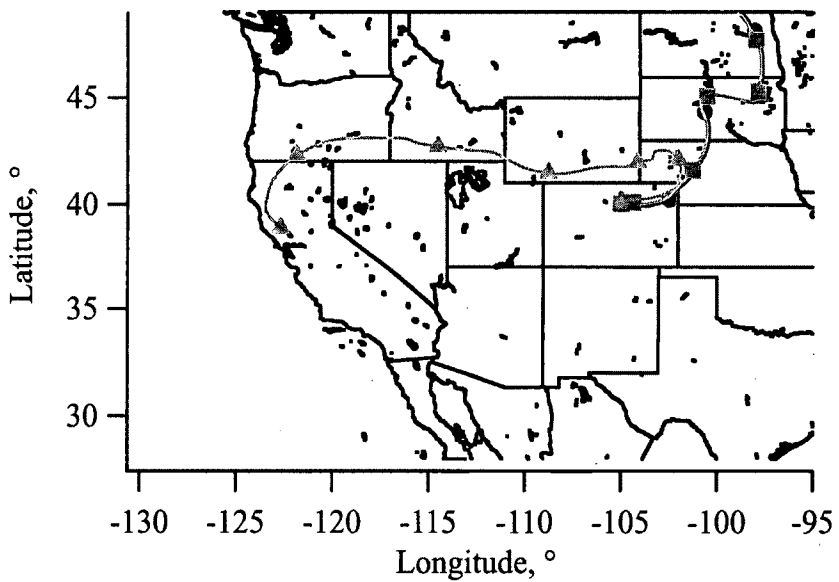
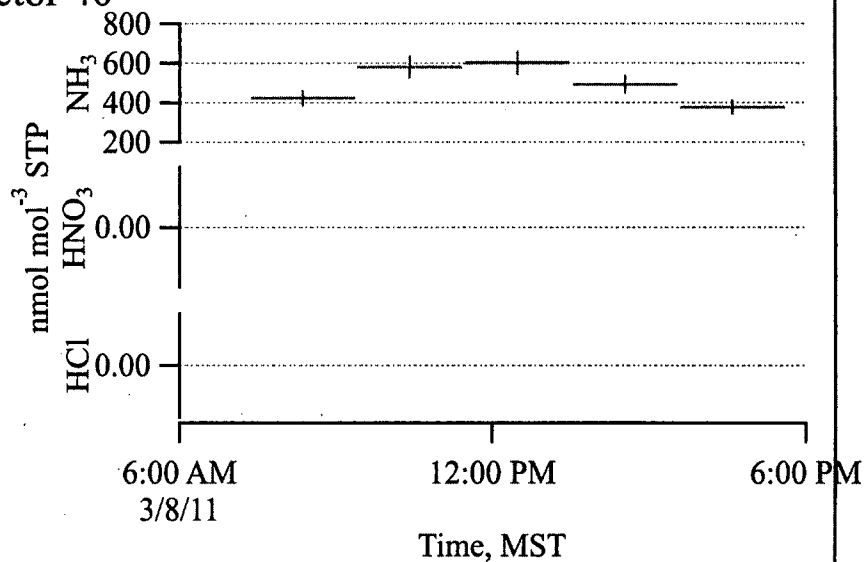
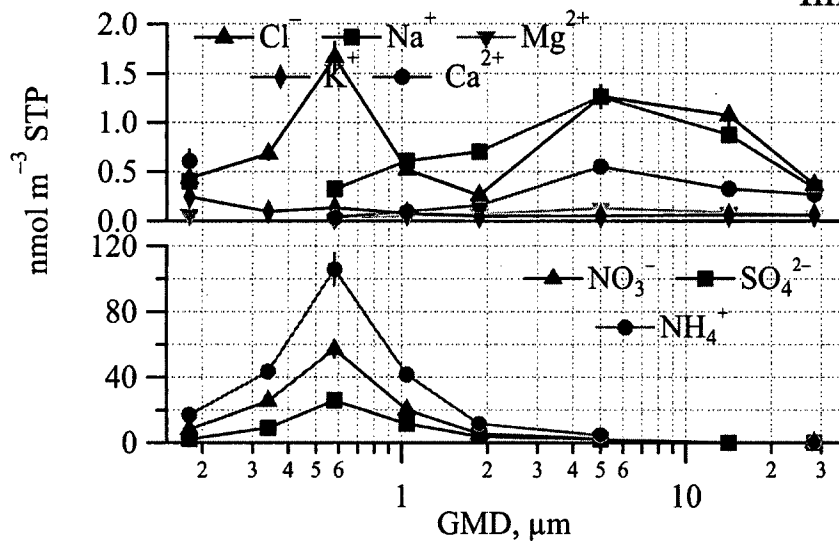
Impactor 38



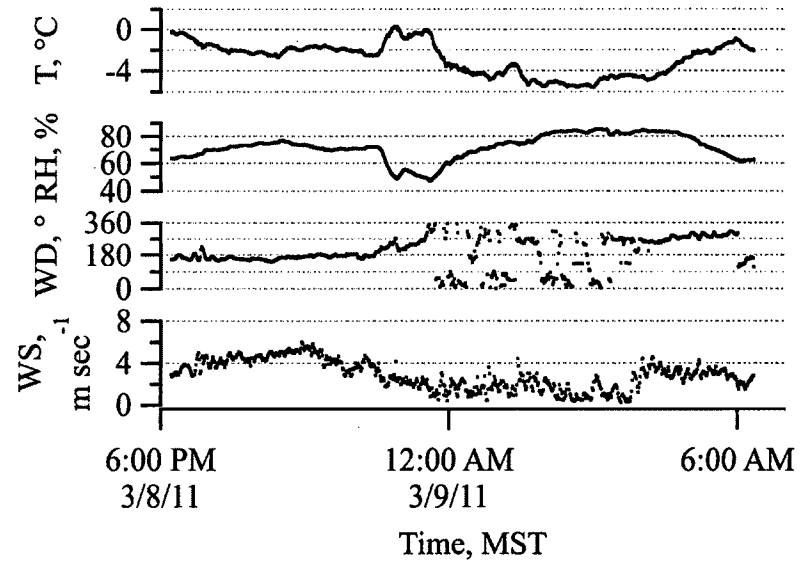
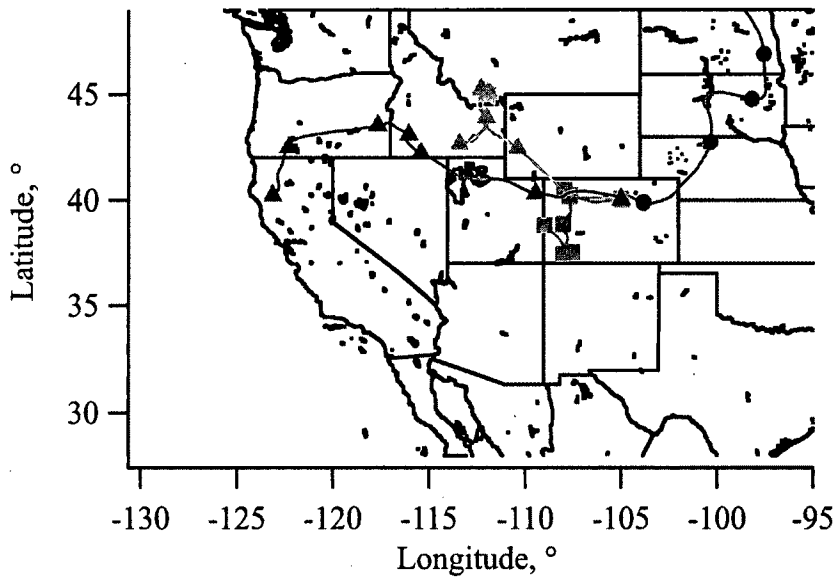
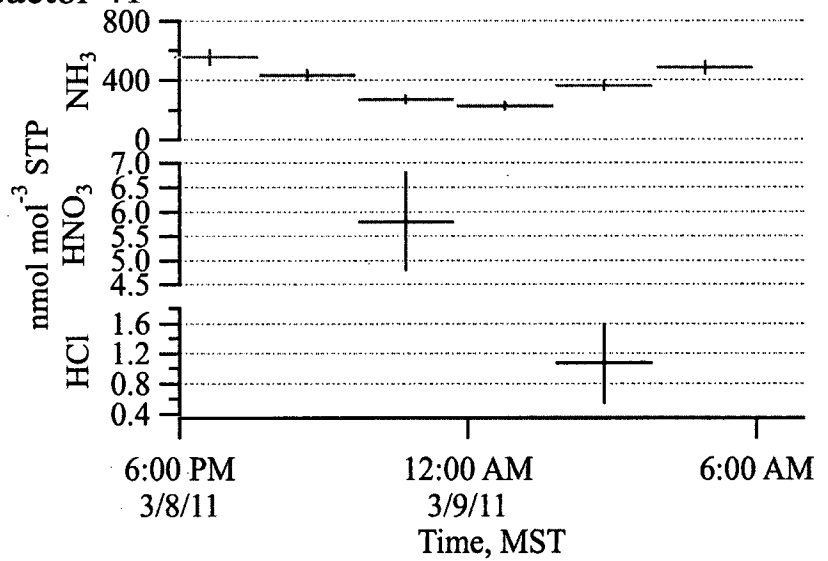
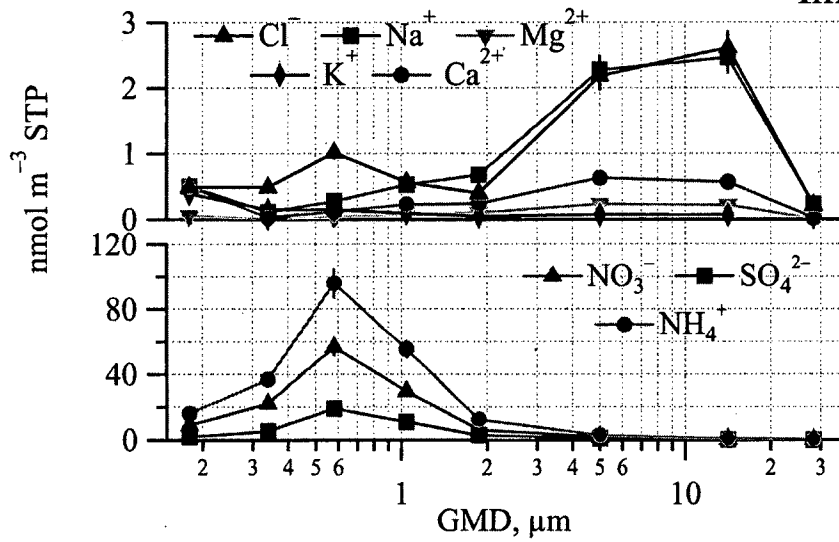
Impactor 39

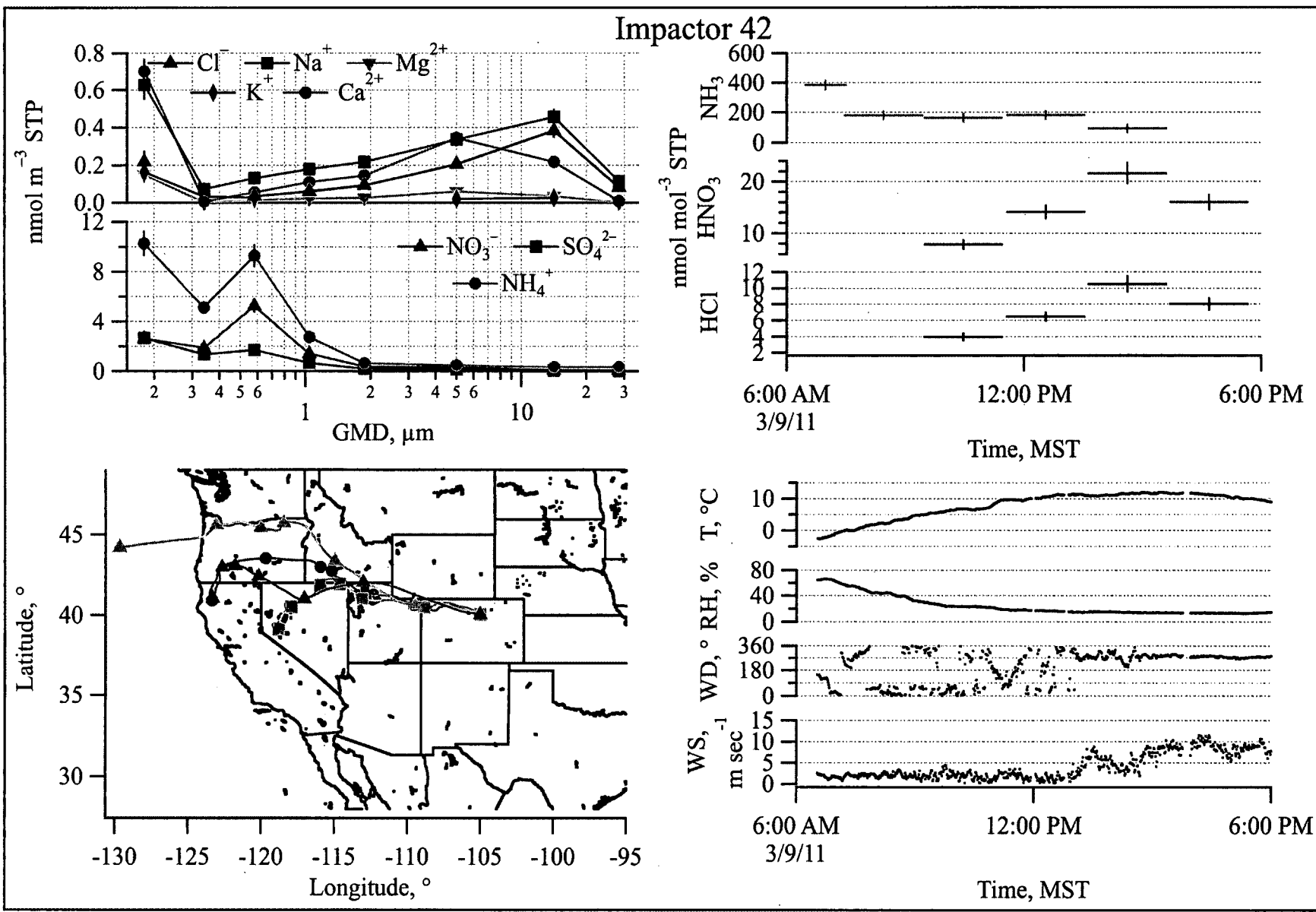


Impactor 40

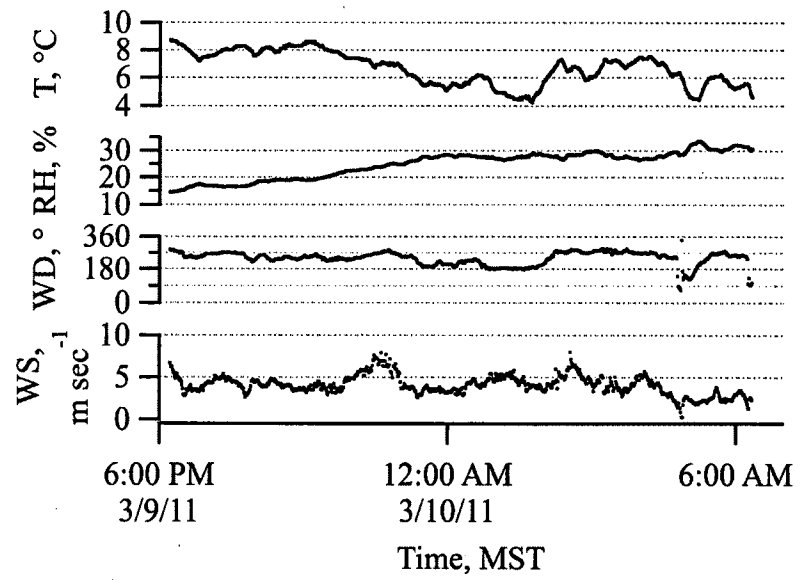
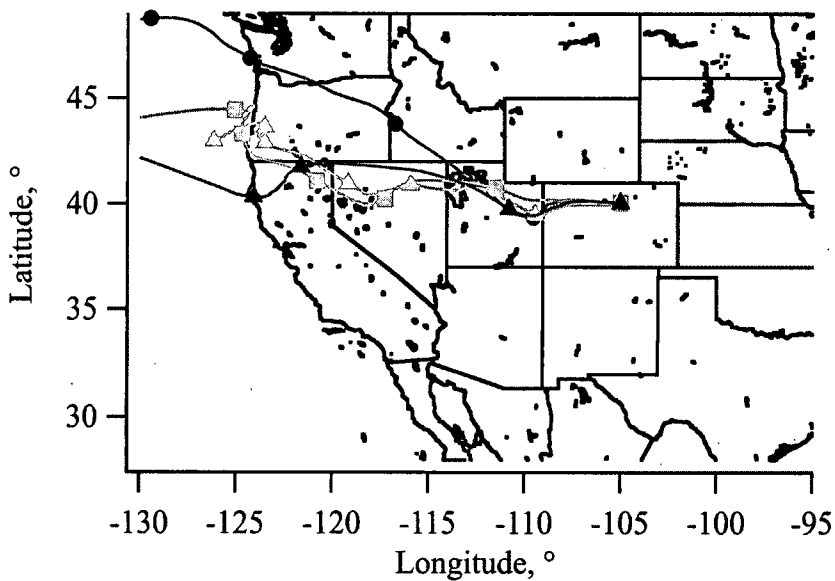
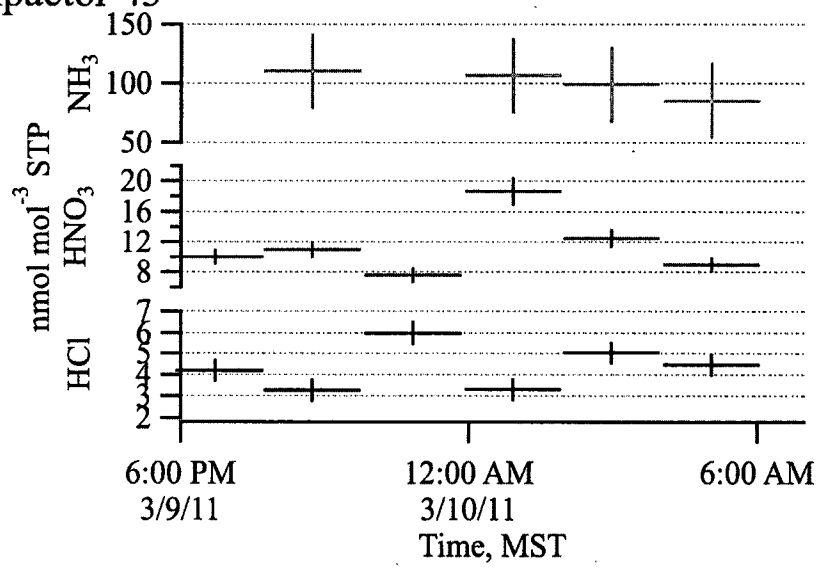
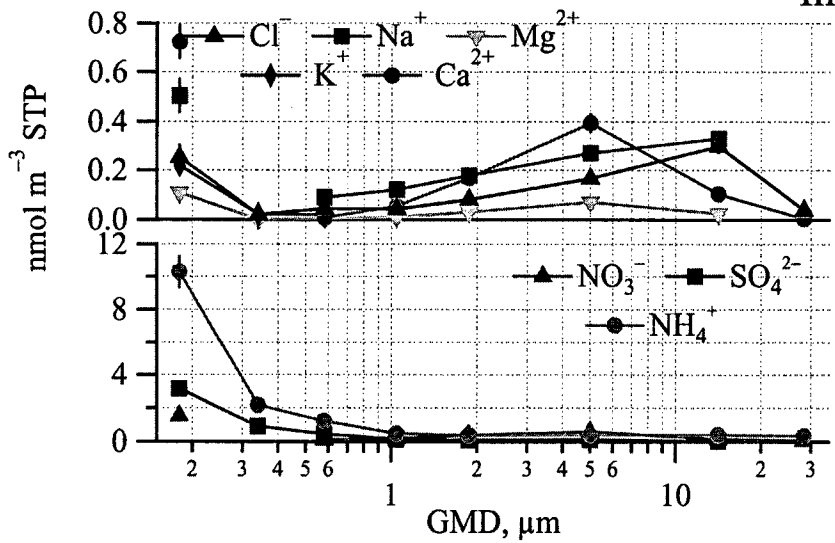


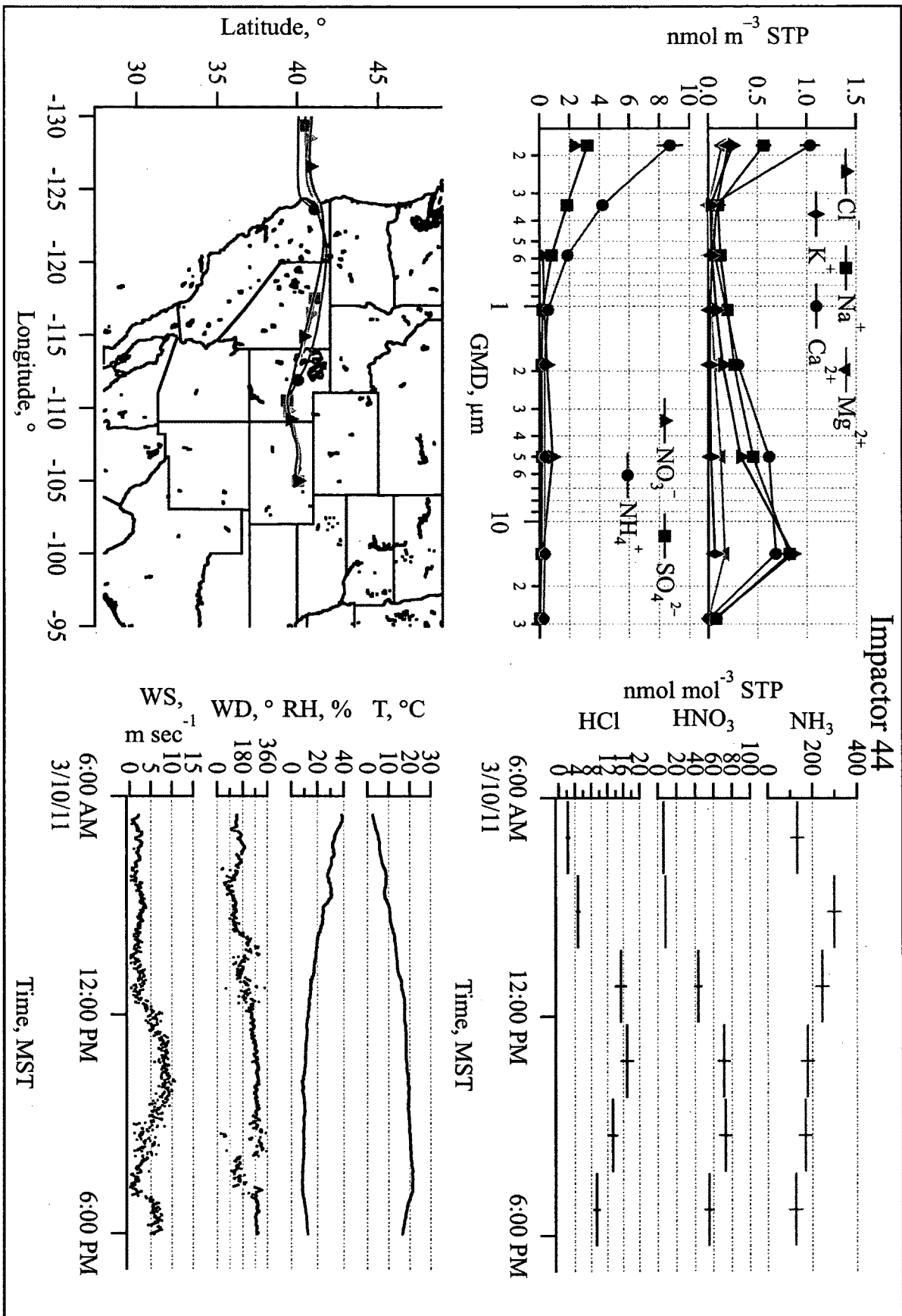
Impactor 41

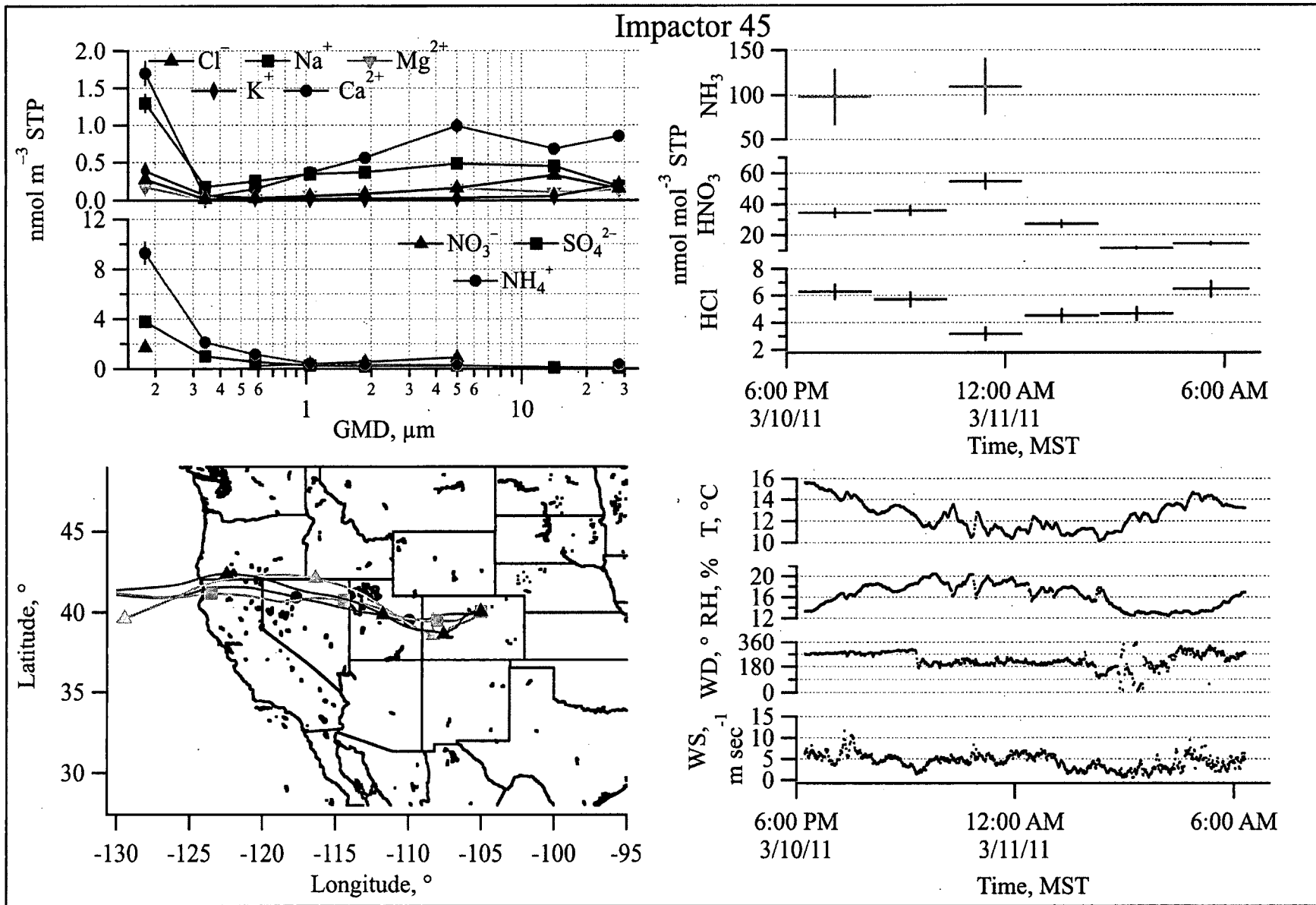


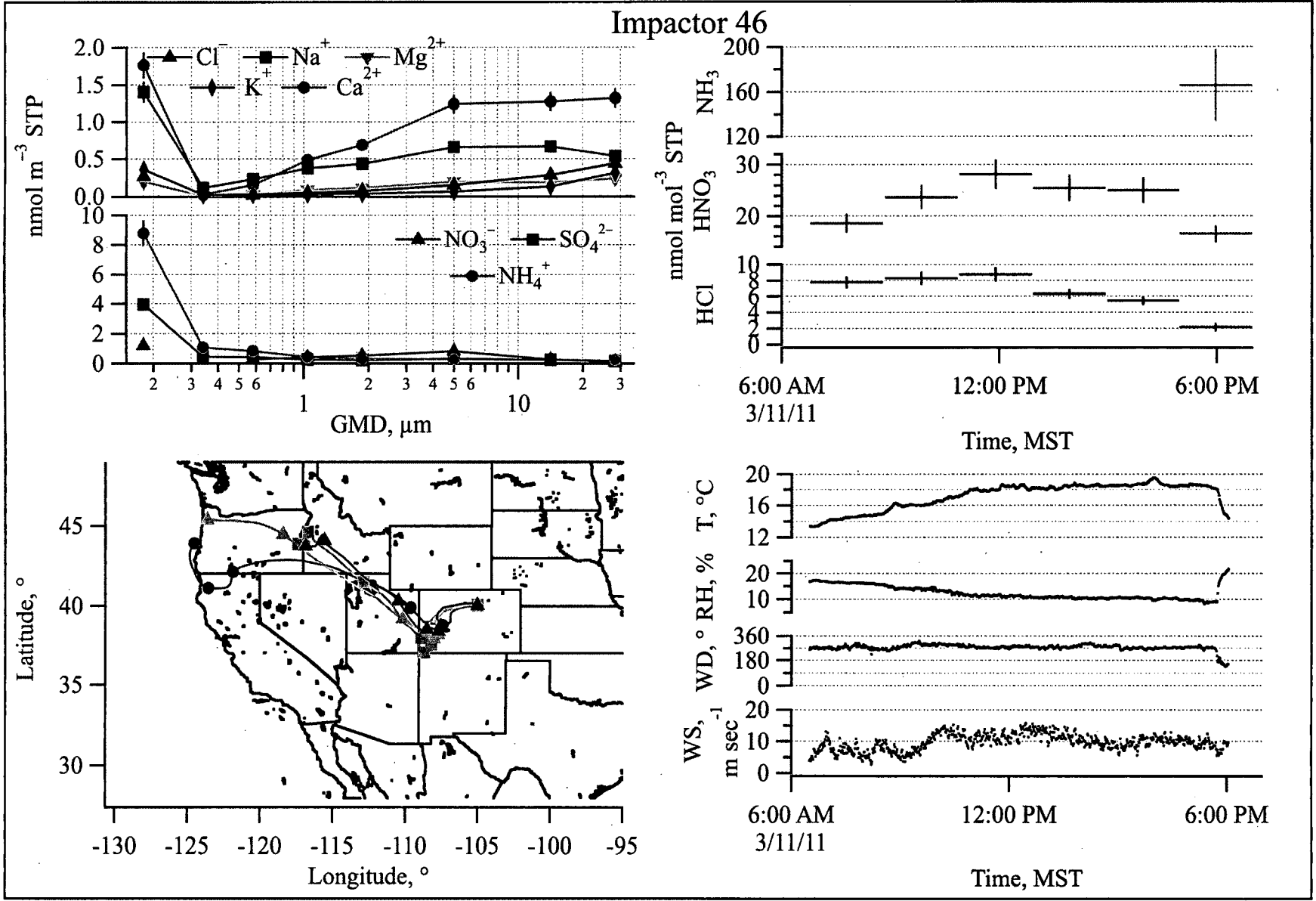


Impactor 43

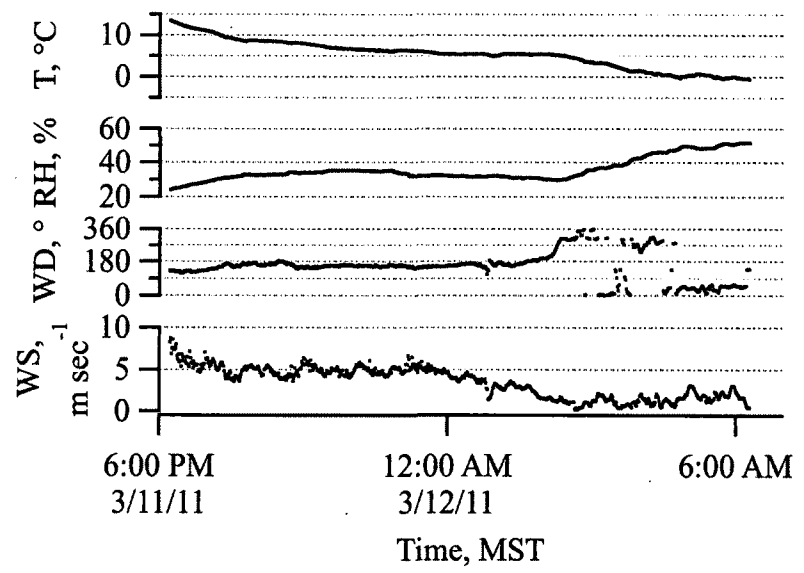
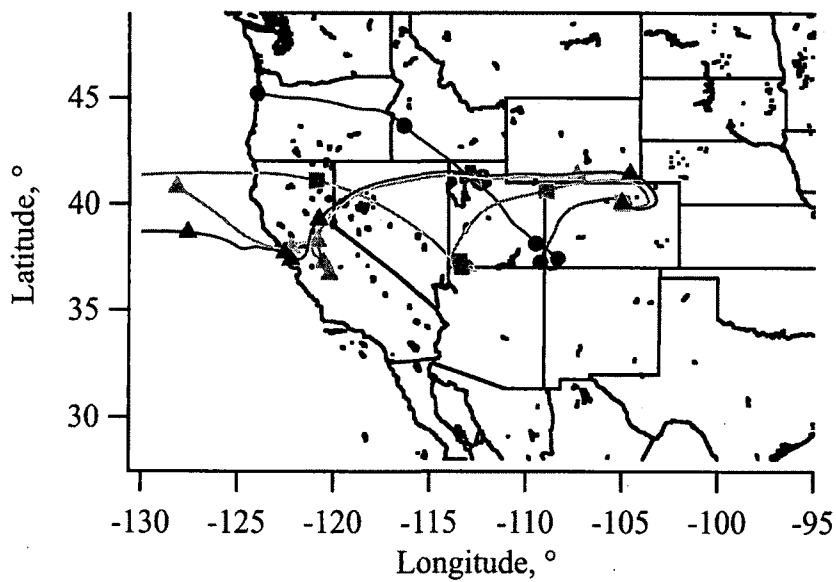
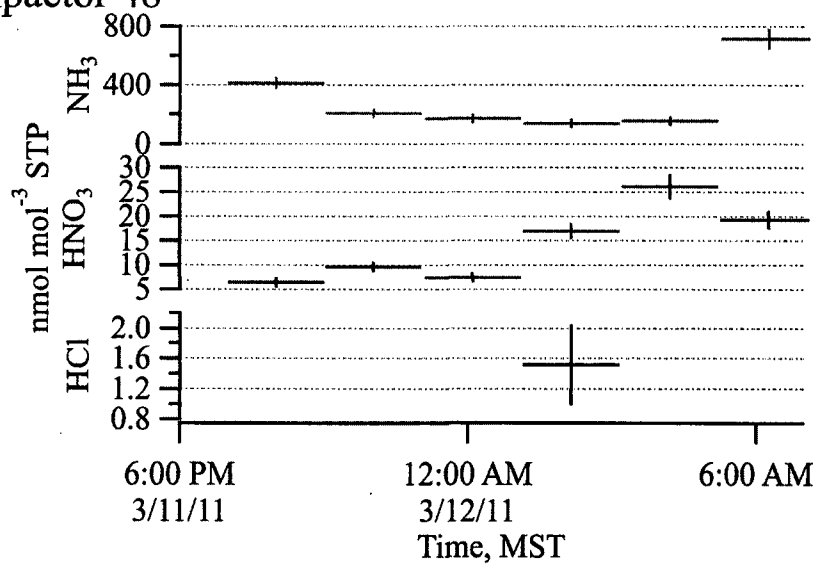
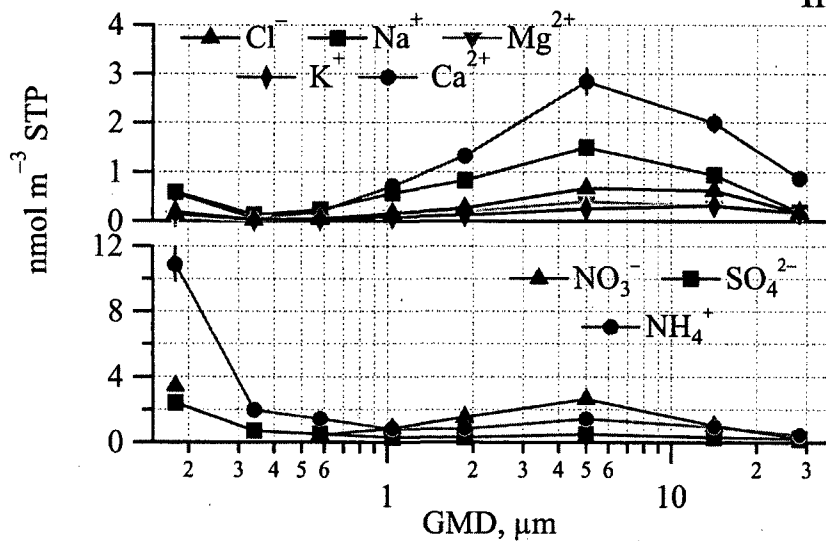


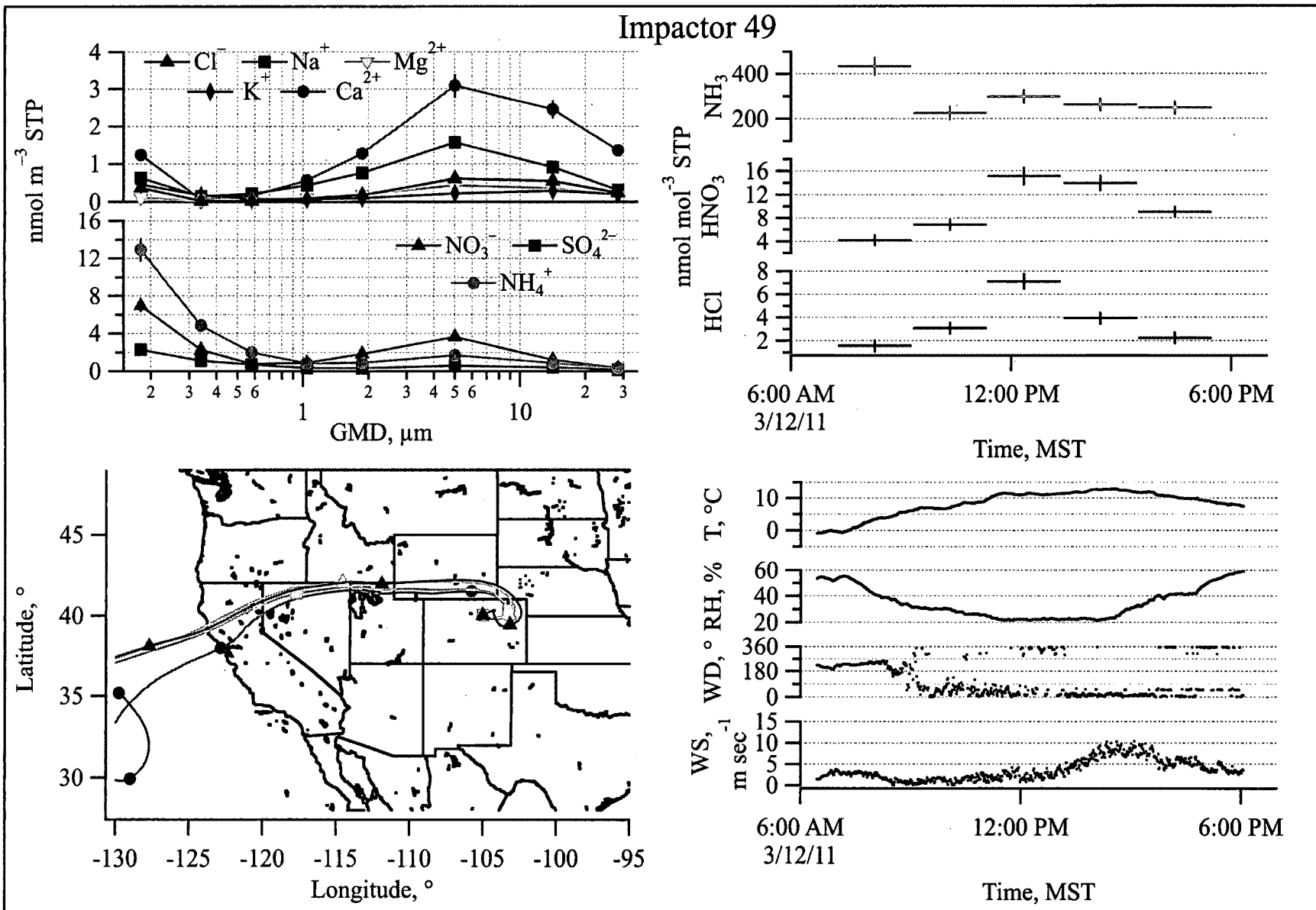






Impactor 48





Impactor 50

